College of Electronics Engineering

Electronic Engineering Department

High Power On-Board Battery Charger for Electric Vehicle

Ali Hussein Sultan
A Thesis in
Electronic Engineering

Supervised by

Assist. Prof.
Dr. Harith Ahmad Mohammed Al-Badrani

1445 A.H.   **2024 A.D.**

I

High Power On-Board Battery Charger for Electric Vehicle

A Thesis Submitted by

Ali Hussein Sultan

To

The Council of the College of Electronics Engineering

Ninevah University

As a Partial Fulfillment of the Requirements

For the Degree of Master of Science

In

Electronic Engineering

Supervised by

Assist. Prof.

Dr. Harith Ahmad Mohammed Al-Badrani

1445 A.H.   **2024 A.D.**

بسم الله الرحمن الرحيم

نَرفعُ دَرجـٰتٍ مَن نَشاء و فَوقَ كُلِ ذي عِلمٍ عَليم

صَدَقَ اللهُ العَظيم

سورة يوسف (٧٦)

ACKNOWLEDGEMENTS

Abstract

Electric Vehicles (EVs) are becoming more and more common. Therefore users must select an appropriate charger without the need for going to charging stations. This study evaluates and simulates an integrated on-board charger specially built for EVs that reliably combines the charging process via the driving components. Generally, the propulsion system's seven-phase inverter and Seven-Phase Induction Motor (7-PIM) are combined during the charging period. As a result of using the inductors in the stator, which function precisely as a grid filter, they experience rotation when an AC current flows through these coils. For this reason, electric cars that operate with an integrated charging system tend to use Multi-Phase Motors (MPMs), depending on the ability to release torque during the charging period. To ensure that the motor remains stationary during charging, an additional phase transposition is implemented, thereby separating the charging and propulsion functions.

Regarding the driving mode, this study provides a comprehensive mathematical analysis of an 7-PIM with the Field-Oriented Control (FOC) algorithm acting as the speed controller. Various controllers, including proportional-integral (PI), sliding mode (SM), and integral sliding mode (ISM) controllers, were employed to achieve a reliable speed control system. The simulation results show that both the SM and ISM controllers, when combined with the FOC algorithm, performed better than the PI controllers in accurately tracking the speed and flux references, even in the presence of disturbances in the system parameters. The simulation results shows that the PI has 0.05% overshoot and 1.2s settling time ,while SMC has no overshoot and 0.25s settling time, and ISMC has no overshoot also and 0.5s for settling time.

On the other hand, this study presents integrated chargers using seven-phase and three-phase sources. When charging from a seven-phase source, the applied parameters ensure a balanced current flow through all coils and preventing the generation of torque. Additionally, joining the three-phase grid presents the potential for an uneven distribution of current consumption among the individual phases of the grid. As a result, inequality exists throughout the grid. The present work uses the VOC technique together with different kinds of current controllers to govern the charging process. The control system included a sliding mode controller, a vector proportional-integral (VPI) controller, and a PI controller with a separation block to regulate the internal loop currents. It focuses explicitly on resolving imbalanced problems and ensuring the attainment of identical current levels. It was performed to deal with the imbalance and termination of the second harmonic generated by the unbalanced grid current. By using sliding mode control instead of other controllers, the degree of harmonics in the grid current is minimized to its lowest amount. The simulation results shows that the VPI has 1% overshoot and 2.5% THD ,while SMC has 0.3% overshoot and 0.25% THD, and PI has 1.3% overshoot and 3.2% THD. The system with the proposed controllers was simulated in MATLAB/Simulink to establish charge and driving management methods.

List of contents

List of Figure

List of Tables

LIST OF ABBREVIATIONS

EV	Electric Vehicles
OBC	On-Board Charger
MP	Multi-Phase
FOC	Field Oriented Control
MPIM	Multi-Phase Induction Motor
V2G	Vehicle to grid
PI	Proportional Integral
VPI	Vector Proportional Integral
7-PIM	Seven-Phase Induction Machine
PLL	Phase-Locked Loop
OESW-FPIM	open-end stator winding five-phase induction motor
SVPWM	Space Vector Pulse Width Modulation
MRAS	Model Reference Adaptive System
SMC	sliding mode control
SO-ISMC	Second Order Integral SMC
FPIM	Five-Phase Induction Motor
IFOC	Indirect Field Oriented Control
DMC	Direct Matrix Converter
PPMIM	Pole Phase Modulation With Multiphase Machines
SWMD	Series-End Winding Motor Drive
WPT	Wireless Power Transfer
APM	Auxiliary Power Module
EMF	Electromotive Force
MMF	Magneto Motive Force
FW	Flux-Weakening
TPIM	Three-Phase Induction Motor
SS	Sliding Surface

LIST OF SYMBOLS

n	Number of phases	1,2,3…
ρ	Angele of rotor flux	degree
ω_e	synchronous speed	Rad/s
V_{ds} ,V_{qs}	direct and quadrature axis of stator voltages	Volt
V_{ns}	stator phase voltages	Volt
Ψ_{ds}, Ψ_{qs}	d and q axis stator flux linkages	web
V_{dr} ,V_{qr}	direct and quadrature axis of rotor voltages	Volt
Ψ_{dr}, Ψ_{qr}	d and q axis of rotor flux linkages	web
P	total number of poles	1,2,3…
J	value of the moment of inertia	kg·m^2
f	friction coefficient	N
T_L	load torque	Nm
T_e	mechanical torque	Nm
ω_r	angular velocity of the rotor part	Rad/s
L_m	mutual inductances	Henry
s	state of the upper switches	1,2,3…
s(t)	Sliding Surface Vector	
e (t)	error signal	
k	sliding mode gain	constant
V_g	grid voltage	volt
V_{con}	converter voltage	volt
V_{drp}	voltage drop	volt
$V_{g\alpha\beta}$	Alpha and beta components of grid voltage in stationary reference frame	volt
V_{gdq}	d and q components of grid voltage in rotating reference frame	volt
C	output Capacitor	faraday
pp	Active power	watt

qq	Reactive power	watt
ω_g	Angular velocity of the grid voltage	Rad/s
θ_g	Position of the grid voltage	degree
R_s	Stator resistance	Ohm
R_r	Rotor resistance	Ohm
L_{ls}	The leakage inductances for stator	Henry
L_{lr}	The leakage inductances of rotor	Henry

CHAPTER 1 : Introduction and Literature Review

1.1 Introduction

Recently, Electric Vehicles (EVs) have gained global attention for a variety of reasons, including global warming because of the vehicles using fossil fuels and internal combustion engines. Furthermore, researchers have linked the environmental pollution these vehicles cause to climate change [1]. In addition, the cost of the fuel is considered high compared to the capacities of electric energy [2].

As a result, changing toward EVs has been adopted by several countries and companies, which can be successfully achieved by considering three factors. The first factor is the ability to store the energy inside the battery to achieve mobility. Consequently, the EV field employs high-quality batteries [3].

The second factor is to supply an appropriate charger for these batteries, using two type of chargers based on the installation location. The first one is an off-board charger, which is located outside the EV at designated stations and requires a specific element for the charging process. This technique provides a fast-charging capabilities based on the efficiency of the charger elements. The second type of EV charger are On-Board Charger (OBC), which utilizes the driving element while charging [4]. This charger provides significant flexibility by allowing charging from any source of electrical energy. The use of driving elements (inverters and motor coils), which are always in a state of non-use during the charging process gives the possibility to benefit from these elements in the battery charging process. However, the passing current through the motor coils causes unwanted rotation. Moreover, three-phase motors are affected by the motor rotation during integrated charging,

demanding a special configuration [5]. As a result, researchers tend to change the direction of Multi-Phase (MP) motors depending on the additional freedom to prevent the motor from rotating [6].

The third factor for success in EVs is applying a driving system with changeable speed and high reliability. MP machines are desirable in EV field applications because of their features [7].

1.2 Literature Review

The operation of electric vehicles with OBC can be separated into two modes. The first mode, known as the driving mode, employs a method for controlling the speed of the electric motor. Since MP motors are the most proposed in the field of electric cars, Field Oriented Control (FOC) technology was applied in this study to control the speed of MP Induction Motors (MPIMs). The second mode represents reusing the elements applied in the driving mode (the motor coils with an inverter) to charge the battery without using an external charger. The biggest challenge in the OBC of EVs is the generation of torque during the charging mode because of the current passing through the motor coils, which act as filters.

Various topologies have been suggested and employed for both the charging process with the OBC of EVs and driving MP machines. However, the following subsections provide a review of the techniques for propulsion systems for MP motors and OBC technologies for EVs.

With respect to MP motors, the currents in the xy sub-planes resulting losses and do not affect the generation of torque. The proposed method by Pescetto P. [8], include the use of FOC with additional PI controllers to eliminate the xy sub-planes by using a zero as desired value.

The design and mathematical representation of an open-ended five-phase motor were proposed in a previous study [9]. The system uses direct and indirect FOC to control the speed of the proposed design under different conditions. The space vector modulation was proposed to generate pulses for the binary inverter, which in turn are connected to the ends of the stator coils of the motor .

However, the indirect FOC method was applied for driving three-phase IM proposed by Paper et al [10]. Integral sliding mode with a reduced order controller applied in feed-back to enhance its capacity to prevent disruptions and accurately follow a desired speed.

A novel control approach for a three-level inverter-supplied Seven-Phase Induction Machine (7-PIM) that employs direct rotor FOC was presented in a previous study by Roumaine R. et al [11]. The machine's model displays non-sequential currents, which reduce current quality and give no torque. A controller based on fuzzy logic is demonstrated to regulate rotor speed and non-sequential components under different conditions.

A previous study presented a method for controlling an open-end stator winding five-phase induction motor (OESW-FPIM) without the need for sensors proposed by Khadar S. et al [12]. The control method is based on field-oriented control (FOC). The use of the FOC approach is linked to the implementation of dual Space Vector Modulation (SVPWM) in order to maintain a consistent switching frequency and reduce the presence of harmonics damage. In addition, a straightforward combination observer is suggested that integrates a Model Reference Adaptive System (MRAS) with a sliding mode (SM) observer.

The study provides a robust Second Order Integral SMC (SO-ISMC) with a five-phase IM drive proposed by Mossa M. et al [13]. The development of the suggested SO-ISMC technique is a methodical method designed to guarantee the stability and appropriate behavior of the five-phase IM.

Rahman K. et al. propose a FOC for a Five-Phase Induction Motor (FPIM) powered by a Direct Matrix Converter (DMC) and controlled by SVPWM in order to remove unwanted elements from spatial vectors proposed by Rahman K. et al [14]. Furthermore, the matrix modulator has the capability to achieve power factor adjustment at the input of the system. The drive's dynamic properties are achieved under various loading scenarios.

In order to obtain a driving system that is not affected by external disturbances and is suitable for EVs the Pole Phase Modulation With Multiphase Machines (PPMIM) was suggested by Iqbal A. et al. [15]. The mathematical modeling and transformation matrices are applied in an rotating reference frame by taking into account every possible arrangement of pole phases. The Indirect FOC (IFOC) is suggested with an individual PI controller was established and used to regulate the current components in rotating reference frame for all pole-phase modes. The suggested IFOC system is resilient and suitable for any modulation technique.

The study conducted by Surada R. et al.provides a thorough analysis of a unified charging system for a single phase integrated charger [16]. This method employs two inverter legs and can operate in both the Vehicle-to-Grid (V2G) and charging modes. The system uses a

bidirectional DC-DC converter and a three-phase inverter, as shown in Figure 1.1. During charging, it is essential to separate the motor from the system. A significant drawback of the concept is its need for several system restructuring elements, like a grid filter.
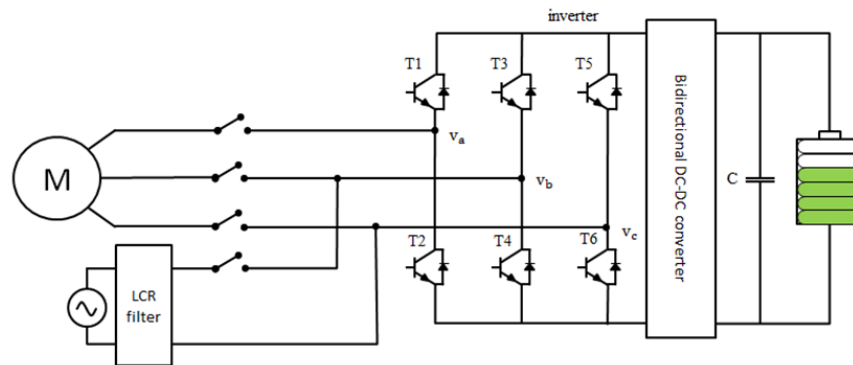
Figure 1.1 The configuration of only integrated three-phase inverter with DC-DC converter [16]

During the charging process, five-phase driving elements are combined to provide a quick charging system, which was proposed by Subotic I. et al. [17]. This proposed study can expanded and applied to any multiphase system with a natural including a single neutral point. Hardware reconfiguration can be accomplished by imposing additional switches to achieve comfortable conversion between driving and charging modes. In order to achieve balance in the network current in addition to reducing the effect of harmonics, whether due to load imbalance or due to the deadtime of the inverter, a Vector Proportional Integral Controller (VPI) with selective harmonic ability has been proposed as a current controller.

Kollar B. et al. conducted a study that examines the different configurations of the nine-phase machine-based OBC [18]. Machines that have nine phases provide extra torque and reduce copper damage. An important drawback of these inverters is the increased number of

semiconductor switches and the resulting complexity of the regulating circuit, as shown in Figure 1.2.
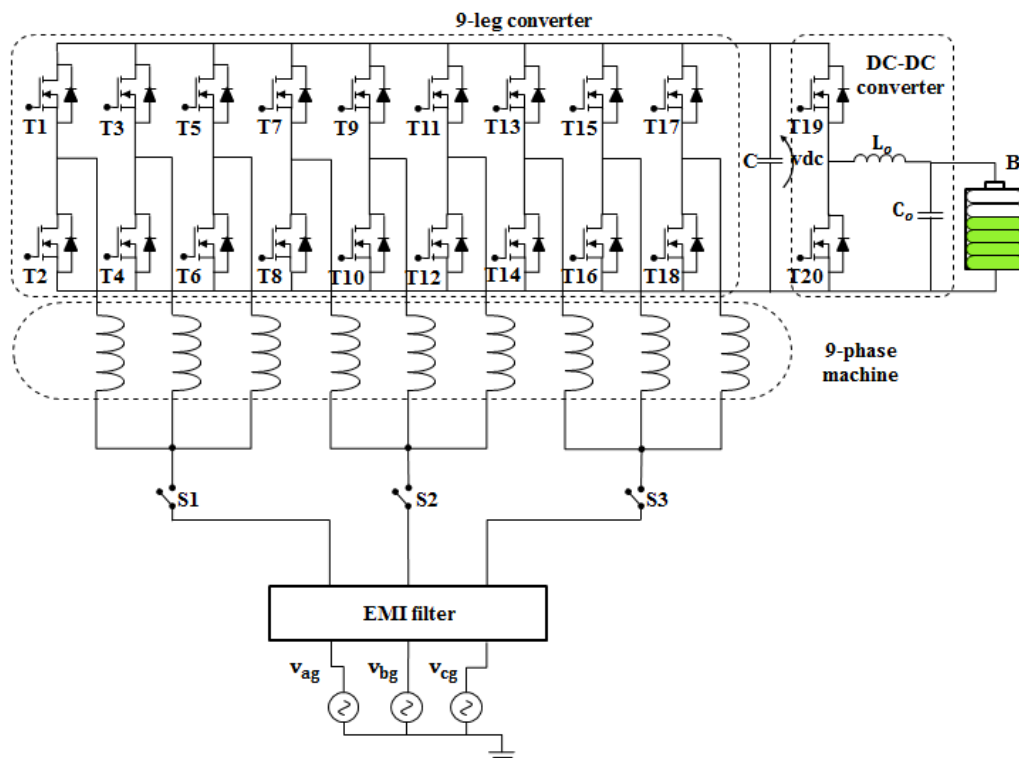
Figure 1.2 Nine-phase OBC with DC-DC converter [18]

Chinmaya K. A. et al. proposed a bidirectional DC/DC converter for coupling a six-phase IM with a Power Electronic Interface (PEI). [19]. This DC/DC converter functions as a Power Factor Correction (PFC) when operating in plug-in charging mode, and it also acts as a single switch inverting buck/boost converter under driving and regenerative braking modes. The use of a six-phase induction machine improves the PEI's efficiency. In addition, this study provides a FOC strategy with a PI controller during a driving mode.

In a recent study proposed by Herrera D. et al [20], a reluctance motor with a six-phase permanent motor was implemented for EVs. The suggested stator design has two separate rows of three-phase windings that are precisely aligned at a zero-degree angle to their counterparts. The

motor has the capability to be used for both traction and charging purposes, with the ability to operate via a centralized control system. During a charging process, the stator windings are rearranged or separated in such a way that there are two sets of three separate phases to avoid the motor rotating. The first set is linked to the inverter, while the second set is connected to the grid independently, devoid of requiring synchronization, as shown in Figure 1.3.
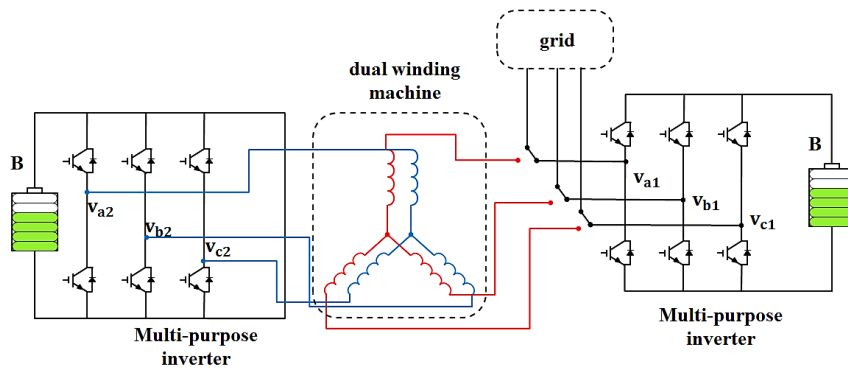
Figure 1.3 The proposed configuration of six-phase permanent magnet motor during OBC [20]

The integrated battery charger is based on open end winding in conjunction with an asymmetric hybrid multilevel inverter mechanism proposed by Foti S. et al [21]. The proposed battery charger may draw power directly from a standard AC single-phase grid for standard charging, or it can use a DC power supply, enabling rapid charging, as shown in Figure 1.4.
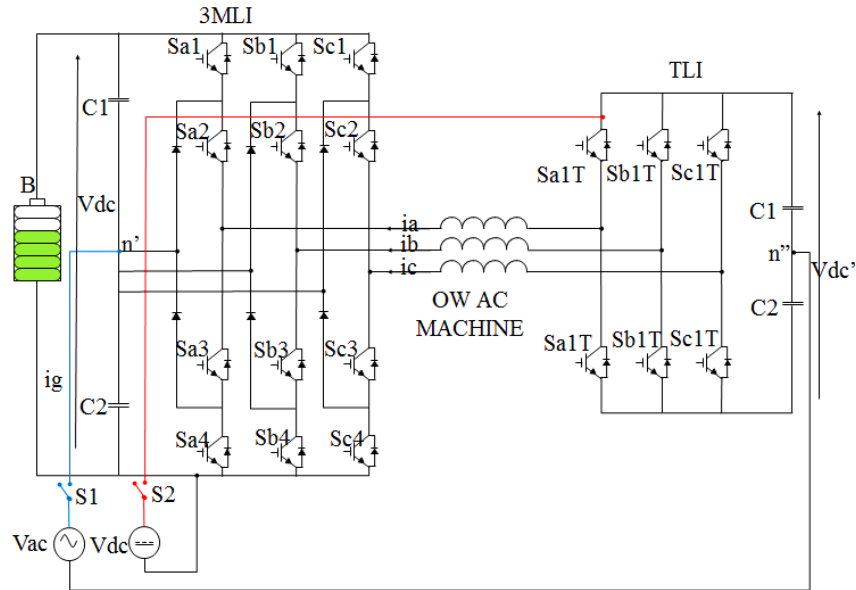
Figure 1.4 Three-level inverter with open end winding machine with ability to charging form AC or DC source [21]

A nine-phase motor for electric cars was proposed by the authors in the driving and charging cases with a three-phase and single-phase grid supply proposed by Singh U. et al in [22] and [23], respectively. The proposed mechanisms do not require any additional components for charging or even vehicle-to-grid mode. In addition, a robust current controller was applied to eliminate the harmonic caused by the dead time of the inverter during battery charging mode.

The three-phase IM with segmented stator coils with suitable configuration was proposed by Sharma S. et al [5]. The proposed configuration is applied to prevent the motor from rotating during the charging time. This configuration is considered more complex than the multi-phase one.

Based on the advantages of the five-phase motor the ability to eliminate torque during the combined charging process uses three-phase source. The proposed study by Tong M. et al [24], imposes the presence

of two stages in order to obtain the appropriate voltages at the output. Additionally, a technique for regulating the current balance in charge mode, devoid of a Phase-Locked Loop (PLL) circuit is used in order to minimize the number of voltage sensors and reducing the weight and cost of the vehicles.

The proposed configuration for an EV with a multi-phase machine proposed by Raherimihaja H. et al [25] involves the use of a symmetrical six-phase open-end coil machine and a twelve-leg with bidirectional DC-DC converter. The battery charging circuit is created by simply joining the three-phase AC grid to the midpoint of the machine's phase coil. This setup causes the grid currents to divide equally and pass in opposing directions, eliminating the need for an additional hardware change. In addition, this setup has the capability to cancel the rotation of the motor and obtain a high input filter (inductance).

Figure 1.5 illustrates the use of a six-phase machine as a transformer proposed by Pescetto P. et al [26].This machine provides galvanic separation for all three-phase and single-phase input operations. Significantly, it has the unique ability to provide torque-free operation when configured in a charging setup.
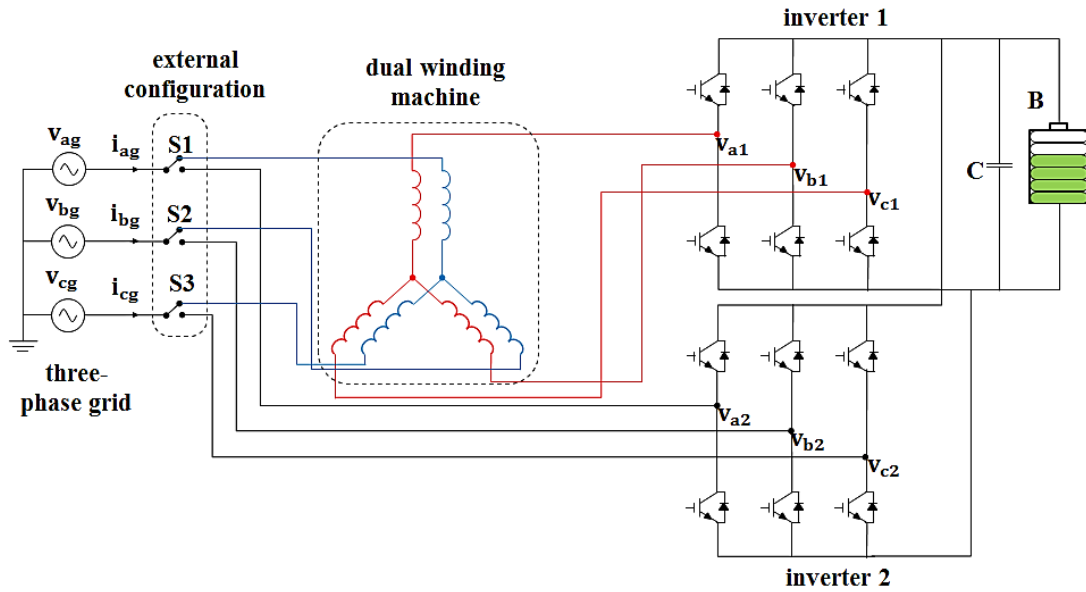
Figure 1.5 OBC mode for six-phase dual winding machine [26]

According to the characteristics of MP motors proposed by Abdel-majeed M. et al [27], a six-phase IM was proposed in order to provide a suitable design for the motor windings during the battery charging process in an EV, which eliminates the phenomenon of motor rotation, as shown in Figure 1.6. In addition, a current controller mechanism is suggested to maintain grid currents balanced during normal or one-phase fault scenarios.
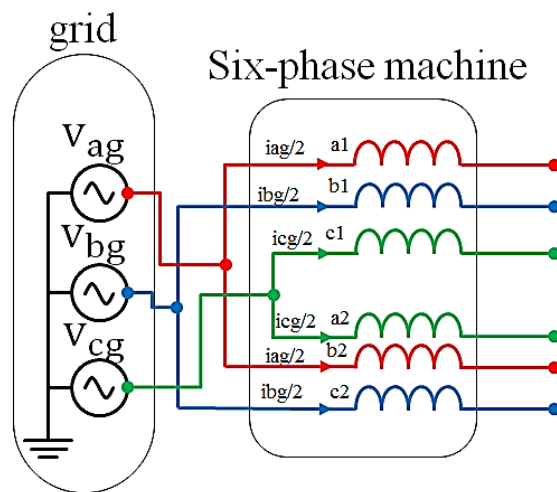
Figure 1.6 The configuration of six-phase IM during the battery charging period [27]

A recent study proposed by Abdel-wahed A. et al [28], focuses on the analysis and enhancement of a six-phase inside permanent magnet motor that has an integrated onboard battery charger. The investigation covers both sides of the motor's driving capabilities and its ability to charge the battery. The suggested approach uses a genetic algorithm method in conjunction with finite-element analysis to optimize the system's design. The objective is to maximize torque while minimizing the ripple of torque and core losses.

In another recent study proposed by Jiang D. et al [29], the authors examine the utilization of electric cars. In the Series-End Winding Motor Drive (SWMD) charging scenario, a single-phase source is used to charge the battery by connecting it to one of the motor coils. This configuration guarantees that no torque is produced throughout the charging process. Additionally, it allows for advantages to be gained from the increased flexibility in the zero axis and the utilization of grid current when charging. By controlling the d-axis and the 0-axis voltages during the charging phase, the motor's voltage may be reduced, leading to fewer losses.

Depending on the possibility of using Wireless Power Transfer (WPT) to charge electric cars, plug-in charging is used with WPT and the Auxiliary Power Module (APM) proposed by Liang Z. et al [30]. With respect to other studies, each component, including plug-in charging, WPT, and APM, is developed, produced, and fitted separately. However, this research explored the potential of combining integrated charging with WPT and APM. This feature is achieved by the utilization

of a variable dual magnetic coupler, which subsequently minimizes the dimensions, expenses, and intricacy of the charging system.

1.3 Thesis Objectives

The primary goal of this study is to create an integrated charging system for electric cars to achieve mobile charging, in addition to eliminating the phenomenon of motor rotation during the charging process. The primary goal can be accomplished by following these steps:

1. Critically evaluate the existing OBC configuration and MP driving methods and identifying the limitations of them.
2. Modeling the seven-phase induction motor and analyzing its operation as a vehicle propulsion system.
3. Design and analysis of the FOC speed controller and testing it with different controllers to obtain a propulsion system that meets the requirements without being affected by external disturbances.
4. Designing and discussing the OBC available configuration for a seven-phase motor when the source is seven- or three-phase.
5. Ensuring that the motor does not need a mechanical break during the charging mode.
6. Modeling and discussing the Voltage Oriented Control method with a seven-phase system to obtain a unity power factor and a smooth DC-output voltage.
7. Applying appropriate controllers to eliminate the harmonics that appear due to the unbalance of the drawn current from the grid if the source is three-phase.

1.4 Thesis Outline

This thesis is divided into five chapters.

Chapter Two analyzes and discusses the drive system of a 7-PIM using FOC technology with appropriate controllers to ensure that it is not affected by disturbances.

Chapter Three discusses several topographies to achieve integrated charging for an electric car driven by a 7-PIM with the application of VOC technology to achieve appropriate charging with several controllers in order to reduce the harmonics that affect the grid current.

Chapter 4 explains and discusses simulation results for driving and charging systems.

Chapter Five provides a conclusion to the studies and offers ideas for potential future work that might expand upon this study.

CHAPTER 2 : Propulsion Mode with Seven Phase Induction Machine

2.1 Introduction

One of the most important reasons for the widespread adaptation of three-phase motors is the compatibility between the power sources and the number of phases required by these motors. This eliminates the necessity of power-form transformation in order to run these engines. Through decades, the discovery of semiconductor devices led to the emergence of ways to convert power from one form to another, and one of these methods was the appearance of an inverter that could convert DC power into AC power at any number of phases. This discovery was the main reason for the development of another type of motor with more than three phases, known as multi-phase motors. When an AC machine is powered by an inverter, the need for a predefined number of phases on the stator, such as three, is eliminated, and variable phase numbers can be used instead. This led to the first interest in multi-phase motors nearly five decades ago, particularly in 1969, when the most likely initial proposal for a multiphase variable speed electric drive was a five-phase induction motor drive [31]. Over time, many of the benefits of multi-phase motors have become apparent.

By considering the next characteristics of multiphase drives, it is acceptable to achieve the Preferred implementation in electric vehicles.

2.1.1 Reliability

One of the most important reasons for the spread of multi-phase motors is their great reliability. Multi-phase motors have more fault tolerance compared to three-phase motors, which in turn gives them the ability to remain in work even if an error occurs in one phase, leading to the utilization of this technology to increase the chances of using multi-phase motors in traction industries [32],[33]. A seven-phase machine, as in the case of this study, can still work if one or two phases of the power sources are damaged [34].

2.1.2 Safe Operation

In electric cars, the drive system requires a high current to pass through each phase due to the use of a high voltage source. More than one transistor was connected in parallel to overcome the large current passing through each phase and create a synthetic transistor with an enhanced rating. But on the other hand, this solution leads to the appearance of many problems, like variations in the on/off time caused by variations in the gate driver units' properties and the paralleled transistors' fabrication procedures. Moreover, it is important to consider managing the heat dissipation of each transistor to ensure none exceeds the allowed thermal range. Another significant issue is that each transistor has its own lifetime. Consequently, many of the drawbacks of parallel transistors are solved by employing multiphase machines to distribute power among a large number of phases and inverter legs. However, rather than having multiple parallel elements supply for each phase of the power, an inverter leg with just one element does so. For the same DC-bus voltage and power, traditional three-phase drives have a higher current per phase rating for inverters and machine windings [7], [35].

2.1.3 Reduction in torque ripple

A typical three-phase machine is typically constructed with distributed stator windings, resulting in the generation of a sinusoidal back-EMF (sinusoidal field distribution). Consequently, the application of sinusoidal currents leads to the production of a regular torque. With respect to multi-phase machines, the most significant axial have been identified as the ones responsible for generating torque, while the other axes are regarded as sources of energy losses. Indeed, the use of the decoupling (Park's) transformation results in a collection of n equations that are contingent upon the number of phases. These equations are allocated to pairs, with each pair being designated a sub-plane. The first pair, known as the d−q pair, is the same as the comparable pair of equations used for a three-phase system. As a result, d−q pair present the characteristics of multiphase machines. A constant torque may be achieved under ideal conditions when only one harmonic of currents and back-EMFs are presented in each reference frame, excluding the zero-sequence frames. If a multiphase machine is designed well, the torque that non-sinusoidal back-EMFs produce may stay the same even during dynamic performance as long as the d-q currents stay the same in any reference plane [36]. This feature is not present in a three-phase machine. To summarize, a multiphase machine allows for the achievement of a consistent torque by maintaining constant d-q currents in many reference planes. On the other hand, a three-phase machine necessitates the traditional limitation on sinusoidal back-EMFs and currents. Consequently, a multiphase machine imposes fewer design limitations than a three-phase machine.

Compared to a standard three-phase machine, an electric machine with multi-phases produces fewer torque ripples, as mentioned in

references [37], [38]. In fact, only odd harmonics have back-EMF effects on an n-phase drive; for odd n, the minimum harmonic order for torque ripples is 2n. In this regard, in 3-phase drives, the lowest harmonic order of torque ripples is 6; in 5-phase drives, it is 10; and in 7-phase drives, it is 14, and so on. For example, the minimum level of fluctuation in torque in a 6-phase symmetrical machine is in the sixth harmonic order, which is the same as that of a 3-phase machine. For even values of n, the minimum harmonic order of the 6-phase asymmetrical machine exhibits torque ripples at the lowest harmonic order of 12, comparable to a 12-phase symmetrical machine. Consequently, a rise in the quantity of phases leads to an advancement in the frequency of torque fluctuations. This characteristic is intriguing since it eliminates the mechanical resonance of an electric motor at high frequencies. Consequently, a multiphase drive's torque exhibits more smoothness than that of a three-phase drive.

2.1.4 Less Restriction for Stator Winding Arrangements

By implementing Flux-Weakening (FW), the configuration mode of the machine stator windings enables the manipulation of the torque-speed relationship, thereby granting greater flexibility in the face of imposed restrictions. The speed range may be expanded by using combinations of flux-weakening methods [39], [40], and various couplings of stator windings. Multi-phase drives provide a more comprehensive range of choices for stator winding arrangements, specifically designed for applications with high-speed range. In an n-phase machine, (n+1)/2 options are available for connecting the stator's windings. With a 3-phase machine, there are two connection options: delta and star [41].

2.2 Modeling of a multiphase induction machine

MPIMprinciple of operation is similar to that of a three-phase induction ones, applying Faraday's Law of Electromagnetic Induction. The induction motor, created by Nikola Tesla in 1886, is often regarded as the most prevalent motor in the industrial world [42]. The wide acceptance of this particular type of motor may be attributed to its several benefits, including:

- Efficiency and longevity in the installation process,
- significantly lower cost in comparison to other motors,
- the level of maintenance required is low,
- the potential to create it with a wide range of capabilities and
- unlike other motors, it does not require the use of field current.

The drawbacks of this type of motors include:
- challenges in regulating speed,
- a high beginning current relative to the total load current and
- a poor power factor at low load levels.

The induction motor has two primary components: the stator and the rotor. One of the basic concepts of induction machines is the generation of a magnetic field that rotates and distributes in a sinusoidal pattern in the air gap. The construction of a 7-PIMused in this thesis includes employing a total of fourteen phase straps, each spanning 25.714 degrees around the stator. This results in a physical shifting of 51.428 degrees among phases. The squirrel cage of the rotor is considered to be a similar seven-phase with identical features as the three-phase one. Multi-phase induction machines operate at slip speed when functioning as motors, and when functioning as generators, they operate at a speed greater than synchronous speed. If the rotor is originally at rest, the relationship

between the magnetic field in the air gap and the rotor's Magnetic Motive Force (MMF) generates no electromagnetic torque. If the rotor reaches the synchronous speed, there is no induction in the rotor, and no electromagnetic torque is generated. At any other speed, the difference between the synchronous speed and the rotor speed, known as slip speed, induces rotor current, and electromagnetic torque is then created [42].

2.2.1 Mathematical model of the multi-phase induction machine

An efficient analysis of an IM's functioning necessitates the use of a dynamic mathematical model. The mathematical model of the MPIM, which is similar to the modeling of standard TPIM, must contain the correlation of the electromagnetic torque and all the electrical and mechanical parameters of the machine. An essential initial process in comprehending the induction machine and developing a control scheme is the modeling and analysis of its dynamic system [35].

The induction machine's control relies on a model that is organized as sets of equations; this model will be discussed in more detail in the following section [43], [44].

2.2.2 Phase variable model of 7-PIM

This theory offers a very practical instrument for fully treating multi-phase systems. Given the practicality of this theory in three-phase systems, it has been applied to explain the dynamic characteristics of the multi-phase induction machine. The phase variable model is capable of processing variables that represent the instantaneous values of multi-phase quantities. As a result, it can be applied to describing steady-state manners but is also applicable to transient states and non-sinusoidal modeling. When developing a mathematical model of MPIMs, many

factors must be considered in the design to simplify the modelling, including:

- The stator consists of n-phase windings with a varying angular shift.
- The shape of the distributed field along the outer margin of the air gap has a sinusoidal pattern.
- Each phase winding features a sinusoidal distribution and is positioned at an electrical angle displacement of $2\pi/n$ with respect to the other.
- A perfect iron is defined as a metal that does not experience any losses or magnetic saturation events.
- The air gap diameter is assumed to be regular, disregarding the existence of stator slots and rotor bars.
- The rotor bars are evenly spaced over the surface of the squirrel rotor cage.
- Hysteresis, eddy currents, anisotropy effects, core loss, and skin effects have not been taken into consideration.
- Complete separation of the leakage fluxes throughout the stator and rotor.

2.2.3 Coordinate Transformation

To reduce the complexity of the MP machine model, it is essential to implement a coordinate transformation that will eliminate the complication. For this reason, the following method for transformation is thus employed for the modeling of the seven-phase machine:

2.2.3.1 Clark Transformation

In the case of multi-phase induction machines, an original n-phase machine with sinusoidal-field distribution is mathematically divided into

(n+1)/2 pairs of axes if n is odd, or (n+2)/2 pairs of axis if n is even. In the case of 7-PIM, it contains three planes ranging as (α-β), (x_1, y_1) and (x_2, y_2). Furthermore, when n is an odd number, there is only one zero-sequence machine that corresponds to a single one-dimensional reference frame.

When applying mathematical expressions to a MPIM, it is thought to change the equations that describe how the motor works from a multi-phase coordinate axes system to a dual coordinate axes system to make analysis easier. This conversion process requires careful attention to the following considerations [32], [35]:

- The total number of elements before and after the transformation must be constant.
- The multiphase coordinate axes system represents the actual system.
- The dual orthogonal coordinate axes system is a hypothetical system that was suggested to simplify the equations derived in a multi-phase axis system.
- The initial pair, denoted as α−β, is equivalent to the comparable set of equations for a three-phase machine.
- The last equation, or the last two equations for phase numbers that are even, represents the zero-sequence equation, which is identical to that of a conventional three-phase machine.
- The x−y equations follow the same structure as the zero-sequence component, indicating that the impedance for the x−y stator current components is essentially the leakage impedance of the stator winding.
- If the input provided to the motor is a pure sinusoidal waveform and the magnetic field is also sinusoidal, then there will be no

21

current flowing through the motor windings, and any of the x-y voltage components will be equal to zero.

- It is possible to transform from the dual orthogonal coordinate axes system to the multi-phase system and vice versa, so the transformation may be reversed.

In (2.1), you can find the Clark transformation matrix that is used to convert the seven-phase stator variables into a two-phase α-β stationary reference frame [7], [35].

$$
C = \begin{matrix} \alpha \\ \beta \\ x_1 \\ y_1 \\ x_2 \\ y_2 \\ 0 \end{matrix}
\begin{bmatrix}
1 & cosa & cos2a & cos3a & cos3a & cos2a & cosa \\
0 & sina & sin2a & sin3a & -sin3a & -sin2a & -sina \\
1 & cos2a & cos4a & cos6a & cos6a & cos4a & cos2a \\
0 & sin2a & sin4a & sin6a & -sin6a & -sin4a & -sin2a \\
1 & cos3a & cos6a & cos9a & cos9a & cos6a & cos3a \\
1 & sin3a & sin6a & sin9a & -sin9a & -sin6a & -sin3a \\
1 & \frac{1}{\sqrt{2}} & \frac{1}{\sqrt{2}} & \frac{1}{\sqrt{2}} & \frac{1}{\sqrt{2}} & \frac{1}{\sqrt{2}} & \frac{1}{\sqrt{2}}
\end{bmatrix}
\begin{matrix} a \\ b \\ c \\ d \\ e \\ f \\ g \end{matrix}
\quad (2.1)
$$

Where $a = 2\pi/7$.

2.2.3.2 Park Transformation

In a multi-phase system, rotational transformation is restricted to applying to the two sets of equations in α, β since the stator-to-rotor interaction occurs only in these equations. The configuration of the machine is identical to that of a three-phase machine [7].

$$
D=\begin{array}{c}\alpha\\\beta\\x_1\\y_1\\x_2\\y_2\\0\end{array}\begin{bmatrix}cos\rho & sin\rho & 0 & ... & 0\\-sin & cos\rho & 0 & ... & 0\\0 & ... & 0 & \vdots & 0\\\vdots & ... & ... & \vdots & \vdots\\0 & ... & ... & ... & 0\end{bmatrix} \tag{2.2}
$$

$$
D=\begin{array}{c}\alpha\\\beta\\x_1\\y_1\\x_2\\y_2\\0\end{array}\begin{bmatrix}cos\rho & -sin\rho & 0 & ... & 0\\sin & cos\rho & 0 & ... & 0\\0 & ... & 0 & \vdots & 0\\\vdots & ... & ... & \vdots & \vdots\\0 & ... & ... & ... & 0\end{bmatrix} \tag{2.3}
$$

The term ρ specifies the actual angular position of the d-axis in the rotating frame referring to the magnetic axis of phase "1" with respect to the transformed value.

$$\rho = \int \omega_e dt \tag{2.4}$$

where ω_e represents the synchronous speed.

2.2.4 Modeling of the machine in rotating reference frame

The modeling of a multi-phase induction motor is similar to the modeling of a three-phase one, excluding the existence of x-y component equations, which represent flux and torque-independent components as shown in Figure 2.1. In order to represent a mathematical model of a seven-phase motor, the phases voltages supplied to it are balanced and expressed by the following equations:
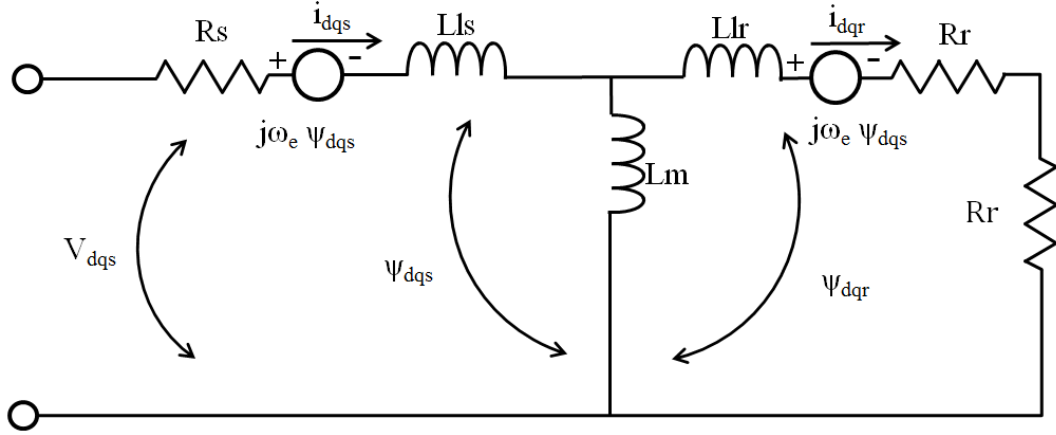
Figure 2.1 Modeling of 7-PIM in dq reference frame

$$V_{ns} = V_m \sin(2\pi f t), l = 0,1, \dots ,6 \quad n = a, b, \dots , g \quad (2.5)$$

$V_{as}, \dots, V_{gs}$ are stator phase voltages.

The phase voltage variables can be converted into three sets of perpendicular axes (d-q, x_1-y_1, and x_2-y_2). Use the transformation matrix shown in equations (2.2) for the stator and rotor, respectively [7], [35].

The following are the formulas for the stator voltage representation in the rotating referencing frame (ds and qs) :

$$V_{qs} = R_s i_{qs} + \omega_e \psi_{ds} + \frac{d\psi_{ds}}{dt} \qquad (2.6)$$

$$V_{ds} = R_s i_{ds} - \omega_e \psi_{qs} + \frac{d\psi_{qs}}{dt} \qquad (2.7)$$

$$V_{x1s} = R_s i_{x1s} + \frac{d\psi_{x1s}}{dt} \qquad (2.8)$$

$$V_{y1s} = R_s i_{y1s} + \frac{d\psi_{y1s}}{dt} \qquad (2.9)$$

$$V_{x2s} = R_s i_{x2s} + \frac{d\psi_{x2s}}{dt} \qquad (2.10)$$

$$V_{y2s} = R_s i_{y2s} + \frac{d\psi_{y2s}}{dt} \qquad (2.11)$$

$$V_{0s} = R_s i_{0s} + \frac{d\psi_{0s}}{dt} \qquad (2.12)$$

Where, V_{ds} and V_{qs} present as direct and quadrature axis stator voltages, respectively, Where, $V_{x1,2\_s}$, $V_{y1,2\_s}$ and V_{0s} represent x , y and zero axis stator voltages, respectively, and Ψ present as flux linkages.

The following are the rotor side power formulas in the rotating reference frames:

$$V_{qr} = 0 = R_r i_{qr} + (\omega_e - \omega_r)\psi_{qr} + \frac{d\psi_{dr}}{dt} \qquad (2.13)$$

$$V_{dr} = 0 = R_r i_{dr} - (\omega_e - \omega_r)\psi_{dr} + \frac{d\psi_{dr}}{dt} \qquad (2.14)$$

$$V_{x1r} = R_r i_{x1r} + \frac{d\psi_{x1r}}{dt} \qquad (2.15)$$

$$V_{y1r} = R_r i_{y1r} + \frac{d\psi_{y1r}}{dt} \qquad (2.16)$$

$$V_{x2r} = R_r i_{x2r} + \frac{d\psi_{x2r}}{dt} \qquad (2.17)$$

$$V_{y2r} = R_r i_{y2r} + \frac{d\psi_{y2r}}{dt} \qquad (2.18)$$

$$V_{0r} = R_r i_{0r} + \frac{d\psi_{0r}}{dt} \qquad (2.19)$$

The existence of V_{x1}, V_{y1}, V_{x2}, and V_{y2} components makes the 7-PIM model different from the three-phase motor concept. The x-y elements of a squirrel cage rotor are zero.

$$\psi_{ds} = \int(V_{ds} - R_s i_{ds} - \omega_e \psi_{qs}) \qquad (2.20)$$

$$\psi_{qs} = \int(V_{qs} - R_s i_{qs} - \omega_e \psi_{ds}) \qquad (2.21)$$

$$\psi_{dr} = \int(V_{dr} - R_r i_{dr} - (\omega_e - \omega_r)\psi_{qr}) \qquad (2.22)$$

$$\psi_{qr} = \int(V_{qr} - R_r i_{qr} + (\omega_e - \omega_r)\psi_{dr}) \qquad (2.23)$$

$$i_{ds} = \frac{\psi_{ds}(L_{lr}+L_m)-L_m\psi_{dr}}{(L_{lr}L_m+L_{ls}L_m+L_{lr}L_{ls})} \qquad (2.24)$$

$$i_{qs} = \frac{\psi_{qs}(L_{lr}+L_m)-L_m\psi_{qr}}{(L_{lr}L_m+L_{ls}L_m+L_{lr}L_{ls})} \qquad (2.25)$$

$$i_{dr} = \frac{\psi_{dr}(L_{ls}+L_m)-L_m\psi_{ds}}{(L_{lr}L_m+L_{ls}L_m+L_{lr}L_{ls})} \qquad (2.26)$$

$$i_{qr} = \frac{\psi_{qr}(L_{ls}+L_m)-L_m\psi_{qs}}{(L_{lr}L_m+L_{ls}L_m+L_{lr}L_{ls})} \qquad (2.27)$$

However, the electromechanical torque is created from the aforementioned equations, and rotor speed can also be calculated from them. The equation governing the relationship between angular speed ω_r and torque is as follows:

$$T_e = T_L + J\frac{d\omega_r}{dt} \qquad (2.28)$$

$$T_e = \frac{3p}{4}(\psi_{ds}i_{qs} - \psi_{qs}i_{ds}) = \frac{3p}{4}(\psi_{dr}i_{qr} - \psi_{qr}i_{dr}) \qquad (2.29)$$

$$\frac{d\omega_r}{dt} = (p(T_e - T_L) - f\omega_r)/J \qquad (2.30)$$

$$\omega_r = \int \frac{T_e-T_L}{J} dt \qquad (2.31)$$

Where, R_s, R_r is stator and rotor resistance respectively.

Lls, Llr stator and rotor leakage inductance respectively.

P is the total number of poles.

J is the value of the moment of inertia.

f is the friction coefficient.

T_L is the load torque.

T_e is the mechanical torque.

ω_r is the angular velocity of the rotor part.

$L_m = (n/2)$ M, where M is the maximum amount of the stator- to rotor mutual inductances.

It is worth noting:

- When $\omega_e = 0$ is used, the above equations can be transformed into a stationary reference frame.
- If the rotor is still fixed, it implies that the ω_r, is equal to zero. The rotor equation will closely resemble the stator equations when expressed in the rotating reference frame.

2.3 Seven-Phase Voltage Source Inverter

The power sources available for multi-phase motors are considered the biggest obstacle that has prevented their widespread use. As a result of the advantages that characterize induction motors, researchers have worked overtime to obtain power sources that adapt to the nature of these motors. There are several methods to acquire a multi-phase supply voltage. The initial approach would include using a transformer that converts three-phase power to n-phase power. Presently, transformer topologies such as three-phase to five-phase transformers [45], and three-phase to seven-phase transformers are well-documented [46]. The multi-phase induction motor can be linked immediately to a conventional, unchanging frequency and voltage multi-phase power supply. The load torque will only dictate the motor speed and slip in these circumstances. Under no-load conditions, the rate of speed is almost equivalent to the synchronous speed. Consequently, the slip is minimal.

Among other possibilities that rely on a power electronic system is a two-step conversion with an n-phase inverter as the resultant step to provide the required power. By using a variable frequency inverter in the induction motor controlling system, it is possible to modify the voltage inputs' amplitude and frequency according to a specific control technique.

The two-level, seven-phase voltage source inverter contains fourteen switches with effective capacity, as shown in Figure 2.2. The switches are organized into two parts: the upper part and the lower part. The upper part is represented by the upper keys (S1, S3, S5, S7, S9, s11, s13), while the lower switches (S8, S10, s12, s14, S2, S4, S6). The seven-phase inverter is equipped with a DC voltage directly via the battery. The points (a, b, c, d, e, f, and g) correspond to the output of a seven-phase

voltage inverter. The voltage value and frequency may be regulated by manipulating the width of the pulses [44]. The parallel mode of operation is called the six-step operation mode (connection mode). 180° in three-phase inverters is called the fourteen-step operating mode. Each switch is connected for a period of 180°, and the phase difference between each of the two phases is 51.42°. At any moment in time during the operation of the inverter, there will be seven switches in ON state and seven switches in OFF state. The switches that are entered in case the connection is distributed between the upper and lower parts, as for three switches from the upper part on state and four switches from the bottom, or vice versa.
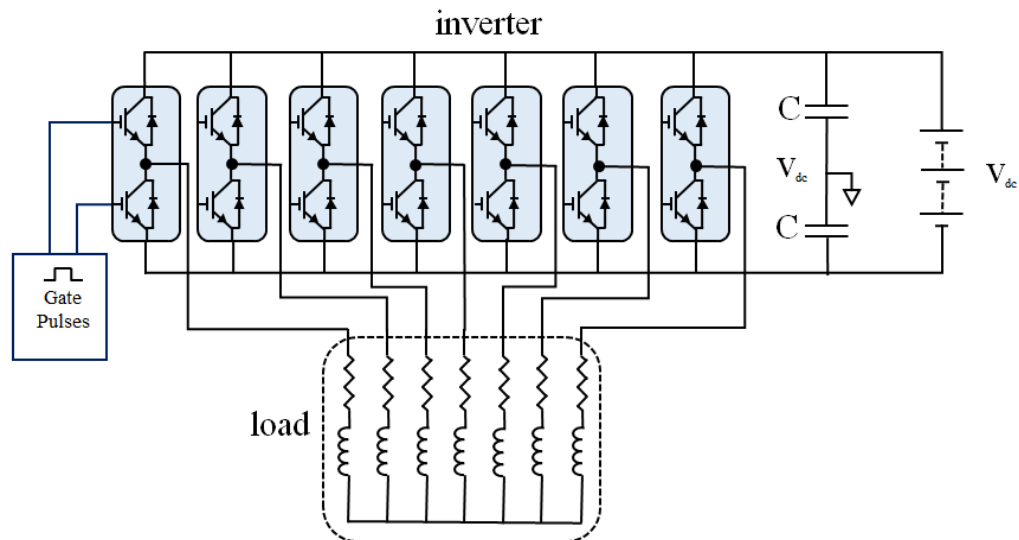
Figure 2.2 Seven-phase voltage source inverter

The seven-phase voltages can be obtained for all possible firing states through the following equation [47].

$$\begin{bmatrix} V_{an}(t) \\ V_{bn}(t) \\ V_{cn}(t) \\ V_{dn}(t) \\ V_{en}(t) \\ V_{fn}(t) \\ V_{gn}(t) \end{bmatrix} = \begin{matrix} \alpha \\ \beta \\ x_1 \\ y_1 \\ x_2 \\ y_2 \\ 0 \end{matrix} \begin{bmatrix} 6 & -1 & -1 & -1 & -1 & -1 & -1 \\ -1 & 6 & -1 & -1 & -1 & -1 & -1 \\ -1 & -1 & 6 & -1 & -1 & -1 & -1 \\ -1 & -1 & -1 & 6 & -1 & -1 & -1 \\ -1 & -1 & -1 & -1 & 6 & -1 & -1 \\ -1 & -1 & -1 & -1 & -1 & -1 & -1 \\ -1 & -1 & -1 & -1 & -1 & -1 & 6 \end{bmatrix} \begin{bmatrix} Sa \\ Sb \\ Sc \\ Sd \\ Se \\ Sf \\ Sg \end{bmatrix} \quad (2.32)$$

When s_a-s_g is state of the upper switches.

2.4 Field Oriented Control

Demand for induction motors has increased due to their proliferation, in addition to the aforementioned benefits. Previously, not enough linear controllers were available to regulate these motors in general, so they continued to function at a constant speed. As a result, the use of these motors in a variety of work locations was restricted. Nowadays, the ability to accomplish smooth control of induction motor speed is attributed to research in the power electronics and inverters areas. In the early 1970s, the researcher introduced the Field-Oriented Control (FOC) algorithm, which had been developed for the first time to control induction motors. The FOC method assumes that induction motors are represented as DC motors in relation to the control process. If the flux in the rotor is constant, the value of the electromagnetic torque is similar to the behavior of the DC motor. Also, the magnetic flux in the rotating part of induction motors is identical to the magnetic flux in a DC motor, except for the flux in the rotating part of induction motors, that depends on the magnetic flux of the stator [42]. For this reason, induction motors have now developed controlling aspects which are comparable to those of DC motors.

2.4.1 Principle of FOC

Due to the heightened difficulty when controlling the AC motor drive. To solve this issue and provide comparable control of AC motors to that of DC motors, FOC technology was applied. When the electromagnetic flux is spread out in a sinusoidal way on the IM, the rotor flux Ψr matches on the d-axis of the rotating reference frame, which is spinning at the synchronous speed ω_e. In the rotating frame, the concept of "i_{ds}" refers to the stator current in the d-axis, and it has an impact on the magnitude of Ψ_r. The, the electromagnetic torque is influenced by the stator current in the q-axis, which is orthogonal in the d-axis in rotating reference frame with respect to stator current transformation. The angle ρ represents the rotor flux angle, and it is used to establish the location in relation to the other two-axis stationary frames (α, β). It is necessary to transform from a stationary to a rotating reference frame. The control process begins with determining the orientation (the angle ρ) and choosing the appropriate inverter control to decouple i_{ds} and i_{qs}. The precise determination of flux values is achieved through either measurement or computation.

As previously mentioned, flux and torque are two components that the field-oriented control can control induction motors, and both are use the stator's current. Due to the rotor flux being aligned with the d-axis, the flux linkage component on the rotating frame's q-axis is equal to zero, as shown in Figure 2.3.
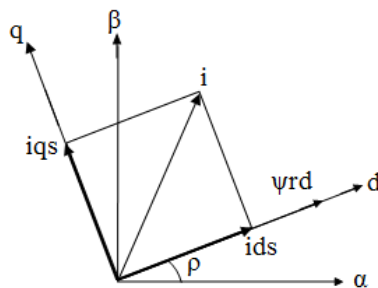
Figure 2.3 The coordinate representation of seven-phase motor

In order to apply the rotor FOC algorithm, the following equations must be achieved [48], [49], [50].

$$\psi_r = \psi_{dr} \tag{2.33}$$

$$\psi_{qr} = 0 \tag{2.34}$$

$$\psi_{qr} = i_{qs}L_m + L_{lr}i_{qr} = 0 \tag{2.35}$$

Therefore, the equations of the mathematical model of the induction motor (2.26) translate into the following equations :

$$i_{qr} = \frac{-L_m i_{qs}}{L_{lr}} \tag{2.36}$$

$$T_e = \frac{3p}{4}\psi_{dr}i_{qr} \tag{2.37}$$

When the system is in a steady state, the voltage on the rotor's q-axis can be expressed as follows using the zero q-axis rotor flux linkage concept:

$$\underbrace{V_{qr}}_{0} = R_r i_{qr} + (\omega_e - \omega_r)\psi_{dr} + \underbrace{\frac{d\psi_{dr}}{dt}}_{0} \tag{2.38}$$

$$\omega_{sl} = (\omega_e - \omega_r) = \frac{R_r i_{qr}}{\psi_{dr}} \tag{2.39}$$

$$\psi dr = Lm\ ids \tag{2.40}$$

As a result, when the stator current's q-axis component is the only source of torque control, the rotor flux linkage is unaffected in any way. On the other hand ,the rotor flux is controlled by only the d-axis component of the stator current. For this system to be linear, the value of ψ_{dr} must stay constant. Then, the electromagnetic torque will only depend on the component of the current i_{sq}. This means that the

mathematical model for the induction motor is now similar to the mathematical model for the DC motor.

The position ρ can calculated by applying the when $idr = 0$, so $\psi dr = Lm\ ids$, and if we substitute that into (2.39):

$$\omega_{sl} = (\omega_e - \omega_r) = \frac{R_r i_{qr}}{L_m i_{ds}} \qquad (2.41)$$

$$\rho = \int(\omega_{sl} + \omega_r)dt \qquad (2.42)$$

And by substituting that into equation (2.38) we get:

$$\psi_{dr} = \frac{R_r L_m}{R_r + L_{lr}} i_{ds} \qquad (2.43)$$

Driving systems based on the FOC algorithm can be designed and built according to the following options:

•Controlling both the torque and rotor flux of the motor directly.

• Controlling both the torque and rotor flux of the motor indirectly by regulating the two components of the current (i_{sd}, i_{sq}).

It is commonly known for practical application in electric cars that each of the previous cases requires measured or estimated information about the variable that is controlled. The motor speed is measured from the speed sensors, and the rotating frame of currents (i_{sd}, i_{sq}) are calculated by applying Clark and Park transformations, respectively, to the seven-phase stator currents that were measured. As a result, the electromagnetic torque (q-axes component) and the rotor flux component (d-axes component),are estimated from i_{sq}, and i_{sd}, respectively, as previously analyzed.

2.5 Outer loop controller

2.5.1 Design of the speed control based on the PI Controller

As previously mentioned, the flux and speed of all asynchronous machines can be controlled with the FOC technique by regulating the rotor speed and flux of the motor directly [51]. Several control methods can be applied for controlling this component. PI controller are commonly employed in induction motor systems due to their simplicity and ease of implementation. However, they exhibit less efficient dynamic performance compared to nonlinear control methodologies, especially when there is a change in system parameters [52], [53]. The system consists of two control loops: the outer loop regulates both speed and flux, while the inner ones regulates currents. The control system includes a pair of PI controllers, which serve as the outer loop responsible for controlling the motor's speed and rotor flux, as shown in Figure 2.4. By using the technique of measuring rotor speed and estimating rotor flux in a rotating reference frame, the controlling parameters are represented as DC quantities, making their management and filtering less challenging. The outer voltage loop utilizes a PI controller to generate a new current reference, as shown in Figure 2.4. The output of the outer loop consists of the i_d reference current derived from flux control, as well as the i_q component generated by the motor speed control.

The signal resulting from the process of controlling the reference value with the measured values of both speed and flux in the outer loop represents a reference current signal. The inner loop refers to controlling the reference signal to generate the switching pulses that are finally routed to the inverter for driving the motor [54].
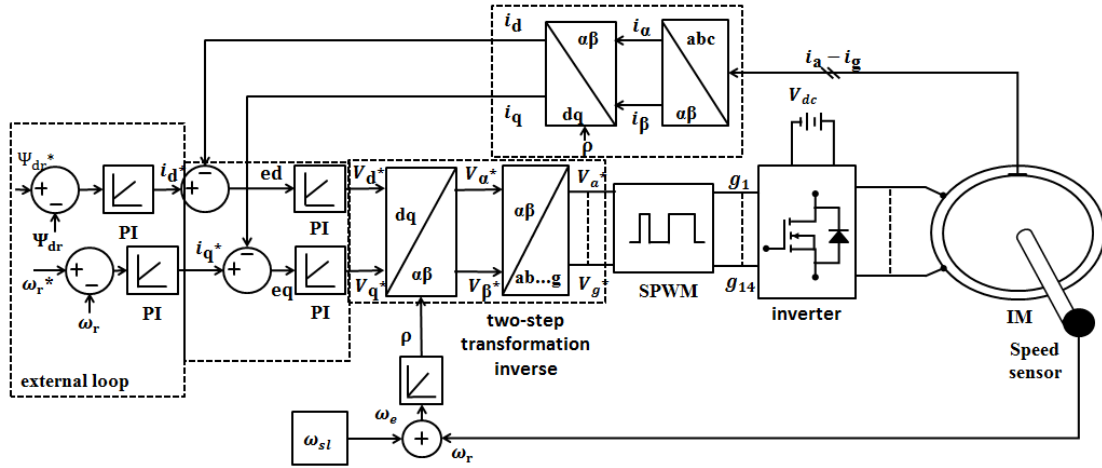
Figure 2.4 FOC system of seven-phase motor with PI controller

2.5.2 Robustness Speed Control Strategy

Due to an increase in the amount of R_r at high temperatures during severe motor functioning, incorrect rotor parameters will cause an assumed rotor flux axis angle to deviate from the real rotor flux angle with time. The external speed loop is going to determine the errorand modify i_{qs} to restore the system to the required motor speed ω_r*.

As a result, the system is non-linear, and traditional controllers such as PI cannot stabilize the system. Sliding Mode Control (SMC), is considered one of the robustness methods of control that offers resilience to load disturbances and parameter variations.
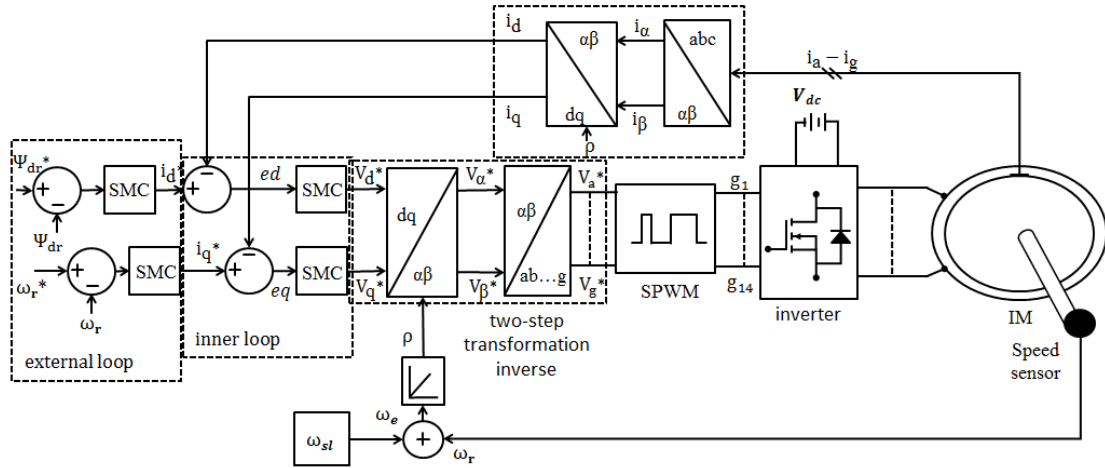
Figure 2.5 FOC system of seven-phase motor with SMC controller

2.5.2.1 Traditional Sliding Mode Control

The SMC ensures that the error in various system states consistently converges until it reaches the Sliding Surface (SS), as shown in Figure 2.5. The sliding surface is determined by the variables of the tracking error (e(t)) of the state the alignment the system with the SS is independent of the system characteristics and additional disturbance [55], [56].

2.5.2.1.1 Traditional SS Design

The SS described in (2.44) ensures statistical stability in conventional sliding mode, with the convergence determined by the value of e(t) [57]. On the other hand, if the error number is zero, this indicates that the controller was successful in producing the planned result and the system adheres appropriately to the sliding surface.

$$s(t) = k_1 e(t) \tag{2.44}$$

$$(t) = x^*(t) - x(t) \tag{2.45}$$

Where s(t) represents the SS vector, it must always be zero, e (t) is defined as the error signal; x is the controlled signal state; x* is the reference of controlled signal state; and k_1 is the sliding mode gain.

2.5.2.1.2 Architecture of equivalent Control

It is important to design the control system in a way that guarantees the controlled variables will reach the sliding surface, follow it, and stay mobile on the surface. Upon reaching the surface, the SS function must fulfill the condition s (t) = ṡ (t) = 0, indicating the presence of a sliding mode. Generally, the sliding control (s_{sm}) consists of a pair of parameters: the equivalent control input and the switching control input.

$$s_{sm} = s_{ip} + s_{sw} \tag{2.46}$$

Where s_{ip} and s_{sw} represent the equivalent control input and switching control input, respectively.

The equivalent control input s_{ip} determined from the general representation of the controlled element under the assumptions s = 0 and S˙ = 0. Generally, s_{ip} is achieves the system's state path towards the SS directly.

On the other hand, the main function of s_{sw} for keeping the conditions on the state trajectory follows the sliding surface, thus achieving the Lyapunov's function in order to ensure the stability of the system. Therefore, it can be presented as follows:

$$s_{sw} = \dot{s}_s = k_2 sgn(s) + k_3(s) \tag{2.47}$$

Where k_n, when n = 1, 2, 3... represents the switching control gain with a constant positive value.

$$Sgn(s) = \begin{cases} 1 & \text{if } s > 0 \\ 0 & \text{if } s = 0 \\ -1 & \text{if } s < 0 \end{cases}$$

Lyapunov's direct technique enables us to assess the stability of a structures. The concept of this theory is satisfied when:

$$V(t) = \frac{1}{2} s(t)^2 > 0$$

and

$$\dot{V}(t) = s(t)\dot{s}(t) \leq 0$$
$$\dot{V}(t) = s(\dot{e})$$

$$\dot{V}(t) = s(-k_1(\frac{dx}{dt})) \leq 0$$

Consequently, V(t) is positive as well as V˙ (t) is clearly negative. Thus, S(t) approaches 0 as time t approaches infinity. Furthermore, all components controlled with S = 0 will eventually stay on the surface. After being on the SS, this system's behavior as stable.

2.5.2.1.3 Controlling of the electric speed using traditional SMC controller:

In order to achieve the FOC consideration, the q-axis rotor flux must be zero. Assume the SS represents the error signal of the rotor speed as follows:

$$s_{wr} = k_1(\omega_{r\_ref} - \omega_r) \tag{2.48}$$

By deriving relationship (2.48)

$$\dot{s}_{\omega_r} = -k_1 \frac{d\omega_r}{dt} \tag{2.49}$$

After substituting the relationship (2.30) with (2.48) and (2.49), we find:

$$\dot{s}_{\omega_r} = -\frac{p^2 L_m i_{qs}}{J L_{lr}} \psi_{dr} + \frac{f \omega_r}{J} \tag{2.50}$$

To maintain ω_r within the reference speed value and preserve alignment with the sliding surface, we apply the relationship for the law of reaching (2.47) in (2.50).

$$i_{qs\_ref} = \left(\frac{f\omega_r}{J} + k_1\big(k_2 sgn(s) + k_3(s)\big) \right) / \frac{p^2 L_m}{JL_{lr}} \psi_{dr} \quad (2.51)$$

2.5.2.1.4 Controlling of d-axes rotor flux using SMC controller

Assume the SS represents the error signal of the d-axis rotor flux as follows:

$$s_{\psi_{dr}} = k_1\big(\psi_{dr\_ref} - \psi_{dr}\big) \qquad\qquad (2.52)$$

By deriving relationship (2.52)

$$s\dot{\psi}_{dr} = -k_1 \frac{d\psi_{dr}}{dt} \qquad\qquad (2.53)$$

After substituting the relationship (2.22) with (2.52) and (2.53), we find the following equation:

$$s\dot{\psi}_{dr} = -\frac{L_m R_r}{L_{lr}} i_{sd} + \frac{R_r}{L_{lr}} \psi_{dr} - (\omega_e - \omega_r)\psi_{qr} \qquad (2.54)$$

For the law of reaching to regulate ψ_{dr} to maintain its value within the limits of the reference rotor flux value, the following relationship can be generated by applying (2.47) in (2.54).

$$i_{ds\_ref} = \left(\frac{R_r}{L_{lr}} \psi_{dr} - (\omega_e - \omega_r)\psi_{qr} + k_1\big(k_2 sgn(s) + k_3(s)\big) \right) / \frac{L_m R_r}{L_{lr}}$$

$$(2.55)$$

2.5.2.1.5 Controlling of rotor angular speed

To ensure the control system is stable despite changing components, the angular speed of the rotor flux is also regulated. Depending on the regulation of the q-axis of rotor flux, the rotor angular speed can be controlled.

By expressing the reference value of the rotor q-axis flux equal to

zero to achieve the FOC condition, the SS is represented as:

$$s_{\psi_{qr}} = \left(-\psi_{qr}\right) \tag{2.56}$$

By deriving the previous relationship :

$$s_{\dot{\psi}_{dr}} = -\frac{d\psi_{qr}}{dt} = 0 \tag{2.57}$$

After substituting the relationship (2.21) with (2.56) and (2.57), we find the following equation:

$$s_{\dot{\psi}_{qr}} = -\frac{L_m R_r}{L_{lr}} i_{sd} + \frac{R_r}{L_{lr}} \psi_{dr} \tag{2.58}$$

For the law of reaching to regulate ψ_{qr} to maintain its value within the limits of the reference rotor flux value, the following relationship can be generated by applying (2.47) in (2.58).

$$\omega_{sl} = \frac{\left(\frac{L_m R_r}{L_{lr}} i_{qs} + k_1\left(k_2 sgn(s) + k_3(s)\right)\right)}{\frac{1}{\psi_{dr}}} \tag{2.59}$$

2.5.2.2 Integral SMC

Traditional SMC improves system resilience despite parameter changes and outer disturbances. Despite the traditional SMC advantages, it also has drawbacks, like chattering efficacy, the reaching condition that cannot ensure resilience [58]. Several forms of Sliding Mode Control (SMC) have been developed to deal with these issues, such as Integral Sliding Mode Control (ISMC), which seeks to minimize the reaching time by maintaining sliding surfaces throughout the system [59].

2.5.2.2.1 SS Design of ISMC

ISMC was developed to address the typical issue of sliding mode control SMC by removing the reaching time, and ensuring the sliding time is maintained for the whole system response.

$$s(t) = k_1 e(t) + k_2 \int e(t) \qquad (2.60)$$

$$e(t) = x(t) - x^*(t) \qquad (2.61)$$

Where s(t) represents the SS vector, it must always be zero, e (t) is defined as the error signal, x is the controlled signal state, x* is the controlled signal state reference, and $k_{1,2}$ is the sliding mode gains. In case of (0) is equal to 0, thereby eliminating the reaching step. The sliding mode will be present starting at time t = 0, and the system will maintain resilience during the whole system response regardless of uncertainty.
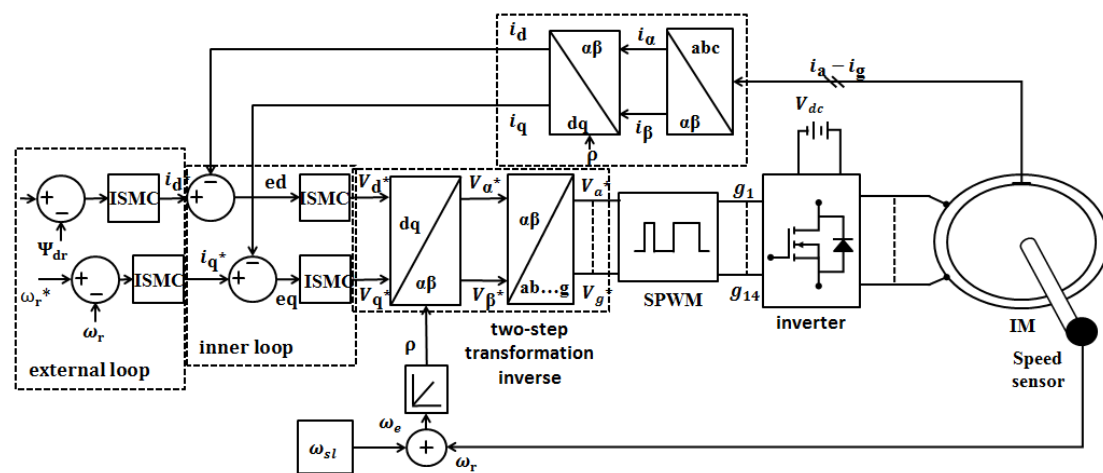
Figure 2.6 FOC system of seven-phase motor with ISMc controller

2.5.2.2.2 Architecture of equivalent Control

To ensure that the controlled variables reach the SS and retain their mobility on it, the ISMC system should be constructed in a manner comparable to that of the traditional SMC, Figure 2.6.

Like the analysis of the SMC, the sliding control s_{sm} consists of the equivalent control input (s_{ip}) and the switching control input (s_{sw}).

$$s_{sm} = s_{ip} + s_{sw} \qquad (2.62)$$

Generally, s_{ip} determined from the general representation of the controlled element under the assumptions S (t) = $\dot{s}$ (t) = 0.

With respect to the switching control input ensures that the state trajectory follows the sliding surface, by implementing the Lyapunov function, the system's stability can be guaranteed. Therefore, it can be presented as follows:

$$s_{sw} = \dot{s}_s = -k_3 sgn(s) - k_4(s) \qquad (2.63)$$

Where k_3 and k_4 are representing the switching control gain with a constant positive value.

Lyapunov's direct technique enables us to assess the stability of a structures. The concept of this theory is satisfied when:

$$V(t) = \frac{1}{2}s(t)^2 > 0$$

and

$$\dot{V}(t) = s(t)\dot{s}(t) \le 0$$

Then by applying (2.63) in V(t)(Lyapunov's function), If c is positive, then v(t) is positive, meeting the initial condition of Lyapunov's theory.

$$V = \frac{1}{2}(k_1 e + k_2 \int e)^2$$

In the same way if the k_1, k_2, k_3, and k_4 have positive values and k_1 is equal or greater than k_2, v(t) will have a negative value, satisfying the second condition.

$$\dot{V} = s(k_1 \dot{e} + k_2 e)$$

$$= s(k_1(-k_3 Sgn(s) - k_4(s)) + k_2 e)$$
$$= s(-k_1 k_3 Sgn(s) - k_1 \gamma k_4(s) + k_2 e) \leq 0$$

2.5.2.2.3 Design of FOC with ISMC

By representing the general equation of a SS of controlled value as follow:

$$s = k_1(x^* - x) + k_2 \int (x^* - x)dt \qquad \textbf{(2.64)}$$

This leads to the derivation of the relationship as follows:

$$\dot{s} = -k_1 \frac{dx}{dt} + k_2(x^* - x) \qquad \textbf{(2.65)}$$

When regulating the speed, the equation (2.30) can be combined with (2.64) and (2.65) as controlled values to generate i_{sq}* as follows:

$$i_{qs\_ref} = \left(k_1 \frac{f\omega_r}{J} + k_2(\omega_{r\_ref} - \omega_r) + (k_3 sgn(s_2) + k_4(s_2)) \right) /$$
$$k_1 \frac{p^2 L_m}{J L_{lr}} \psi_{dr} \qquad \textbf{(2.66)}$$

In a similar way, the controlling of the d-axis rotor flux to generate i_{sd}* is equating from (2.22), (2.64), and (2.65) as follows:

$$i_{ds\_ref} = \left(k_1 \frac{R_r}{L_{lr}} \psi_{dr} + k_2(\psi_{dr\_ref} - \psi_{dr}) + (k_3 sgn(s_1) + k_4(s_1)) \right) /$$
$$k_1 \frac{L_m R_r}{L_{lr}} \qquad \textbf{(2.67)}$$

For controlling the angular speed of the rotor flux, the following equation comes from (2.21), (2.64), and (2.65).

$$\omega_{sl} = \left(k_1 \frac{L_m R_r}{L_{lr}} i_{qs} + (k_3 sgn(s_1) + k_4(s_1)) \right) / k_1 \frac{1}{\psi_{dr}} \textbf{(2.68)}$$

2.6 Inner loop control with ISMC

In order to control the inner loop (controlling the reference current), use the same controller applied in outer loop again. The signal resulting is a reference current signal in the rotating reference frame. This signals is converted from the rotating reference frame to a seven-phase reference voltage signal through the inverse Park and Clark transformation respectively. Thus, the seven-phase reference voltage signals are applied to the sine pulse width wave modulator(SPWM), Figure 2.7.
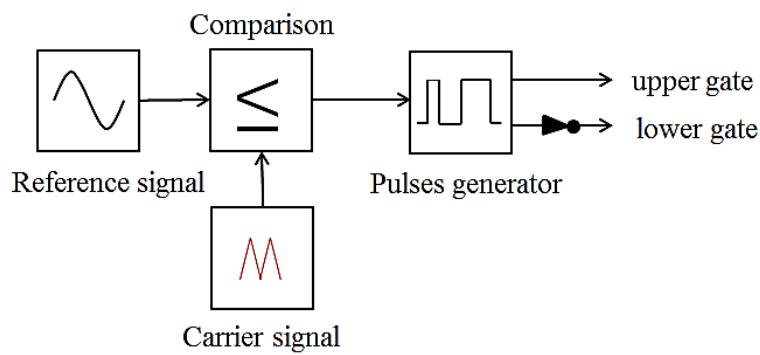
Figure 2.7 The mechanism of sin-pulse width modulation technique
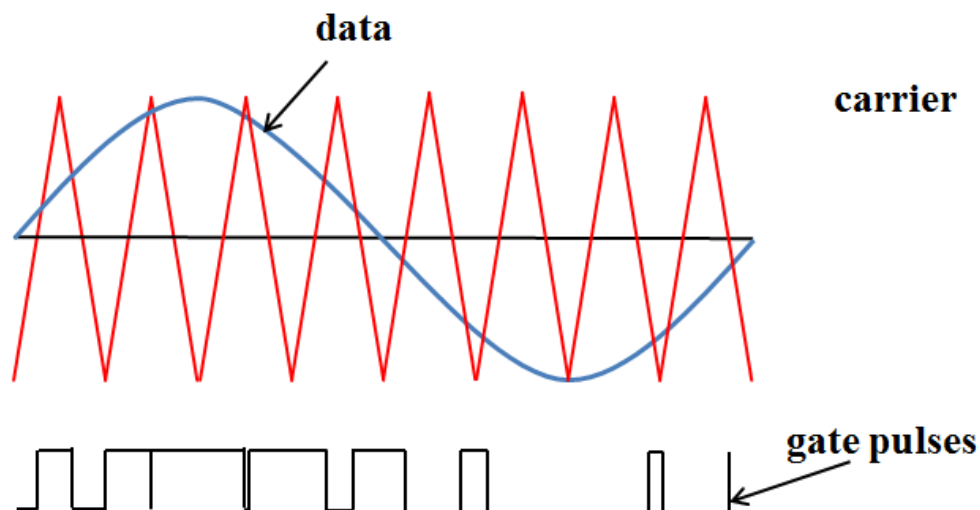
Figure 2.8 Pulses generator for SPWM technique

SPWM, on the other hand, is responsible for producing pulses that are directed to the inverter switches by comparing reference voltage signals with a triangular carrier wave [60], [61]. If the reference voltage signal is higher than the carrier wave, the upper switch will be activated for the leg that has the same address as the reference signal. In this case, the lower switch will be in the opposite state from the top switch, and vice versa.

CHAPTER 3 : Integrated on board charger

3.1 Introduction

Due to the advantages of multi-phase electric machines in propulsion, previously discussed, they are appropriate for use in electric vehicles. Furthermore, these machines provide supplementary battery charging features, specifically designed to be integrated into the charging process of electric vehicles [62]. The MPIM contributes to the possibility of charging by passing the current from the power source through its coils without generating torque. On the other hand, a multi-phase inverter is connected to the coils on one side and to the battery on the other, allowing a bidirectional power flow. This technology saves time and space and also eliminates the need for mechanical brakes during the charging process [6], [63].

The design options for charging stations (sources) may be divided into three main categories: multi-phase, single-phase, and three-phase [6], . These classifications are based on the type of supply available at the stations. This chapter deals with the modeling and discussion of the charging mode with the components of the seven-phase motor, the power inverter, and the battery supplied by a three- phase and seven-phase source.

3.2 Mathematical Modeling of 7-phase PWM Rectifier

To achieve integrated charging of electric vehicles, it is essential to utilize the benefits of both the inverter and the motor in the charging process. This is due to the fact that each component possesses the ability to function in two directions. Meanwhile, a specialized control system for the charging process is required for the charge stage to function.

In electric vehicles, the main purpose of power electronics is to feed the propulsion motor with the necessary power to achieve the appropriate level of performance. The progress achieved in power electronics and control systems has enabled bidirectional power conversion, allowing for the transfer of power between different forms.

The main circuit representation of the PWM rectifier combined with motor parameters and battery is shown in Figure 3.1.
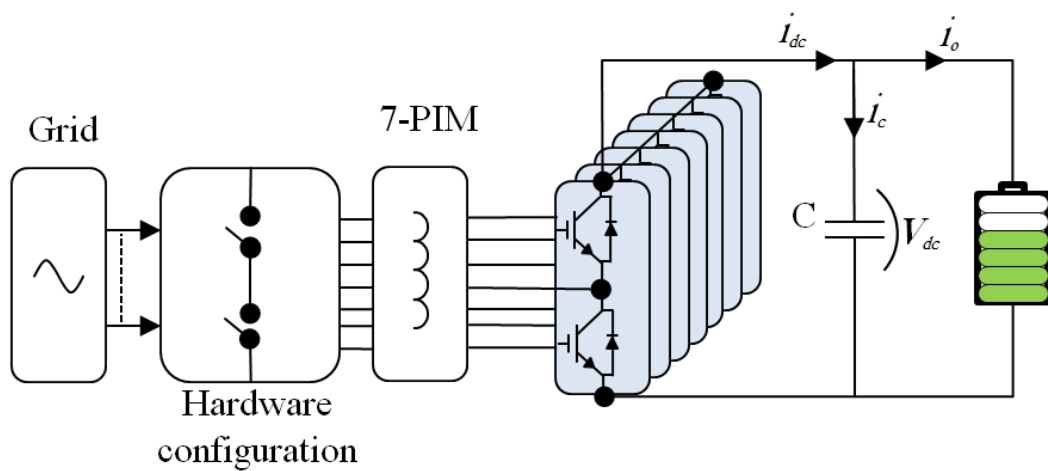
Figure 3.1 seven-phase PWM rectifier connected with motor and battery

Since the rectifiers are primarily nonlinear in their operation, they are responsible for producing harmonic currents in the AC power supply. Many problems arise in the power distribution system as a result of the elevated harmonic in the line current and the low power factor of the load.

From the Figure 3.1 above, it can be concluded that the current that is extracted from the grid may be regulated by adjusting the parameters of the stator's coils (inductor and resistor). The current flow is regulated by reducing the voltage drop (V_{drp}) produced at the coils. In other words, the

voltage drop is the resultant of the differences between grid voltage (V_g) and converter voltage (V_{con}).

$$V_{dep} = V_g + V_{con} \qquad \text{(3.1)}$$

By controlling the phase angle and the amplitude of the converter voltage V_{con}, the phase and amplitude of the line current can be indirectly regulated. Similarly, the average DC value and polarity can be controlled by adjusting according to the active power across the converter.

The rectifier may be characterized by a set of equations that explain the current and voltage.

$$V_{gn} = R_s i_n + L_{ls} \frac{di_n}{dt} + V_{con\_n} \qquad \text{(3.2)}$$

$$
\begin{bmatrix} V_{ag} \\ V_{bg} \\ V_{cg} \\ V_{dg} \\ V_{eg} \\ V_{fg} \\ V_{gg} \end{bmatrix} = R_s * \begin{bmatrix} i_a \\ i_b \\ i_c \\ i_d \\ i_e \\ i_f \\ i_g \end{bmatrix} + L_{ls}\frac{d}{dt} \begin{bmatrix} i_a \\ i_b \\ i_c \\ i_d \\ i_e \\ i_f \\ i_g \end{bmatrix} + \begin{bmatrix} V_{con\_a} \\ V_{con\_b} \\ V_{con\_c} \\ V_{con\_d} \\ V_{con\_e} \\ V_{con\_f} \\ V_{con\_g} \end{bmatrix} \qquad \text{(3.3)}
$$

Where n represents the phase number, n = a, b, c, d, e, f, and g.

For the current equation:

$$C\frac{dV_{dc}}{dt} = i_{dc} - i_L \qquad \text{(3.4)}$$

Where

$$i_{dc} = \begin{bmatrix} S_a \\ S_b \\ S_c \\ S_d \\ S_e \\ S_f \\ S_g \end{bmatrix} \times [i_a \quad i_b \quad i_c \quad i_d \quad i_e \quad i_f \quad i_g] \qquad (3.5)$$

according to the S_n switching, state of operating is given by:

$$S_n = \begin{cases} 1 & upeer\ switch\ ON \\ 0 & lower\ switch\ ON \end{cases}$$

With n is a phase number, n = a, b, c, d, e, f, g.

By using the Clark transformation in the stationary reference frame on equation (2.1), we will obtain:

$$V_{g\_\alpha\beta} = R_s i_{\alpha\beta} + L_{ls}\frac{di_{\alpha\beta}}{dt} + V_{con\_\alpha\beta} \qquad \textbf{(3.6)}$$

By considering $x_{\alpha\beta} = x_{dq}\,e^{j\omega t}$, the equation (3.6) will be transformed into equation (3.7) in the rotating reference frame.

$$V_{g\_dq} = \left(R_s + j\omega_g L_{ls}\right)i_{dq} + L_{ls}\frac{di_{dq}}{dt} + V_{con\_dq} \qquad \textbf{(3.7)}$$

By using the decoupling technique on the d and q components

$$V_{g\_d} = R_s i_d + j\omega_g L_{ls} i_d + L_{ls}\frac{di_d}{dt} + V_{con\_d} \qquad \textbf{(3.8)}$$

$$V_{g\_q} = R_s i_q + j\omega_g L_{ls} i_q + L_{ls}\frac{di_q}{dt} + V_{con\_q} \qquad \textbf{(3.9)}$$

It can be observed that the relationship between the voltages on the d-axis and the q-axis is decoupled through the coefficients $L\omega_g i_d$ and $L\omega_g i_q$.

The following formulas are used to calculate the active and reactive power delivered by the source:

$$pp = Re\{v * i\} = v_{g\_d}i_{g\_d} + v_{g\_q}i_{g\_q} \qquad \textbf{(3.10)}$$

$$qq = \text{Im}\{v * i\} = v_{g\_q}i_{g\_q} + v_{g\_d}i_{g\_q} \qquad (3.11)$$

3.3 Architecture Of on-board Charger

3.3.1 Architecture of Charging System by Seven-Phase sorce

The key consideration in the integrated charging stage is the absence of torque generation throughout the charging time. When the charging current flows through the motor coils, it generates a magnetic field that causes the motor to rotate during the charging process. To overcome this problem, motors with a unique design of the stator coils can be used, or an external mechanical brake can be applied. Similarly, multi-phase motors provide more flexibility as they prevent motor rotation during charging. The degree of freedom offered by MPIM is a direct result of their operating characteristics. Multi-phase motors can switch between producing torque planes and not producing torque planes to avoid rotation or the need for external brakes.

The prevention of motor rotation relies on the specific configuration between the grid and the motor coils. At the same time, a seven-phase star-connected motor with a single neutral point is used in the drive state, the switch (s) to a column (a). For the charging state, it is essential to keep the neutral point open while charging from a seven-phase source. This can be achieved by shifting the switch (s) to a column (b). Subsequently, the individual stator coils are interconnected with the source phases, as depicted in[64].

The goal of the connection shown in the Figure 3.2 is to induce the motor to function at planes where torque is not generated utilizing the characteristics of multi-phase motors. Consequently, the motor remains

stationary while it is being charged, without the need for an additional mechanical brake [65].
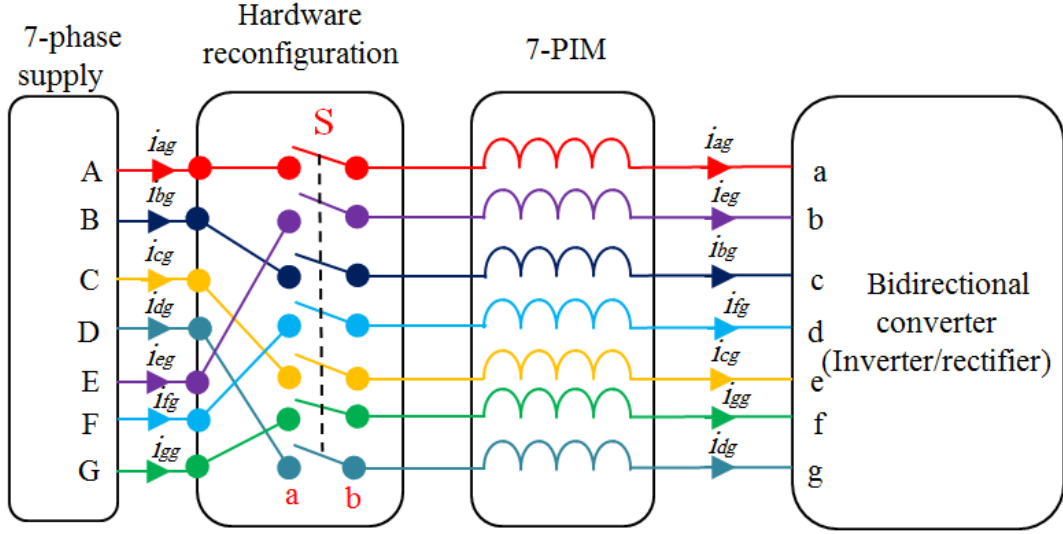

Figure 3.2 Hardware configuration of integrating seven-phase charging from sevev-phase source

On the other hand, several methods exist to acquire a multiphase power supply in a charging station. The elementary approach would include using a transformer that converts three-phase power to n-phase power. Nowadays, there are identified transformer topologies, such as (in this case) three-phase to seven-phase transformers [46]. Other possibilities rely on power electronic inverters and require the addition of output voltage filtering. Form grid current:

$$i_{kg} = \sqrt{2}I\cos\left(\omega_g t - \frac{l2\pi}{7}\right) l = 0, 1, \dots, 7 \ k = a, b, \dots, g \ \textbf{(3.12)}$$

By applying the phase configuration shown in above:

$$i_a = i_{ag}, i_b = i_{eg}, i_c = i_{bg}, i_d = i_{fg}, i_e = i_{cg}, i_f = i_{gg}, i_g = i_{dg} \ \textbf{(3.13)}$$

The first guide is the generic transformation matrix (2.1), specifically for a seven-phase system.

$$f_{\alpha\_\beta} = f_\alpha + jf_\beta = \sqrt{2/7}\,(f_a + \underline{a}\,f_b + \underline{a}^2\,f_c + \underline{a}^3\,f_d + \underline{a}^4\,f_e + \underline{a}^5\,f_f + \underline{a}^6\,f_g) \tag{3.14}$$

$$f_{x1\_y1} = f_{x1} + jf_{y1} = \sqrt{2/7}\,(f_a + \underline{a}^2\,f_b + \underline{a}^4\,f_c + \underline{a}^6\,f_d + \underline{a}^8\,f_e + \underline{a}^{10}\,f_f + \underline{a}^{12}\,f_g) \tag{3.15}$$

$$f_{x2\_y2} = f_{x2} + jf_{y2} = \sqrt{2/7}\,(f_a + \underline{a}^3\,f_b + \underline{a}^6\,f_c + \underline{a}^9\,f_d + \underline{a}^{12}\,f_e + \underline{a}^{15}\,f_f + \underline{a}^{18}\,f_g) \tag{3.16}$$

$$\underline{a} = e^{j\delta}, \quad \delta = 2\pi/7$$

By substituting equation (3.13) into equations (3.14, 3.15, 3.16), we can get the space vectors in the seven-planes given the interaction shown in above:

$$i_{\alpha\_\beta} = 0$$

$$i_{x1\_y1} = \sqrt{7}I\,e^{j\omega t}$$

$$i_{x2\_y2} = 0$$

The preceding calculations show that throughout the charging phase, the motor will rely on the second xy plane, which is incapable of producing torque, utilizing the advantage of multi-phase motors.

3.3.2 Architecture Of Charging System by three-Phase Grid

Various approaches may be developed to facilitate charging from the three-phase grid, depending on the machine's phases amount and the number of neutral points, various approaches can facilitate charging from the three-phase grid [66], [67], [68]. If the motor's winding is seven-phase, as in this thesis, the machine must have at least three separate neutral points. The idea outlined in the previous section for using a seven-phase power source may be adapted for employing a three-phase power

supply in a charging state. Unlike the options discussed in the previous section, hardware modification is complex in this case. A minimum of three separate neutral points is required by connecting each phase of the grid supply to a single neutral point (switch (s) opened), as shown in Figure 3.3.
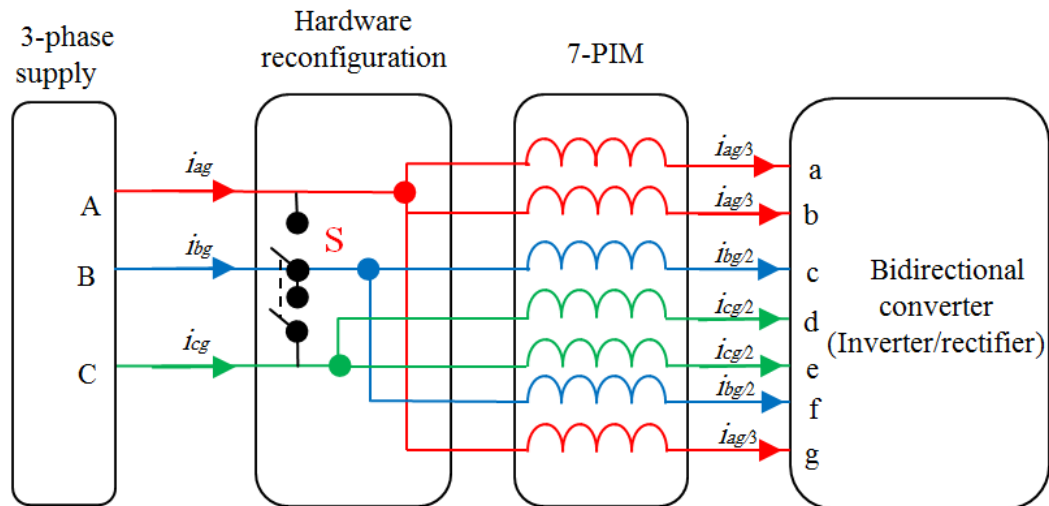

Figure 3.3 Hardware configuration of integrating seven-phase charging from three-phase source

In the case of a three-phase grid, the current can be written as follows:

$$i_{ng} = \sqrt{2}I cos\left(\omega_g t - \frac{l2\pi}{3}\right) \quad l = 0, 1, 2 \quad n = a, b, c \quad \textbf{(3.17)}$$

In this figure, the connection between the grid phases and the stator windings can be represented as follows:

$$i_a = i_b = i_g = \frac{i_{ag}}{3}, i_c = i_f = \frac{i_{bg}}{2}, i_d = i_e = \frac{i_{cg}}{2} \quad \textbf{(3.18)}$$

Applying (3.18) to (3.17) results in the next stimulation:

$$i_{\alpha\_\beta} = 1.0858 * I \cos(\omega_g t - 0.4214)$$

$$i_{x1\_y1} = 1.0274 * I \cos(\omega_g t + 1.3304)$$

$$i_{x2\_y2} = 0.6751 * I \cos(\omega_g t - 2.139)$$

Without a doubt, the excitation in the torque-generating plane is only oriented along the α-axis (real part). By maintaining the β-component at zero (the imaginary part), the magnetic field in this situation will oscillate and cannot generate any initial torque [24]. Consequently, the rotor of the machine will remain stationary.

3.4 Methods of Controlling PWM Rectifier

To control a PWM rectifier, there are two common techniques:

Voltage-Oriented Control (VOC): this technique ensures superior dynamic and static efficiency by using an inner current regulation loop. However, accuracy mostly relies on the existing control approach .

Direct Power Control (DPC): in this technique, real-time control of both active and reactive power is utilized. There is an absence of an internal current control loop and a PWM section. The switching condition is computed using a switching table that relies on the instantaneous errors caused by the requested and calculated quantities of active and reactive power [69].

VOC may be considered a parallel control technique to FOC in the drive system of induction motors, as previously described. In the same regard, the DPC technology has parallels to direct torque control (DTC) used for induction motors. The control focuses on regulating the instantaneous active and reactive powers, instead of manipulating torque and stator flux.

3.4.1 Voltage Oriented Control

The control algorithm generally maintains a DC voltage level by managing the current flow that charges the capacitor. This is achieved by producing specific pulses for the power electronic switches, which are adjusted in amplitude and angle according to the operating circumstances.

The VOC technique converts the grid current from stationary coordinates αβ to a synchronous rotating reference frame dq, in order to controlling direct DC currents to eliminate any steady-state inaccuracy. This method ensures fast transient responses and excellent static behavior through inner current regulation loops as illustrate in Figure 3.4. Hence, the ultimate arrangement and efficiency of the system heavily rely on the performance of the implemented current control. Assuming that the dq-axes are oriented at the angular speed ω_g so that the d-axis applies to the grid voltage vector while the q-axes equal zero.

According to equations (3.10) and (3.11), the active power P and the reactive power Q in the PWM rectifier can be controlled by separately controlling the values of the components i_d and i_q. In turn, controlling both active and reactive power allows determining the value of the power factor on the input terminal of the rectifier [70].

To obtain a unity power factor, the reference current value (i_q*) is set to zero. This hypothesis suggests that controlling the current id, which is in phase with the grid voltage, allows the active power to be controlled directly, as (3.6) shows. At the same time, it is possible to control the value of V_{dc} indirectly as the value of the constant voltage on the output terminals. Directly based on the difference between the active power provided by the PWM rectifier and the power consumed by the

load on the output of the rectifier. Generally, only when the electrical load current is equal to the PWM rectifier current, the voltage become a DC value on the capacitor terminals.
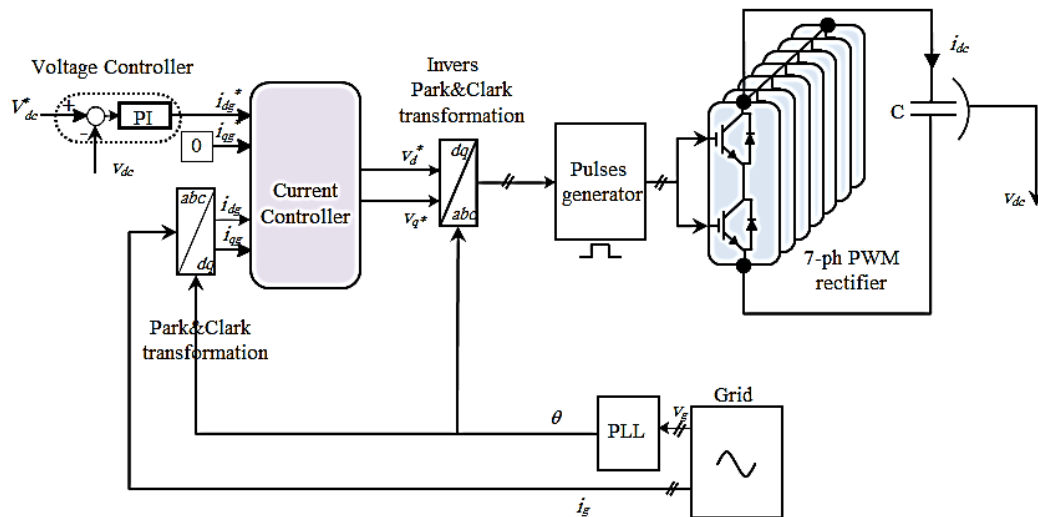

Figure 3.4 VOC mechanism for seven-phase system

3.5 Phase Locked Loop (PLL) Algorithm

A phase-locked loop (PLL) obtains the grid voltage position and then sends it to the park transformation block. The angle derived by the phase-locked loop (PLL) and the grid currents allows us to determine the components of the grid currents in the dq form. A diagram, as shown in Figure, aids in the extraction of these components. This block diagram operates based on the double Synchronous Reference Frame (SRF) theory strategy [71].

The SRF-PLL is a closed-loop control system that rapidly detects the grid voltage's phase angle (θ_g). The grid voltages, whether from a three-phase or a seven-phase source in this system, are initially monitored, after that, the variables V_α and V_β are obtained by applying the Clarke transformation to the grid voltage; subsequently, the variables

V_d and V_q were obtained as modified rotational frames by applying the Park transformation. The grid voltage's estimated phase angle (θ_g*) is used as feedback to control the operation of the abc (for simplicity) to dq block, enabling the execution of the Park transformation. The PI controller is frequently utilized to control the Synchronous Reference Frame SRF-PLL mechanism. The PI controller functions as a loop filter in the system, regulating V_{qg} and detecting the system's dynamics, as shown in Figure 3.5. Furthermore, a simple low-pass filter can achieve stability and effectively address the issue of decreased bandwidth due to network imbalance [72].
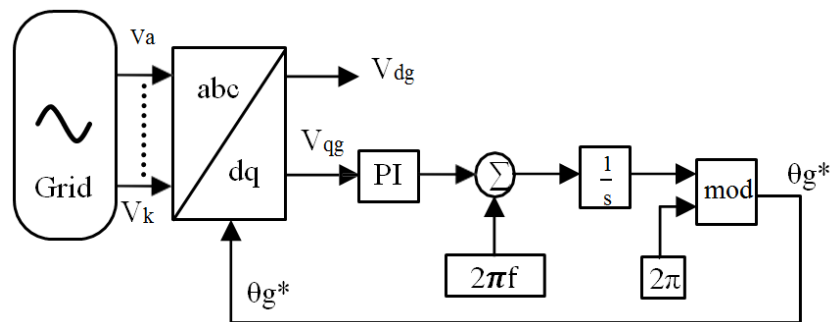

Figure 3.5 PLL diagram designed by SRF technique

3.6 Control Under Balance Conditions

3.6.1 Introduction

As shown in Figure 3.2, each single phase of the grid directly connects to a single phase of the stator windings, ensuring an identical current draw from the seven-phase network for all phases. The equality of the motor windings, which function as a filter in the state of charge, is the reason for the balanced connections. The VOC control technology allows for controlling both the external loops, which regulate the output voltage, and the internal loop, which represents the reference current controller.

Depending on the linear load, traditional controllers can control these loops, including the PI controller and the hysteresis current controller.

3.6.2 VOC for Balanced Condition

PI controllers are known for their straightforward implementation and uncomplicated nature.

3.6.2.1 PI controller

It is appropriate to use a PI controller to regulate both the internal and external loops, depending on whether the components under control are DC components without any disruptions (linear condition) [65].The external loop controls the rectifier output voltage to match its reference value (DC-link voltage controller), thereby achieving the desired output voltage, as shown in Figure 3.4. The outer loop's output signal indicates the current i_d's reference value, which determines the converter's active power. However, as previously indicated, the reference value of the current i_q is set to zero, as shown in Figure 3.6. The regulation of currents, i_d and i_q, functions as the internal loop (current controller) in VOC technology, generating the reference voltages, v_d *, and v_{q*}, the inverse Clark and Park transformation ultimately converts the reference voltages into seven-phase signals. The seven-phase reference values correspond to the input of the SPWM block. Consequently, the module produces pulses that activate the switches to regulate the power flow to the battery.
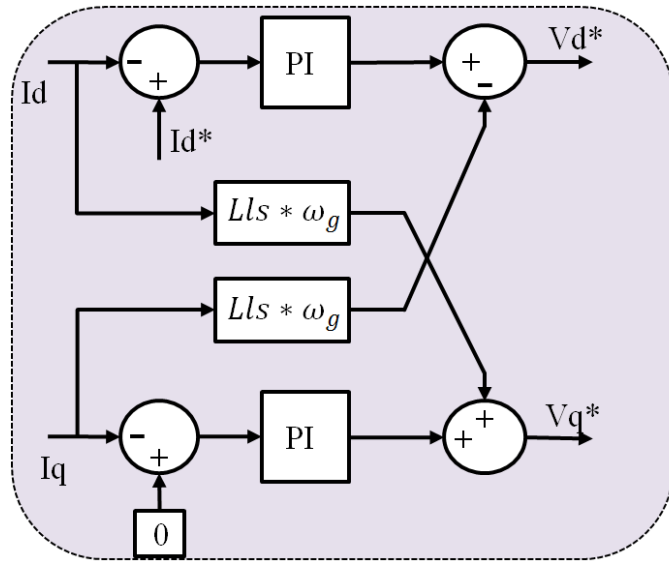
Figure 3.6 Current controller in balance condition

3.7 Control Under Unbalance Condition

According to the configuration of connecting the three-phase grid to the coils of the seven-phase motor, the motor does not rotate during the charging period. Nevertheless, this arrangement causes an asymmetry in the current flowing through the coils of the filter (stator windings). A single phase of the grid supplies a single neutral point, causing the asymmetry in the number of coils connected in parallel. This difference affects the equivalent impedance for each paralleled group. The grid phase (a) connects to the equivalent impedance of three paralleled coils of the motor (a, b, and g), while the other grid phases (b, c) only connect to the equivalent impedance of two paralleled coils each. Consequently, phase (a) supplies a current that is 1/3 times higher in amplitude than phases (b and c).Moreover, it is possible to consider the generated pulsing field as a contributing factor to the imbalance in the stator windings' impedance values, which increases the rotor losses.

3.7.1 DC-Link Voltage Controller

The external loop, which is the output voltage controller, regulate the V_{dc} by adjusting it to its desired reference value, similar to the balanced control scenario. Once again, the PI controller is appropriate as it regulates a DC quantity.

3.7.2 Current Controller

The concept of unbalanced components leads to the rotation of a fundamental component in an anti-synchronous orientation, visible as a harmonic in the d-q reference frame, specifically a negative sequence component that rotates oppositely. The rectifier perceives the fundamental negative-sequence aspect of the input current as a destructive source, oscillating at twice the frequency of the fundamental supply current. A single PI controller is incapable of effectively regulating the positive and negative-sequence components of the grid currents caused by an imbalance in the filter connection. An imbalance in the filter configurations leads to an uneven grid current with elevated total harmonic distortion (THD). Consequently, the filter will experience more losses, resulting in a decrease in the effectiveness of the integrated battery charger. Therefore, several control methods have been devised to mitigate filter losses and ensure a balanced current state coming from the grid.

3.7.2.1 Vector Proportional-Integral VPI Controller

To provide uniform current rms values throughout all phases, it is essential to remove the harmonics caused by an imbalance situation. Vector proportional-integral (VPI) resonant controllers can potentially be used to eliminate harmonics [17]. VPI is considered one of the selective theories for removing harmonics. The VOC control system operates in a rotating reference frame. In this frame, the negative-sequence component appears as the 2nd harmonic (a negative sign indicates rotation in the opposite direction), a sequence of adverse elements, as shown in Figure 3.7. The PI controller manages the fundamental component of the grid current to ensure consistent and smooth functioning of the rectifier, while the VPI completely eliminates any harmonic in the currents.
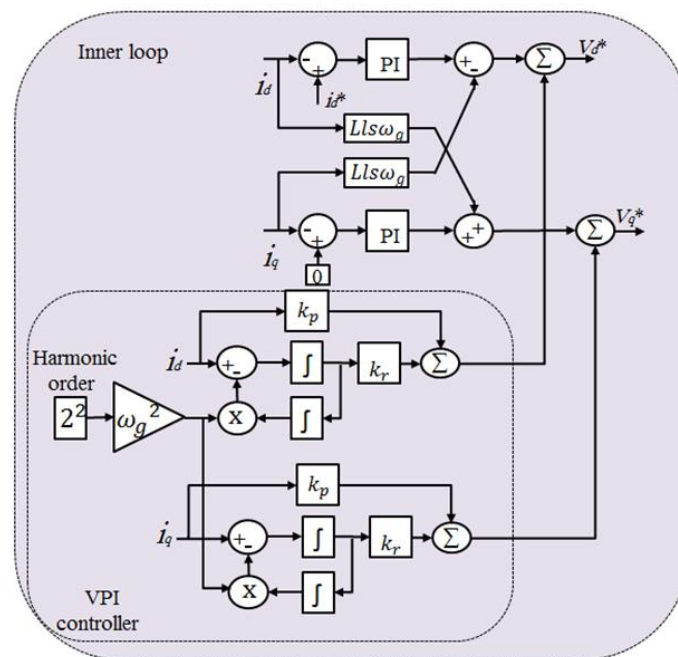

Figure 3.7 The current controller of unbalance case with vector proportional integral controller

3.7.2.2 Sliding Mode Control SMC Current Control

Sliding Mode Control SMC is a highly efficient nonlinear controller that is well-suited for changeable-structure systems, such as power electronics converters, because of its ability to perform switching operations, as shown in Figure 3.8. For this reason, it can function as an inner loop current controller with unbalanced network current [73].

Switching control input can be presented as follows:

$$\dot{S}_d = -k_2 Sgn(S_d) - k_3(e_d) \qquad (3.19)$$

To control the i_d, the SS can be represented by the following equation:

$$S_d = k_1\left(i_{dref} - i_d\right) \qquad (3.20)$$

By deriving the relationship of SS for rectifier (3.20) and applying it to the equation (3.8):

$$\dot{S}_d = i_{dref} + \frac{R_s}{L_{ls}}i_d - \omega_g i_q - \frac{V_d}{L_{ls}} + \frac{V_{con\_d}}{L_{ls}} \qquad \textbf{(3.21)}$$

By applying (3.19) to (3.21), the general control of the rectifier can be described as follows:

$$V_{con\_d_{ref}} = L_{ls}\left(-\dot{i}_{dref} - \frac{R_s}{L_{ls}}i_d + \omega_g i_q + \frac{V_d}{L_{ls}} - k_1(k_2 Sgn(S_d) - k_3(S_d))\right)$$
$$\textbf{(3.22)}$$

In controlling i_q, which is similar to i_d, the SS can be represented as:

$$S_q = k_1\left(i_{qref} - i_q\right) \qquad (3.23)$$

By deriving the relationship (3.23) applying it to the equation (3.9):

$$\dot{S}_q = i_{qref} + \frac{R_s}{L_{ls}}i_d - \omega_g i_d - \frac{V_q}{L_{ls}} + \frac{V_{con\_q}}{L_{ls}} \qquad (3.24)$$

Then

$$V_{con\_qref} = L_{ls}\left(-\dot{\imath}_{qref} - \frac{R_S}{L_{ls}}i_d + \omega_g i_d + \frac{V_q}{L_{ls}} - k_1(k_2 Sgn(S_q) - k_3(S_q))\right)$$
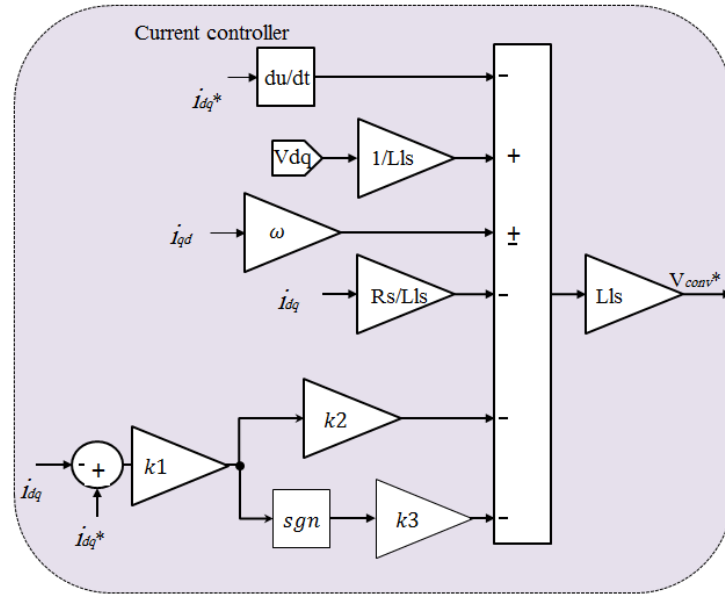
$$(3.25)$$

Figure 3.8 The current controller of unbalance case with sliding-mod controller

3.7.2.3 Separation Method with PI Controller

Since the current drawn from the network contains positive (i_d^+, and i_q^+) and negative (i_d^-, and i_q^-) sequence components, these components can be separated from each other to simplify the controlling process. To mitigate the negative components, the network current components are separated by using the concept of the double synchrony reference frame (DSRF) [5]. The positive (fundamental) components exhibit a rotational motion in the same direction as the voltage vector, while the negative components exhibit a rotational motion in the opposite direction. The PI controller is used to regulate each sequence independently. On the other hand, the reference value of the current i_d^+ is used as the output of the VDC controller. The reference values of the current i_q^+, i_d^-, and i_q^- are all set to zero in order to remove any negative components.

Figure 3.9display the general control block diagram and sequential component separation, shown in Figure **3.10**.
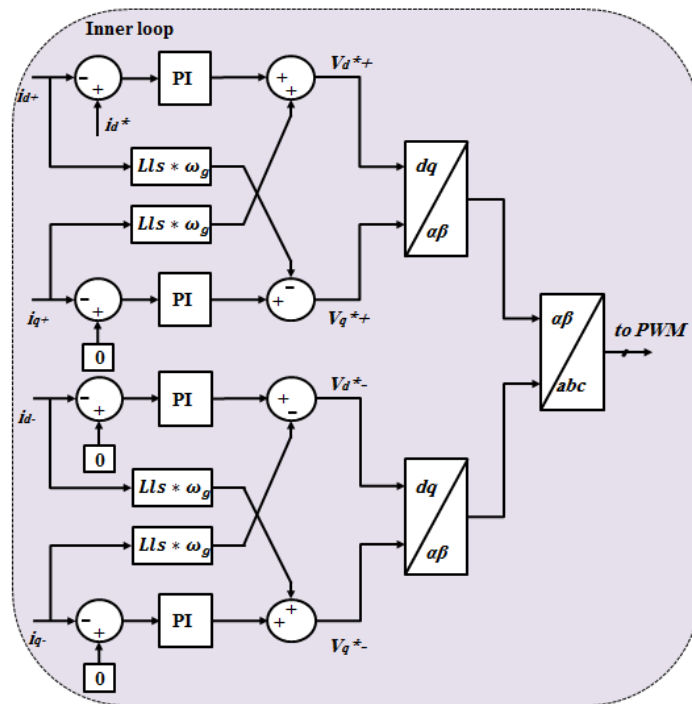

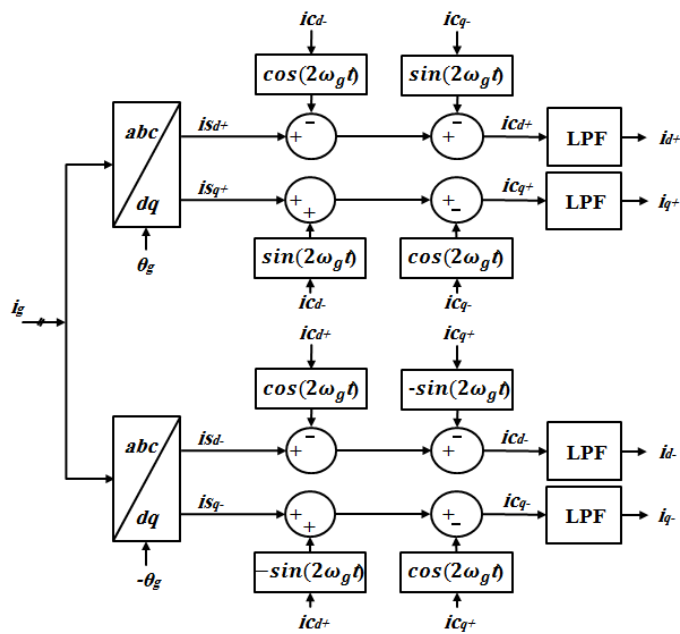Figure 3.9 The current controller of unbalance case with separation method

Figure 3.10 the block diagram of separation the grid current to negative and positive components

CHAPTER 4 : Results and Discussion

4.1 Propulsion Mode

In order to achieve the operating requirements of electric vehicles that operate under various conditions, the FOC drive system for controlling the speed of 7-PIM with the three proposed controllers (PI, SMC, ISMC) was tested using the MATLAB Simulink environment. Table 4.1lists the components of the seven-phase motor used with these controllers. The motor speed was controlled at 150 rad/s, which is considered as the working speed of the motor, and the d-axis rotor flux (ψ_{rd}) was also controlled at 1.4 wb. The propulsion system was tested when an external load of 10 Nm was applied after 2 second. IGBT as a power electronic switches used in this system with switching frequency is 9 kHz.

Table 4.1 Motor's parameters [74]

Rated power (P)	4 kw
Stator resistance (R_s)	10 Ω
Rotor resistance (R_r)	6.3 Ω
Inductance of stator (L_{ls})	0.0412 mH
Inductance of Rotor (L_{lr})	0.0412 mH
Mutual inductance (L_m)	0.42 mH
Moment of Inertia (J)	0.004875 kg.m^2
Poles	4
Rated current	2.5 A
Rated voltage	230V
Rated frequency	50Hz

4.1.1 FOC Drive System with PI Controller

This section discussion the results of applying the FOC with PI controller as speed of 7-PIM with rated parameters. Figure 4.1 Figure 4.2 and Figure 4.3 display the current and voltage of the first phase conjunction with their references. Figure 4.4 shows the system's response to regulating the rotor speed, and Figure 4.5 shows the system's response to regulating the d-axis rotor flux in the rotating reference frame (ψ_{rd}). Figure 4.6 and Figure 4.7 display the component of the stator current.

Table 4.2 The PI parameters for driving mode

	k_p	k_i
ψ_{rd}	200	100
speed controlling	50	80
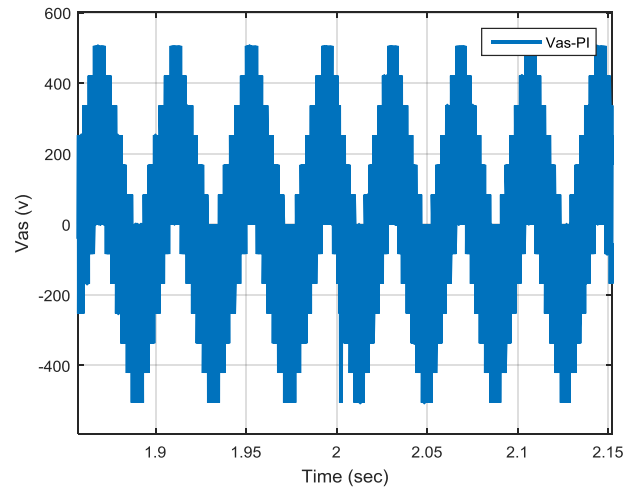
Figure 4.1 The stator voltage of the first phase with respect to its reference value with the PI controller under the rated parameters
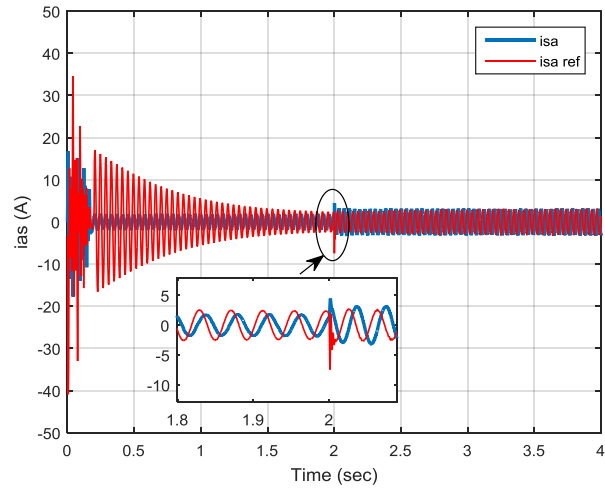
Figure 4.2 The stator current of the first phase with the PI controller under the rated parameters
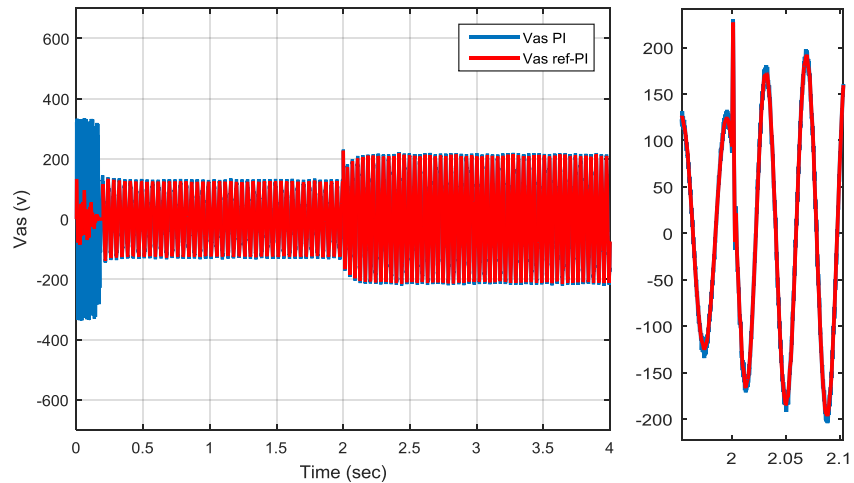

Figure 4.3 The filtered stator voltage of the first phase with respect to its reference value with the PI controller under the rated parameters

Figure 4.1 shows the voltage amplitude with $225V_{rms}$ that is applied to the motor in case of reduced frequency. The machine's load torque value influences the current in, while the stator current responses to its reference value (the reference of the current and voltage multiplied by o.1 at first 0.2s) as shown in Figure 4.2. The output voltage of the inverter is shown in Figure 4.3 after filtration voltage amplitude that is applied to

the motor in order to understanding the behavior of the motor. It changes based on the filtered reference voltage that is generated by the internal control loop and sent to the SPWM block, which in turn drives the inverter.
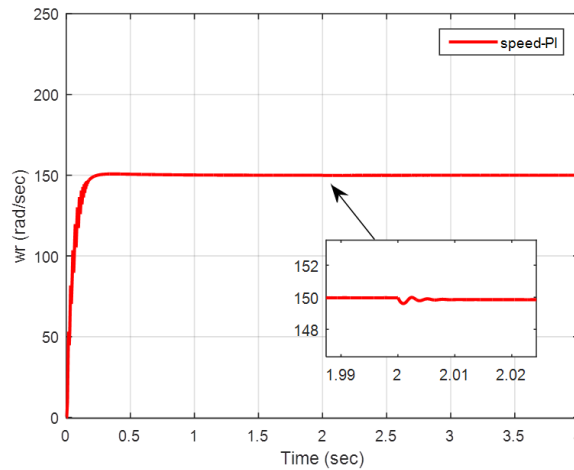

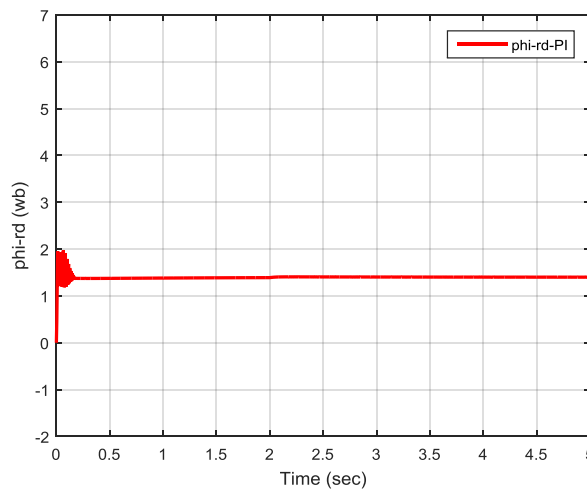Figure 4.4 The motor speed response with PI controller under rated parameters

Figure 4.5 The ψ_{rd} response with PI controller under rated parameters

Figure 4.4 shows that the rotor's actual speed follows the required reference speed before and after applying the load torque, with a zero-

error rate. Figure 4.5 shows that the rotor flux component follows the reference values correctly, where the desired value of ψ_{rd} equal to 1.4wb.
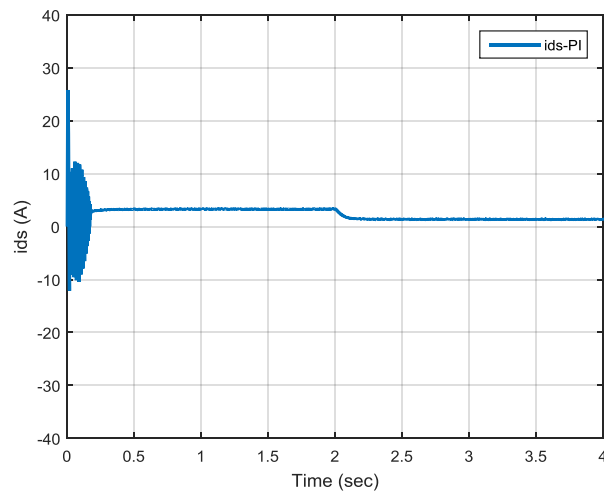

Figure 4.6 The i_{ds} component for the stator current with PI controller under rated parameters
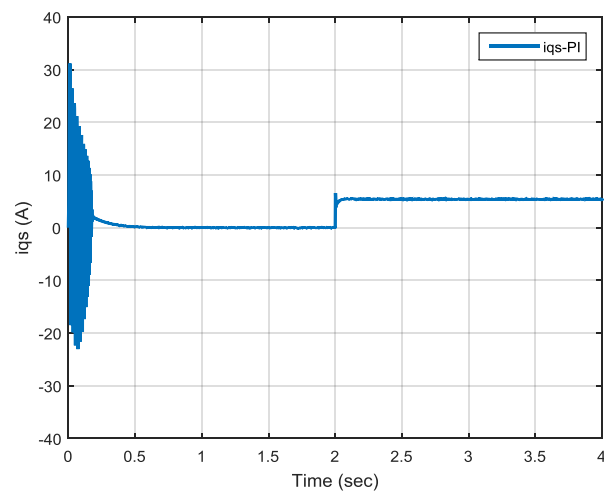

Figure 4.7 The i_{qs} component for the stator current with PI controller under rated parameters

Figure 4.6 and Figure 4.7 displays the response of the stator current component (i_{ds} , i_{qs}) to the system conditions.

To assess the system's stability, the driving system of the PI controller was reactivated under identical conditions, whenever the rotor resistance exceeded 40% of its rated value.
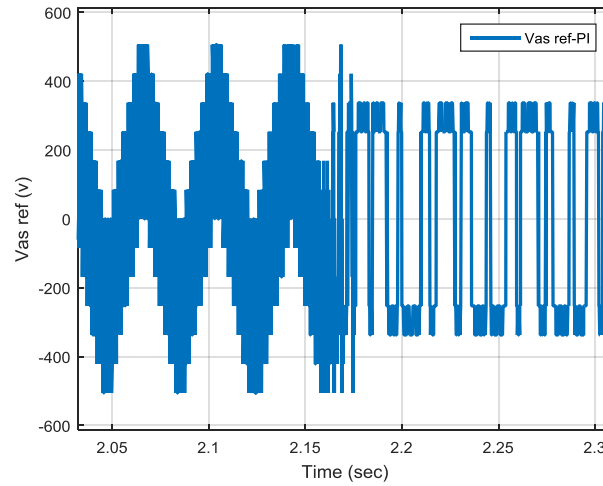

Figure 4.8 The stator voltage of the first phase with the PI controller in driving mode with changing in motor parameters
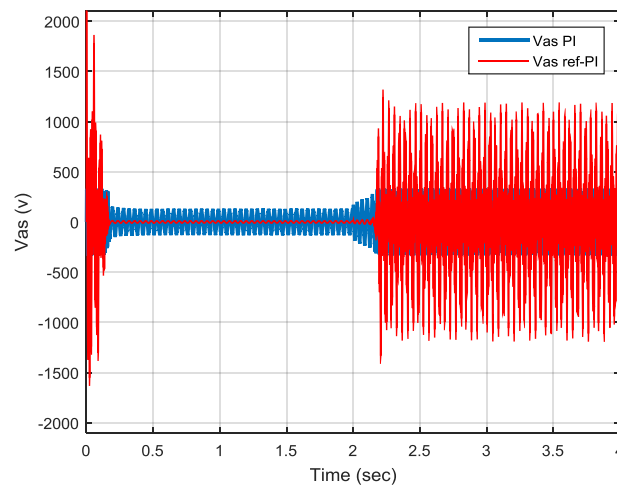

Figure 4.9 The filtered stator voltage of the first phase with the PI controller in driving mode with changing in motor parameters
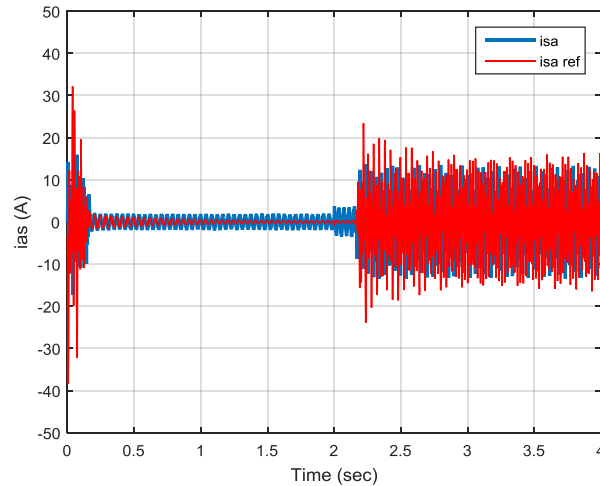
Figure 4.10 The stator current of the first phase with the PI controller in driving mode

Figure 4.8 shows the voltage amplitude with $230V_{rms}$ that is applied to the motor . The output voltage of the inverter is shown in Figure 4.9 after filtration, where an increase in the amplitude after applying the load appeared, following the value of the reference voltage (the reference of the voltage multiplied by 0.09 at first 0.2s) compared to the case of applying a rated value of rotor resistance. On the other hand, disturbances in the motor parameters cause a clear increase in the value of the supplied voltages on the stator compared to the rated values of the motor components. Figure 4.10 shows how the change affects the current, particularly after applying the load (the reference of the stator current multiplied by o.1 at first 0.2s).
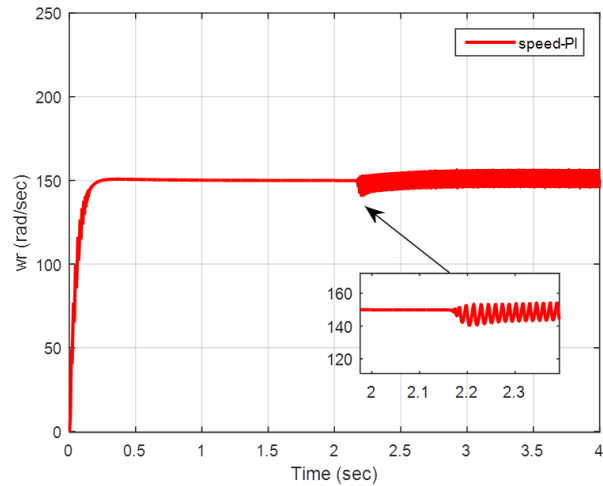
Figure 4.11 The motor speed response with the PI controller in the disturbance case
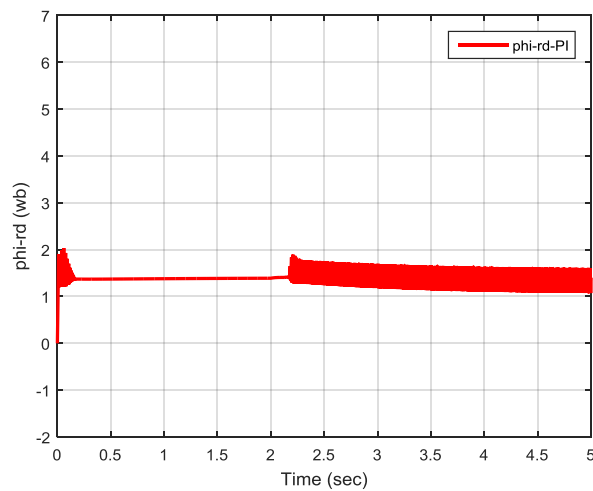

Figure 4.12 The ψ_{rd} response with the PI controller in the disturbance case

Figure 4.11 shows that the actual speed follows the required reference speed before and after applying the load torque, despite some instability after applying the load. Figure 4.12 shows that the ψ_{rd} follows the reference value. However, similar to speed control, the external disturbance causes the rotor resistance to change after applying the load, with the desired value of ψ_{rd} equal to 1.4 wb.
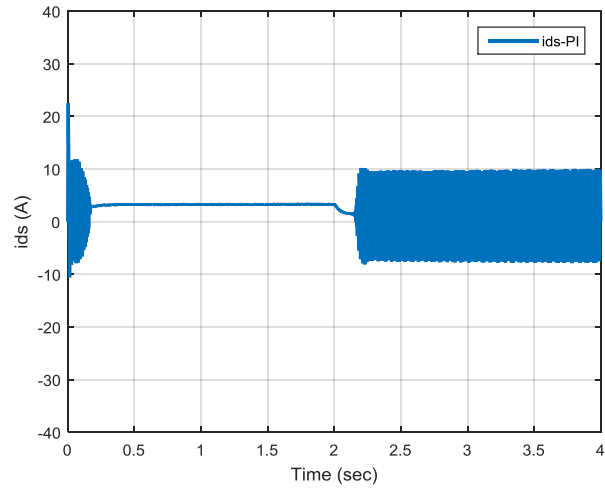
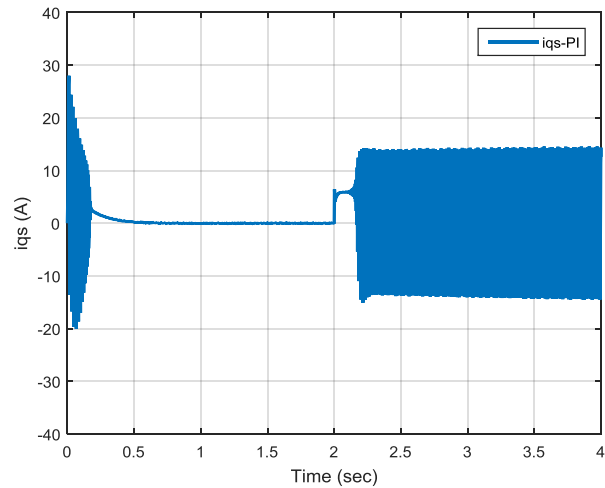Figure 4.13 The i_{ds} component for the stator current with PI controller

Figure 4.14 The i_{qs} component for the stator current with PI controller

Figure 4.13 and Figure 4.14 displays how the stator current component (i_{ds} , i_{qs}) affected by the disturbance in rotor resistance.

4.1.2 FOC Drive System with sliding mode Controller

In this section the illustration and discussion of the results of applying the FOC with SMC controller as speed of 7-PIM with rated parameters are studied. Figure 4.15 and Figure 4.17 show the existing voltage and current of the first phase with their references. Figure 4.18 illustrates what the system is doing to control the speed of the rotor, whereas Figure 4.19 demonstrates the system's response to controlling ψ_{rd}. Figure 4.20 and Figure 4.21 displays the stator current from a rotating reference frame, namely the i_{ds} and i_{qs} components.

Table 4.3 The SMC parameters for driving mode

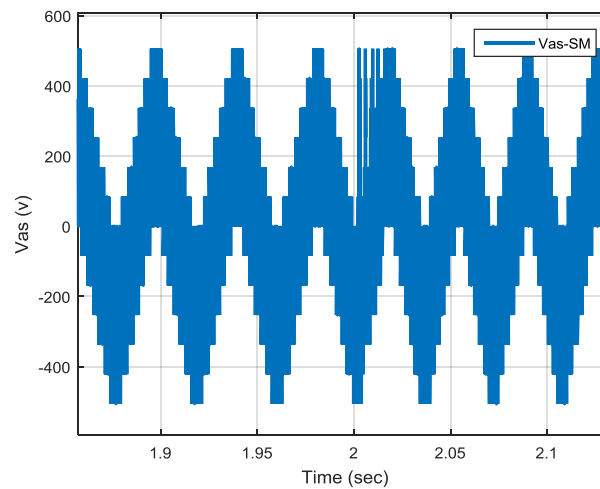|		k_1	k_2	K_3
inner loop	ψ_{rd}	1000	5	20
	speed controlling	1000	7	20
outer loop	ψ_{rd}	10	2	10
	speed controlling	10	2	10

Figure 4.15 The stator voltage of the first phase with the SM controller under rated parameters in driving mode
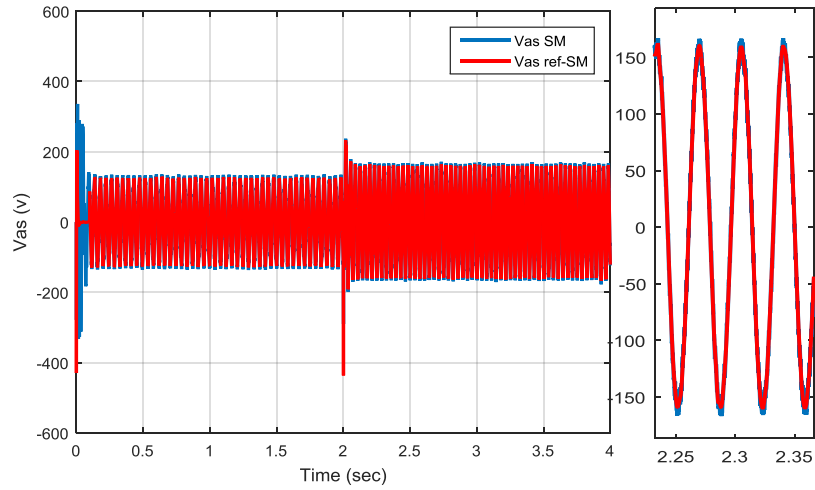
Figure 4.16 The filtered stator voltage of the first phase with the SM controller under rated parameters in driving mode
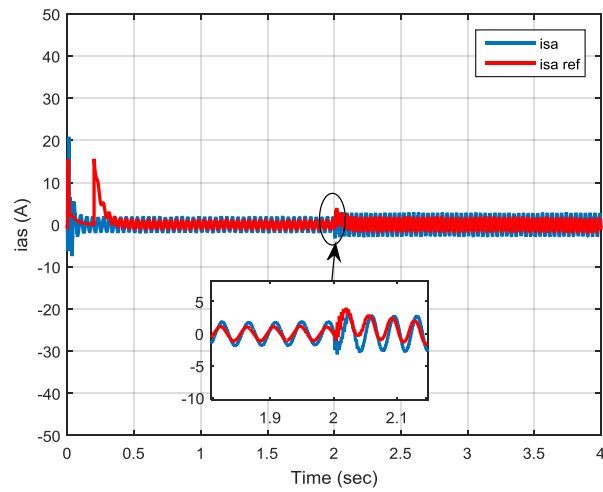

Figure 4.17 The stator current response of the first phase to its reference current with the SM controller under rated parameters
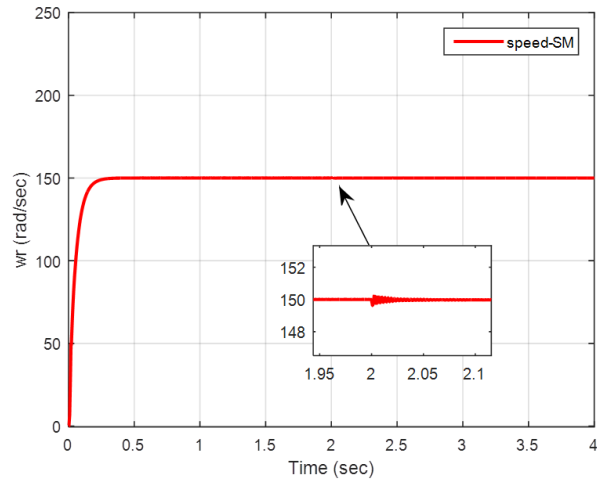
74

Figure 4.18 The motor speed response with the SM controller in the rated parameters
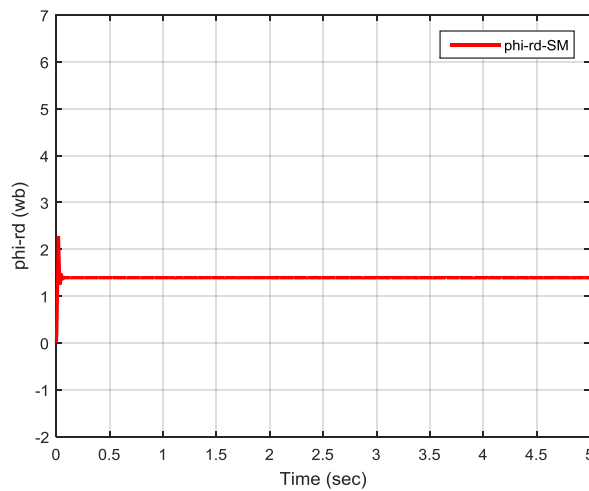

Figure 4.19 The ψ_{rd} response with the SM controller in the rated parameters

Figure 4.15 shows the voltage amplitude with $225V_{rms}$ that is applied to the motor. The output voltage of the inverter is shown in Figure 4.16 after filtration, which aligns with the filtered reference voltage (the value of the reference voltage multiplied by 0.005 at first 0.2s). Figure 4.17 illustrates how the first phase of the stator current is affected by the system operation conditions, while the stator current follow its reference value (the reference of the current multiplied by 0.005 at first 0.2s).

Figure 4.18 illustrates that the rotor's actual speed matches the desired reference speed before and after the load torque is applied, with no deviation. Figure 4.19 illustrates that the ψ_{rd} accurately tracks the reference values, with the desired value of ψ_{rd} equal to 1.4 wb (the required value).
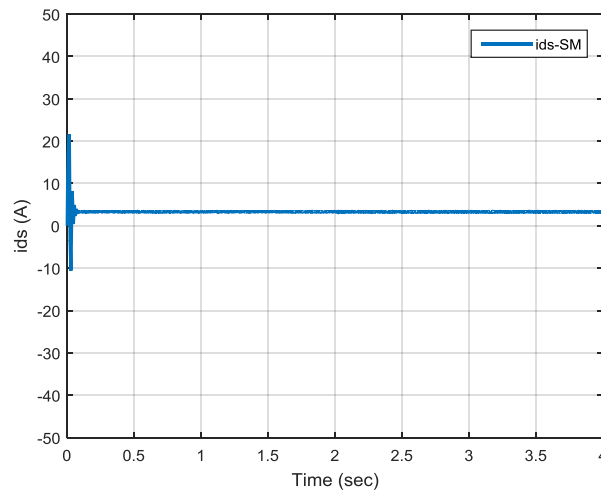

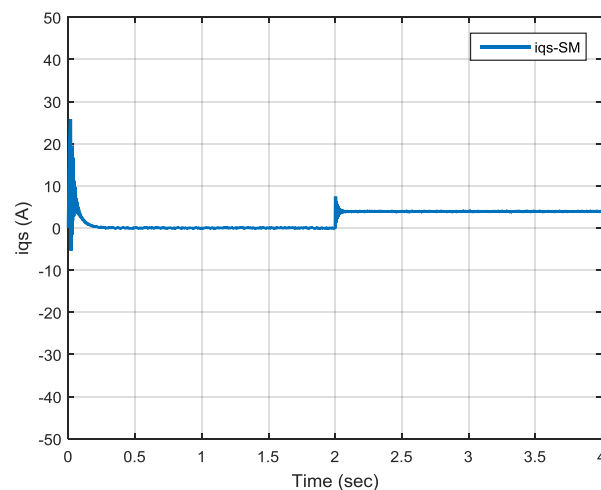Figure 4.20 The ids with the SM controller under rated parameters

Figure 4.21 The i_{qs} with the SM controller under rated parameters

Figure 4.20 and Figure 4.21 shows the rotation reference frame component of the stator current with response on applied load.

To assess the stability of the system, the FOC drive system with SMC controller was tested when the rotor resistance exceeded 40% of its rated value. On the other hand, the other parameters are still at their rated value.
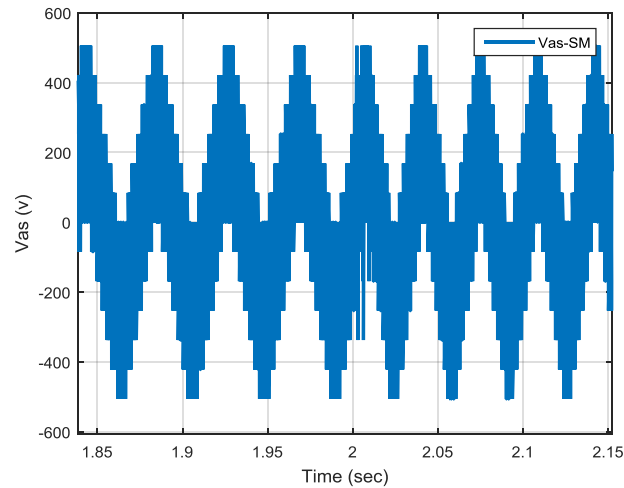

Figure 4.22 The stator voltage of the first phase with the SM controller in the disturbance case with driving mode
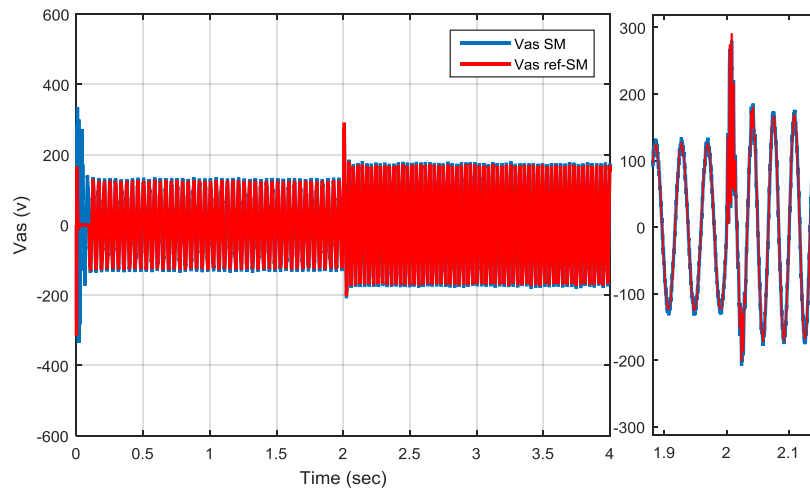
Figure 4.23 The filtered stator voltage of the first phase with the SM controller in the disturbance case
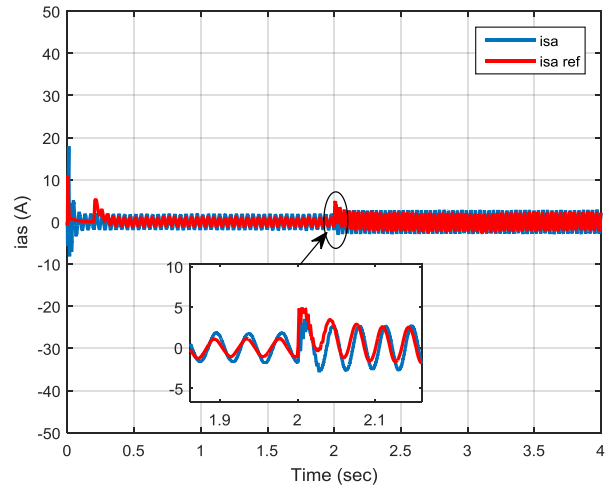
Figure 4.24 The stator current of the first phase with the SM controller in the disturbance case

Figure 4.22 shows the voltage amplitude with 225Vrms that is applied to the motor. The output voltage of the inverter is shown in Figure 4.23 after filtration, correspond to the filtered reference voltage. Figure 4.24 illustrates how the first phase of the stator current is affected by the system operation conditions, while the stator current follow its reference value imposed by the outer control loop. Noting that the reference of the current and voltage multiplied by o.1 at first 0.2s
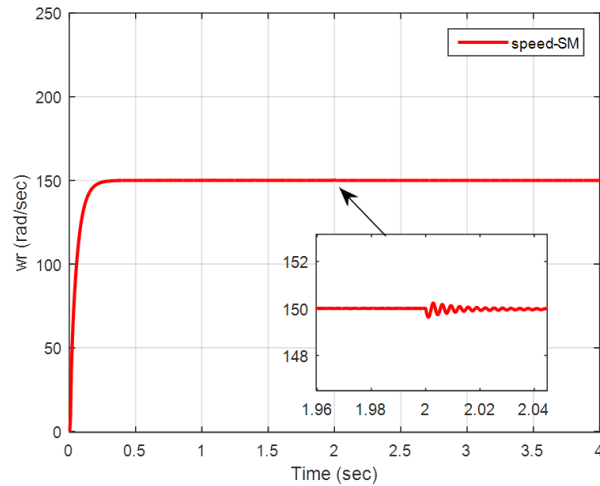
Figure 4.25 The motor speed response with the SM controller in the disturbance case
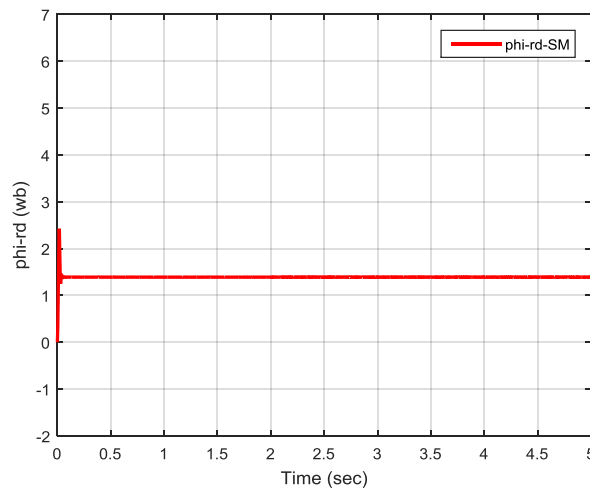
Figure 4.26 The ψrd response with the SM controller in the disturbance case

Figure 4.25 shows that the actual speed matches the required reference speed before and after applying the load torque, as it is not affected by the increase in the rotor resistance value. Figure 4.26 shows that the ψ_{rd} follows the reference value before and after applying the load torque, with the desired value of ψ_{rd} equal to 1.4 wb. It can be observed here that the efficiency of the SMC system in maintaining high dynamic

performance and speed of tracking reference signals, as well as maintaining stable motor operation despite changing system parameters.

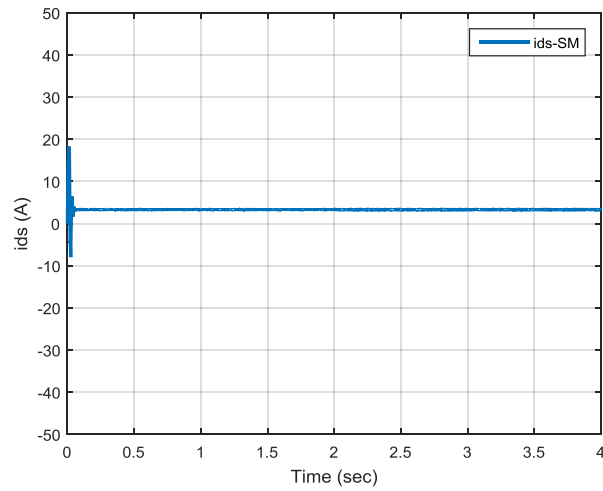
Figure 4.27 The i_{ds} with the SM controller under disturbance case
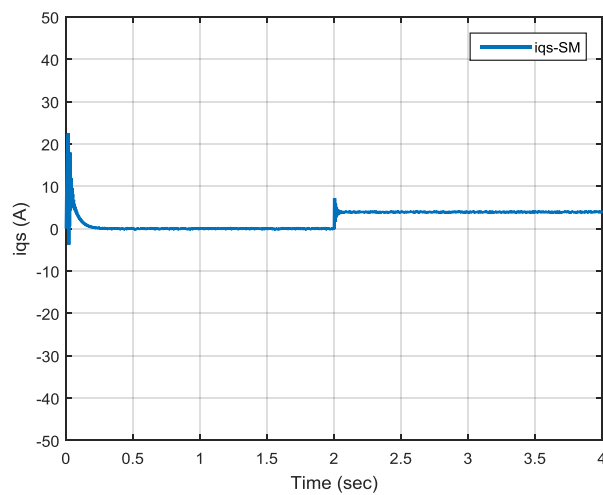
Figure 4٢٨. The i_{qs} with the SM controller under disturbance case

Figure 4.27 and Figure 4٢٨. shows the rotation reference frame component of the stator current with fast response on applied load.

4.1.3 Drive System with integral sliding mode Controller

In this section the illustration and discussion the results of applying the FOC with SMC controller as speed of 7-PIM with rated parameters are studied. Figure 4.29 and Figure 4.31 shows the existing voltage and current of the first phase and the response to their reference values. Figure 4.32 illustrates what the system is doing to control the rotor speed , whereas Figure 4.33 demonstrates the system's response to controlling the rotor flux in the d-axis in the rotating reference frame (ψ_{rd}). Figure 4.34 and Figure 4.35 display the stator current from a rotating reference frame, namely the i_{ds} and i_{qs} components.

Table 4.4 The ISMC parameters for driving mode

		k_1	k_2	K_3	K_4
inner loop	ψ_{rd}	20	5	50	300
	speed controlling	50	30	2	100
outer loop	ψ_{rd}	50	30	1	2
	speed controlling	50	30	1	2

Figure 4.29 The stator voltage of the first phase response to the reference value with the ISM controller under rated parameters

Figure 4.30 The filtered stator voltage of the first phase response to the reference value with the ISM controller under rated parameters

Figure 4.31 The stator current response of the first phase to its reference current with
the ISM controller under rated parameters

Figure 4.32 The motor speed response with the ISM controller under rated parameters

Figure 4.33 The ψrd response with the ISM controller under rated parameters
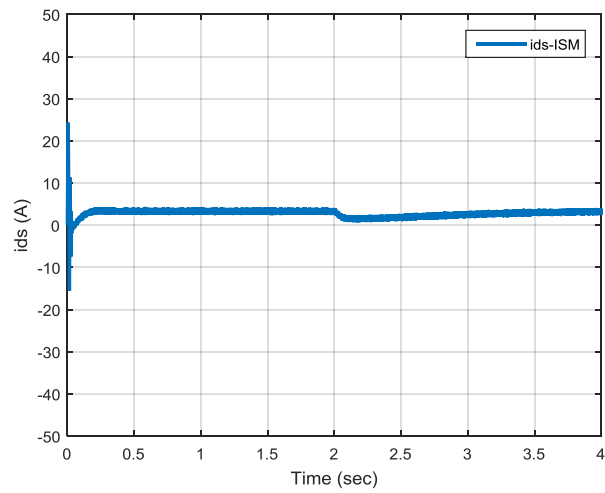
Figure 4.34 The i$_{ds}$ with the ISM controller under rated parameters
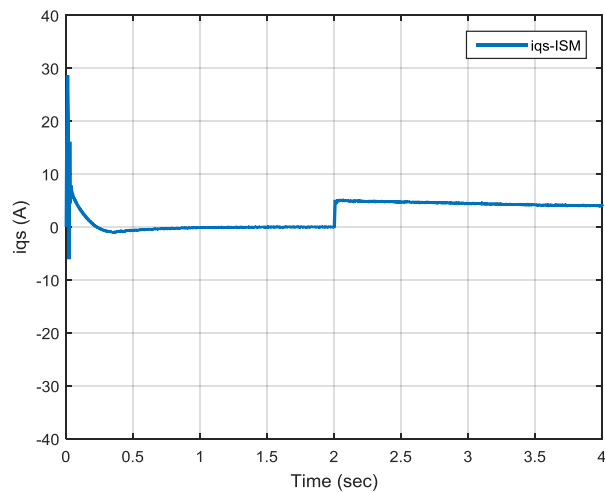
Figure 4.35 The i$_{qs}$ with the ISM controller under rated parameters

To assess the stability of the system, the FOC drive system with ISMC controller was tested when the rotor resistance exceeded 40% of its rated value. on the other hand, the other parameters are still at their rated value.
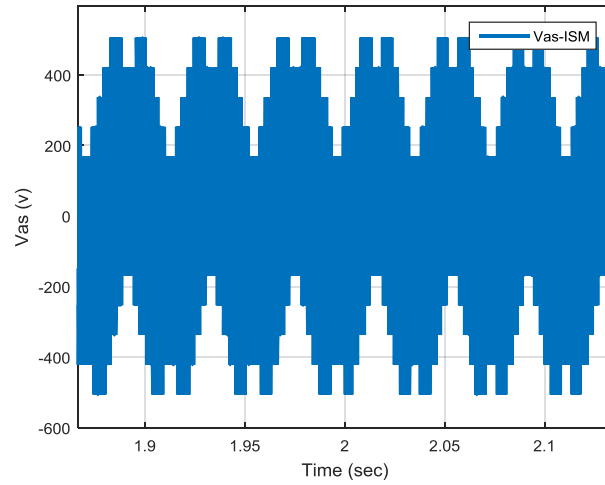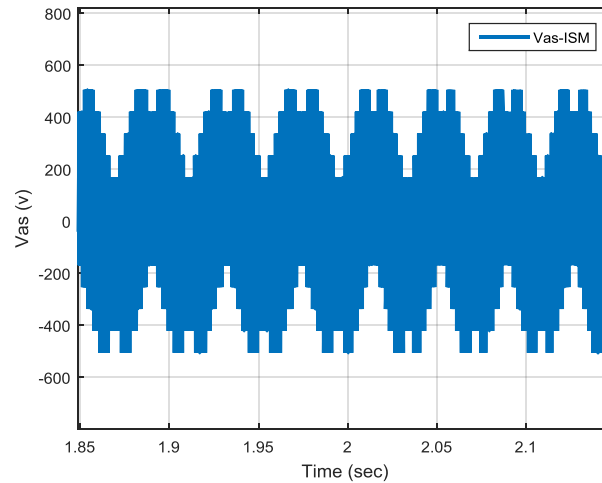

Figure 4.36 The stator voltage of the first phase response to the reference value with the ISM controller under disturbance case
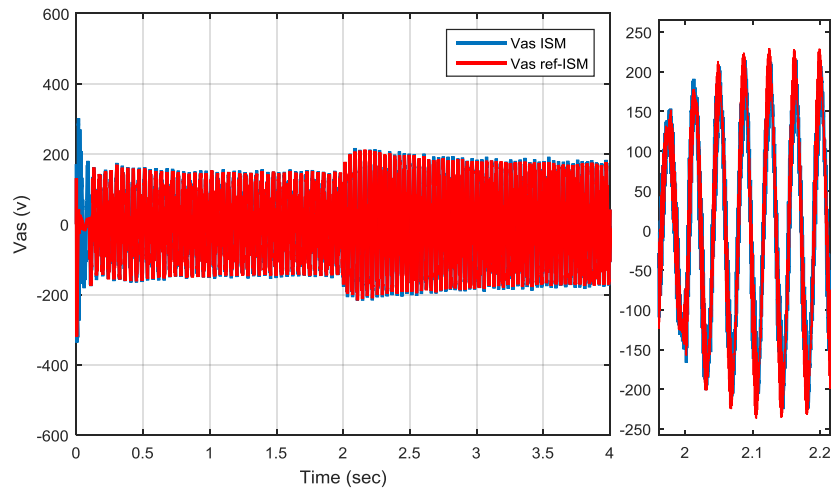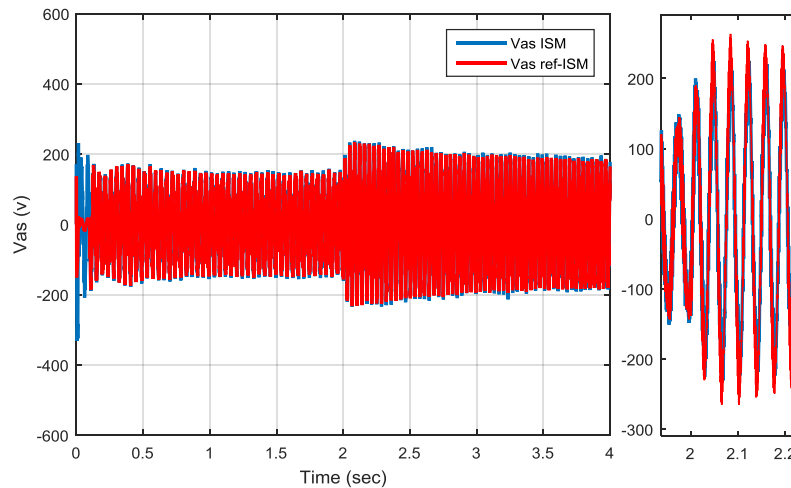

Figure 4.37 The filtered stator voltage of the first phase response to the reference value with the ISM controller under disturbance case
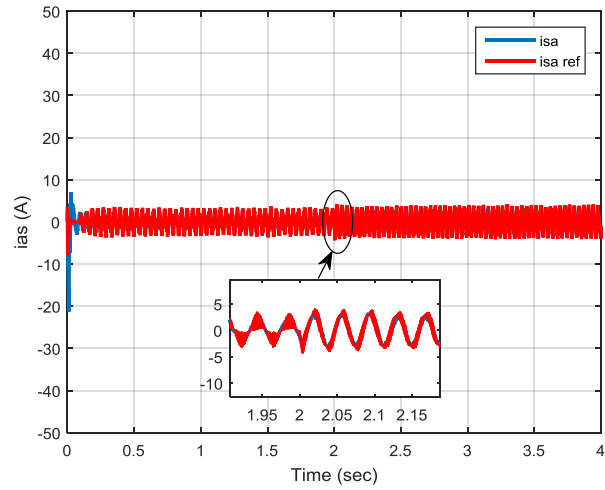
85
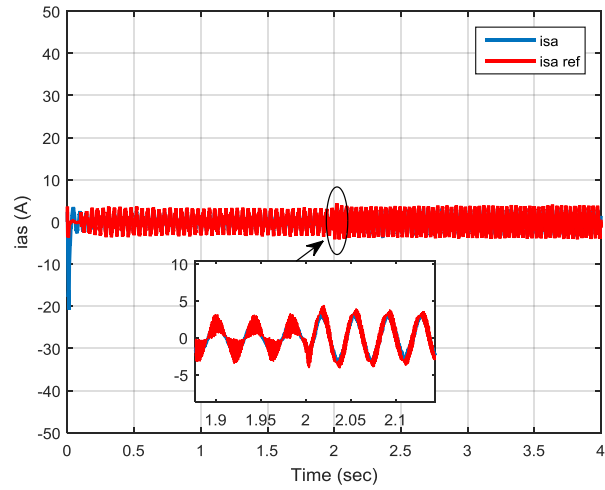
Figure 4.38 The stator current response of the first phase to its reference current with
the ISM controller under disturbance case

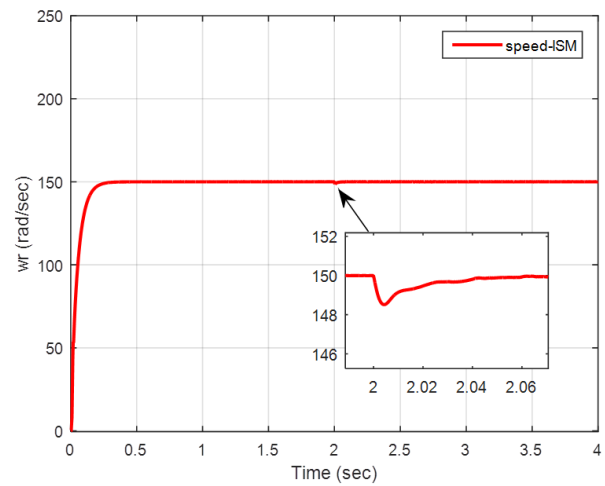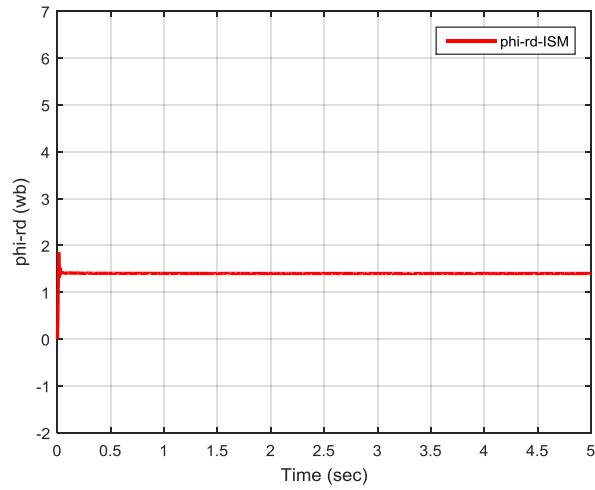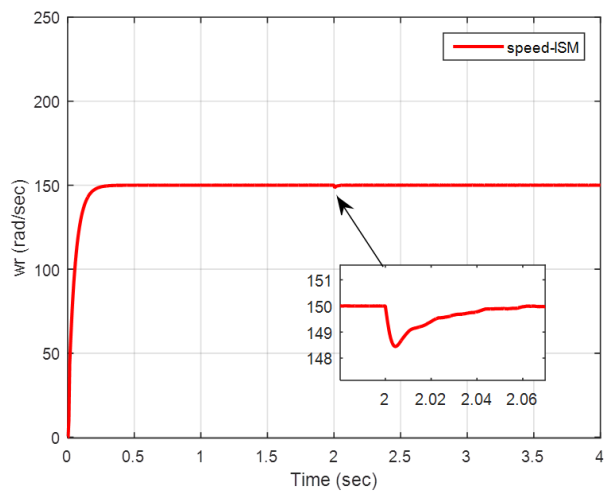Figure 4.39 The motor speed response with the ISM controller in the disturbance case
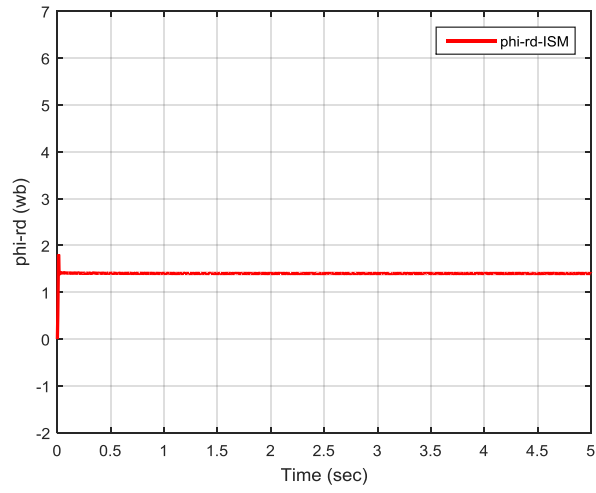
Figure 4.40 The ψ_{rd} response with the ISM controller in the disturbance case
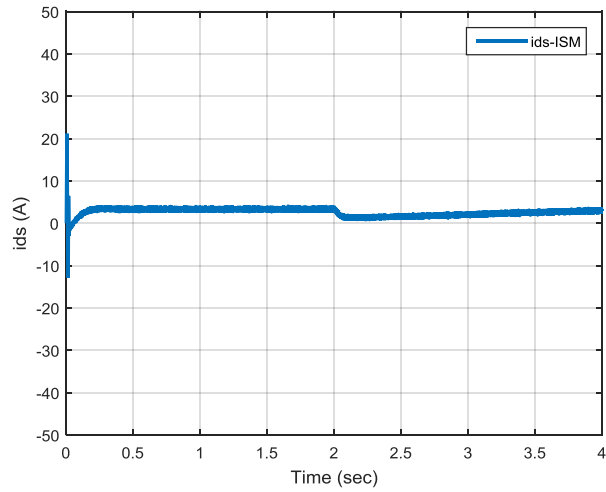
Figure 4.41 The i_{ds} with the ISM controller under disturbance case
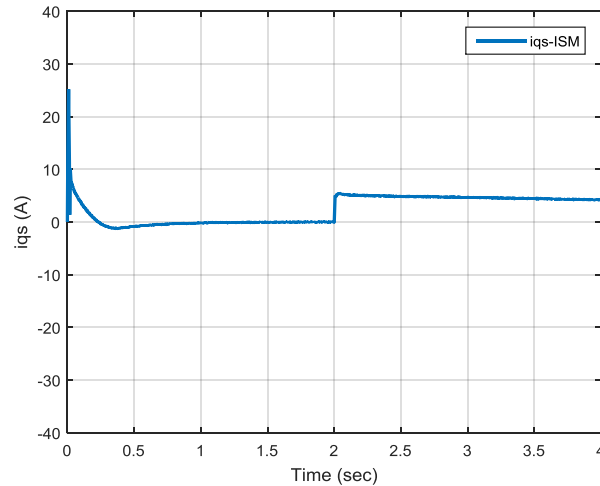
Figure 4.42 The i_{qs} with the ISM controller under disturbance case

Figure 4.36 shows the voltage amplitude with 225Vrms that is applied to the motor. The filtered output voltage of the inverter in order to understanding the behavior of the motor, which corresponds to the filtered reference voltage, is illustrated in Figure 4.37. Figure 4.38 illustrates how the outer control loop specifies the reference value for the first phase of the stator current (the reference of the current and voltage multiplied by o.1 at first 0.2s). The controlled results are close to their reference values obtained from the ISMC controller, especially the speed and flux control, as they were maintained within their reference values despite the system being non-linear. As illustrated in Figure 4.39, the actual speed remains consistent with the required reference speed both before and after the application of load torque, despite the increasing of the rotor resistance value . As illustrated in Figure 4.40, the ψrd remains with the desired value (1.4 wb) in both before and after the application of load torque . The rotation reference frame component of the stator current is illustrated in Figure 4.41 and Figure 4.42.

Table 4.5 summarization of response of driving mode controllers

	Overshoot (%)	Settling time of V_{dc} (sec)	Rise time (sec)
proportional integral	0.05	1.2	0.12
Sliding mode control	0	0.25	0.12
Integral Sliding mode control	0	0.5	0.12

4.2 Results of Charging System Simulation

To achieve an integrated charging system for electric vehicles, the same components of the seven-phase motor used in the driving process mentioned earlier were also employed in the charging process (L_s and R_s). As clarified in Chapter Four, the charging process in this thesis is bifurcated into two segments based on the number of phases of the power supply, while the battery parameters listed in Table 4.1.

Table 4.6 battery parameters

Rated power	3.954 kw
Rate battery voltage	507V
cc charging current	7.8 A
cv charging voltage	575V
Equivalent Battery impedance	50 Ω

4.2.1 Seven-Phase Supply

This section applied a source voltage of 220 V, regardless of the method for obtaining the seven-phase source. PI controller is applied in outer and inner loops in order to obtain the desired DC-output voltage.

Table 4.7 The PI parameters for charging mode with 7-phase source

		k_p	k_i
inner loop	i_d	100	250
	i_q	600	700
outer loop		0.1	3
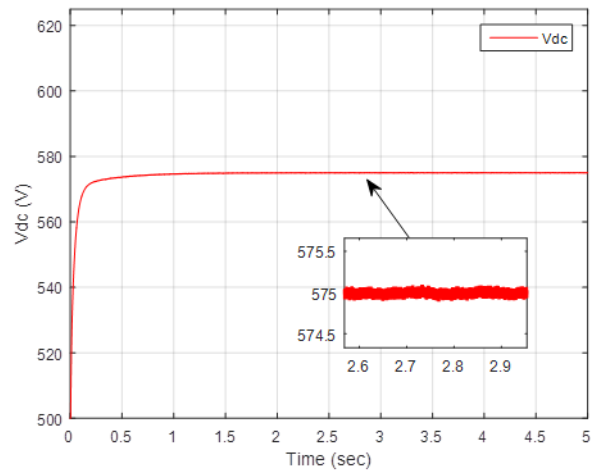
Figure 4.43 The DC output voltage with the seven-phase supply
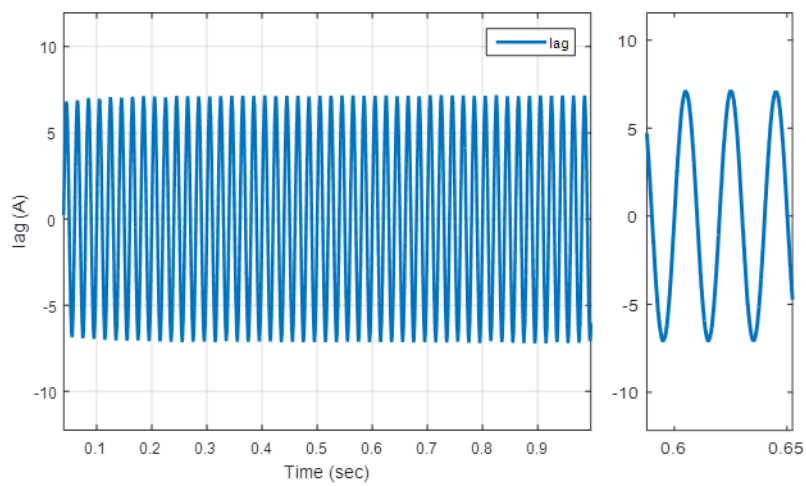
Figure 4.44 The first phase grid current of seven-phase source
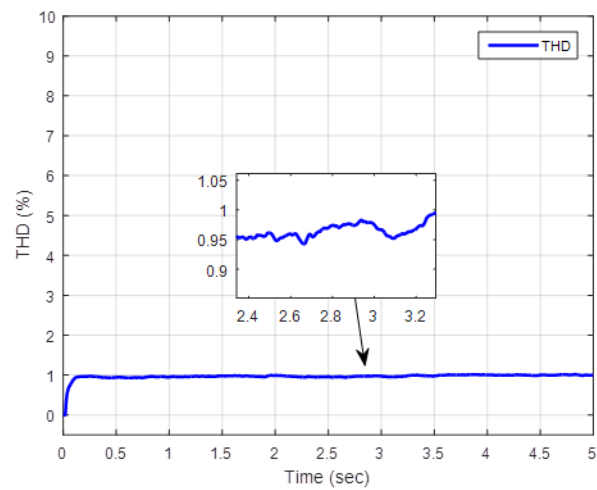
Figure 4.45 The harmonic description of the first grid current
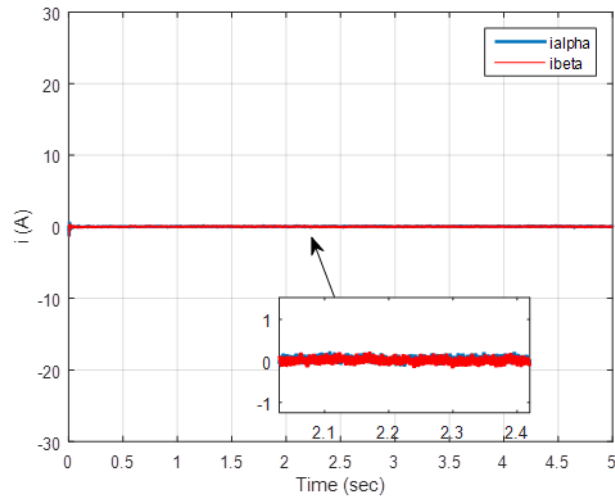
Figure 4.46 The source current first plane in a stationary reference frame

Figure 4.47 The source current second plane in a stationary reference frame in charging mode
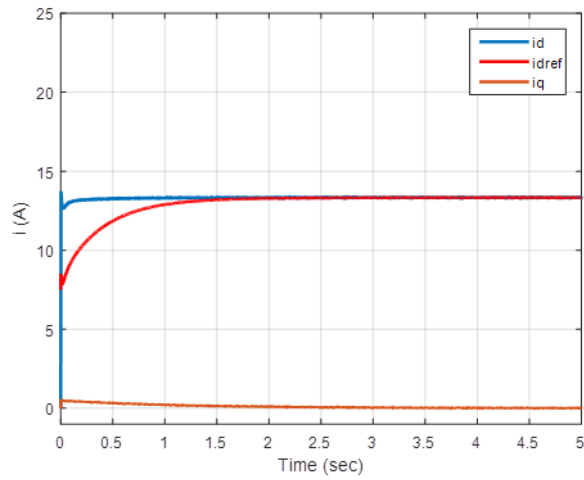
Figure 4.48 The idg and iqg response
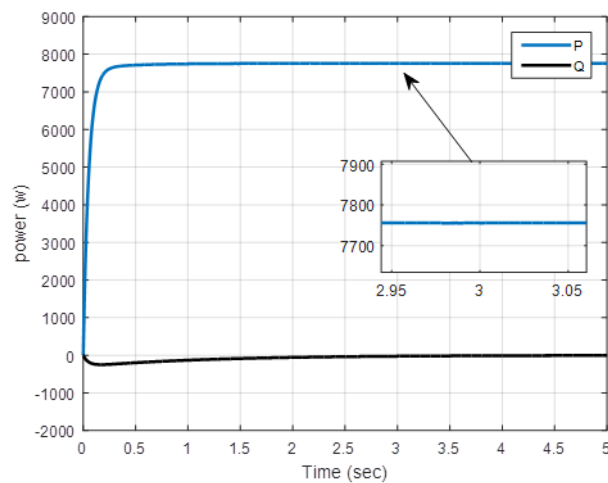
Figure 4.49 The active and reactive power gained with the seven-phase supply

Figure 4.43 shows the response of the output voltage Vdc to the required reference voltage by boosting the grid voltage to 575 V, as it shows the speed of the system's response with a static error rate that may be non-existent. Figure 4.44shows the first phase grid current projected onto the first phase of the stator coil of a seven-phase motor, as it is clear that the disturbances accompanying the drawn current are non-existent. It is worth noting that the currents of all phases are equal to each other as a

result of the equal values of the inductance and resistance of the stator for all phases. Figure 4.45 shows the percentage value of the THD for the first phase current from the source side, that does not exceed 1%, which demonstrates the ability of the PI controller to regulate linear systems as a result of the load being balanced and the current drawn from all phases being equal. Figure 4.46 and Figure 4.47 show the organization of the source currents in a stationary reference frame as a result of the phase conversion between the source and the motor to maintain the motor in a state of rest. It shows that the values of the currents in the first plane, which is responsible for generating torque, are equal to zero, ensuring that the motor does not rotate. Figure 4.48 shows the response of the grid current i_d to the reference current id* (generated from the outer loop). As for the current iq, it was regulated at zero in order to achieve a unity power factor. Figure 4.49 shows the active power and reactive power of the charger, as the value of the power gained from the system is 7750 W.

4.2.2 three-Phase Supply

In the case of a three-phase source with 220 volts equipped, the inverter is regulated as a step-up rectifier to obtain a 575 volt DC bus voltage.

4.2.2.1 virtual proportional integral Controller

The VPI controller was used to overcome the unbalanced state resulting from connecting a three-phase source to a seven-phase motor and inverter within an integrated charging system for electric vehicles.

Table 4.8 The VPI parameters for charging mode with 3-phase source

				k_p	k_i
inner loop	i_d			6777	861
	i_q			8000	2700
	VPI	i_d		1000	1000
		I_q		1000	1000
outer loop				0.1	3
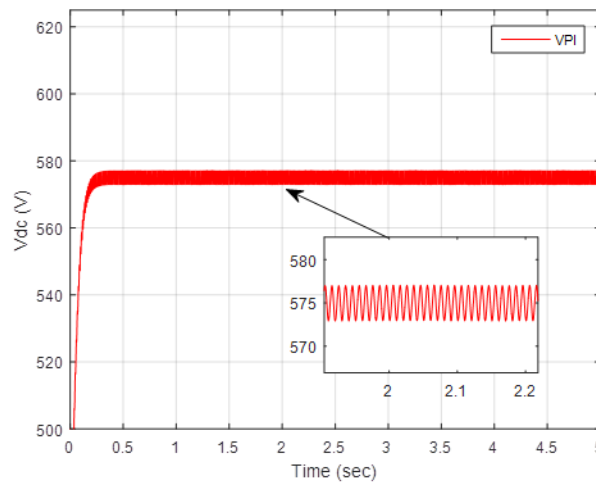
Figure 4.50 The DC output voltage with the VPI controller
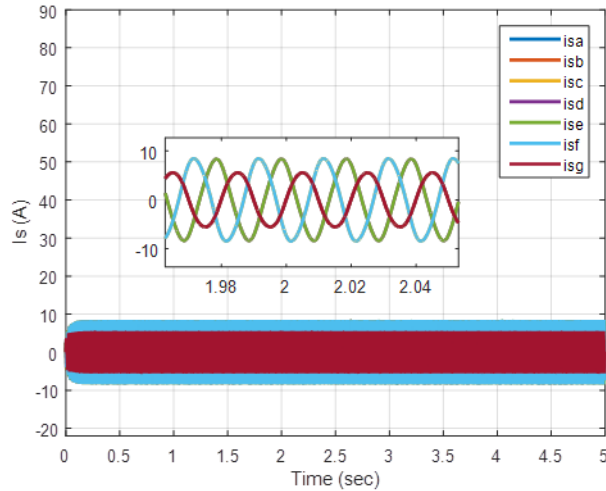
Figure 4.51 The stator current supplied from three-phase source

Figure 4.52 The grid current supplied from three-phase source

Figure 4.50 illustrates the relationship between the output voltage V_{dc} and the desired reference voltage. It demonstrates that the speed at which the system responds (settling time) is 0.27 sec to reach the desired value and indicates that the system has no static error present, although there is a ripple at the output equal to 1 %. Figure 4.51 shows the current passing through the seven phases of the motor coils, noting that the current passing through coils A, B, and G is equal to each other but contain a lower amplitude compared to the current passing through the other coils.

96

Figure 4.53 The harmonic description of the grid current

Figure 4.54 The source currents in a stationary reference frame for the first plane
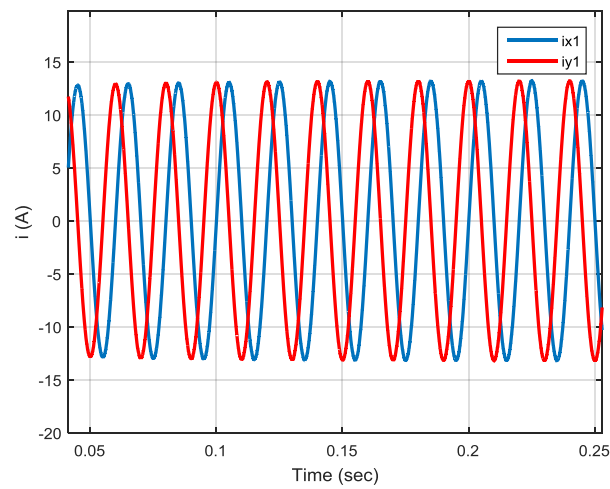
Figure 4.52 shows the grid current projected onto the stator coil of a seven-phase motor, as it is clear that the disturbances accompanying the drawn current are non-existent. It is important to highlight that the current in all phases is equal, which compensates for the imbalance caused by connecting the seven phases of the motor to a three-phase power supply. Figure 4.53 shows the percentage value of the THD for the three-phase grid current from the source side, which does not exceed 2.6%. The reason for this is the VPI controller's capability to select and eliminate the

97

2nd harmonic in systems caused by unbalanced loads and uneven current flow across motor phases.
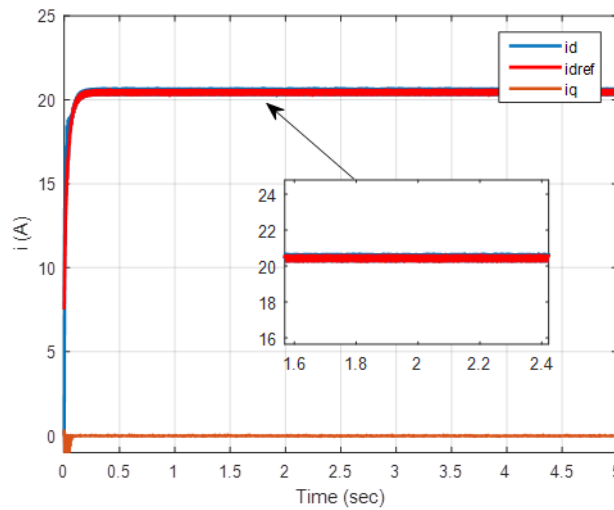
Figure 4.55 The idg and iqg response with VPI controller
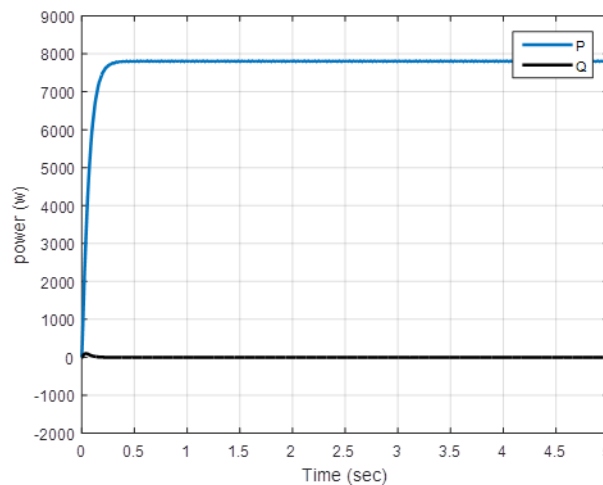
Figure 4.56 The active and reactive power gained with the three-phase supply in the VPI controller

Figure 4.54 depicts the currents passing through the motor coils in a stationary reference frame. Essentially, only the α component is created on the torque-producing (α-β) plane. Consequently, the field is pulsating, which disables the generation of initial torque. Figure 4.55 shows that for the values of the components of the grid current (i_d, i_q), the q-component remains constant at zero, whereas the d-component adheres to its

reference without any leftover mistakes. Figure 4.56 shows the active power and reactive power of the charger, as the value of the power gained from the system is 7750 W.

4.2.2.2 sliding mode Controller

The SM controller was used to rectify the imbalanced condition that arises when a three-phase source is connected to a seven-phase motor and inverter in an integrated charging system, leading to nonlinearity.

Table 4.9 The SMC parameters for charging mode with 3-phase source

|		k_1	k_2	K_3
inner loop	i_d	5000	500	700
	i_q	5000	1000	700
outer loop		$k_p = 0.1$	$K_i = 3$	
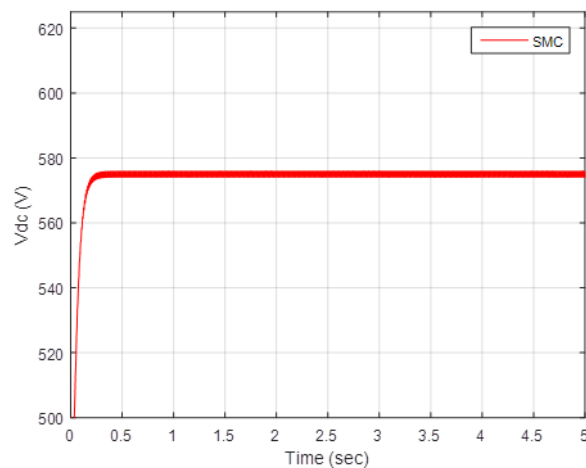
Figure 4.57 The DC output voltage with the SM controller
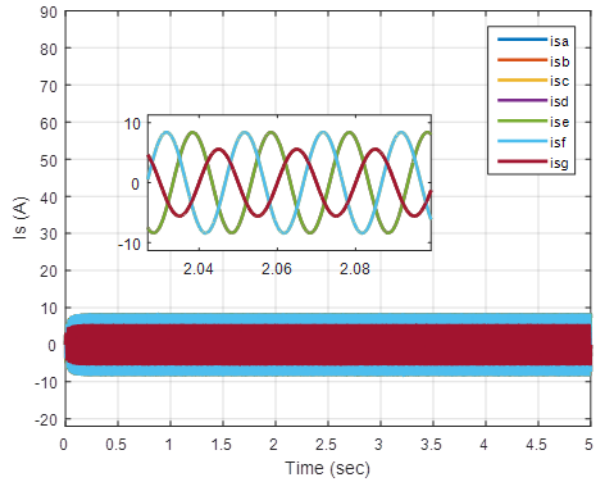
Figure 4.58 The stator current supplied from three-phase source

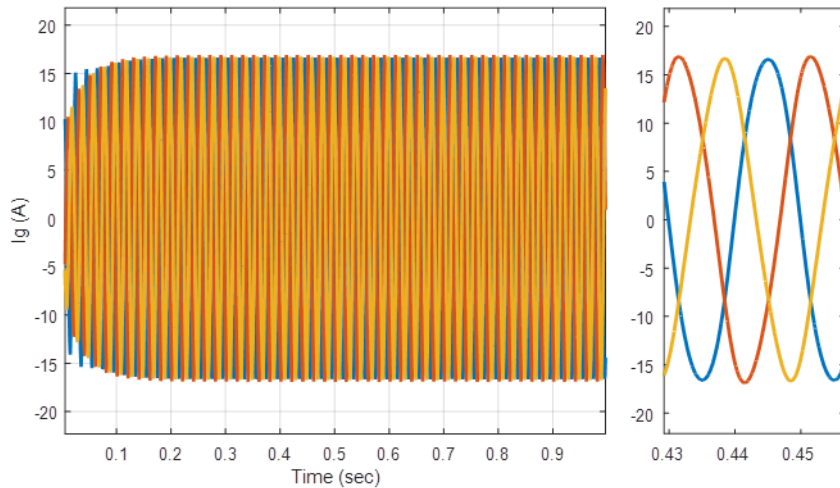Figure 4.59 The grid current supplied from three-phase source
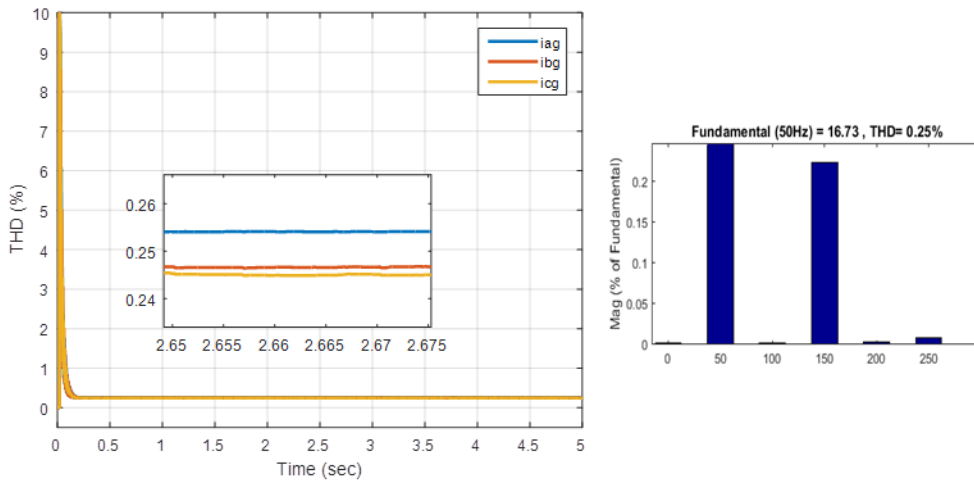
Figure 4.60 The harmonic description of the grid current with SMC

100
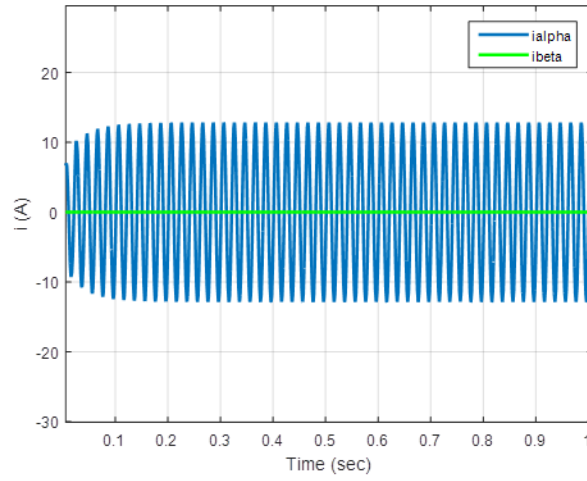
Figure 4.61 The source currents in a stationary reference frame for the first plane
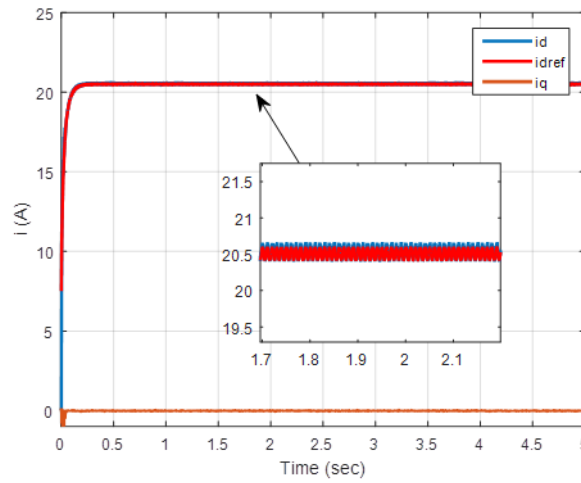
Figure 4.62 The idg and iqg response with SMC
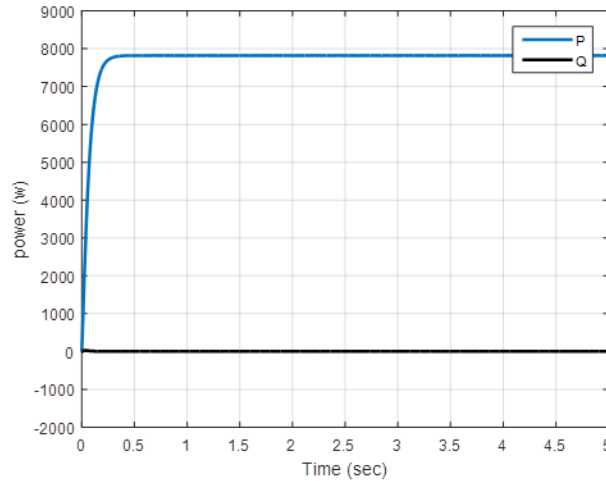
Figure 4.63 The active and reactive power gained with the three-phase supply in the SMC

Figure 4.57 displays the correlation between the DC bus voltage V_{dc} and the reference voltage at 575 V. It shows the system's highest responsiveness (settling time equal to 0.22 sec) and confirms that the system does not have any static errors with a DC bus voltage ripple less than 0.3%. Figure 4.58 shows the current passing through the seven phases of the motor coils, noting that the current passing through coils A, B, and G is equal to each other but contain a lower amplitude compared to t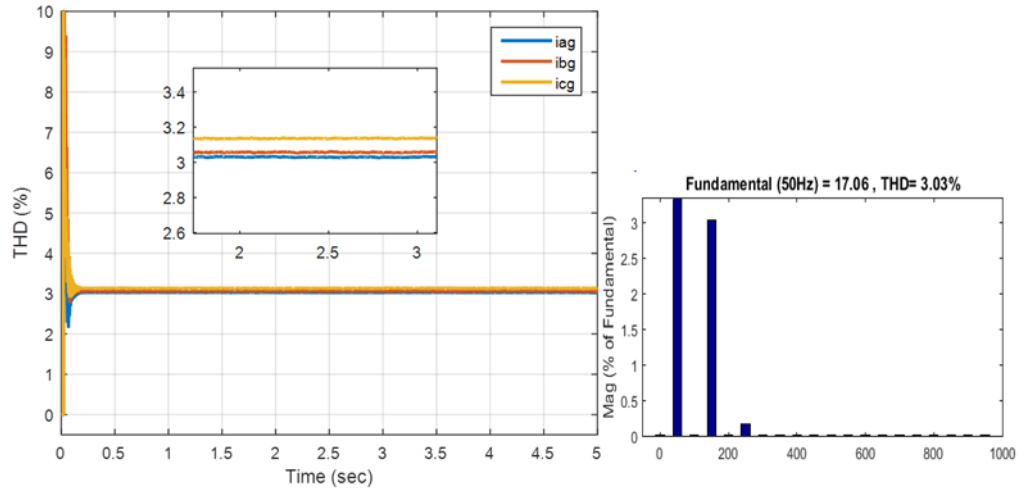he current passing through the other coils. Figure 4.59 shows the grid current supplied to the stato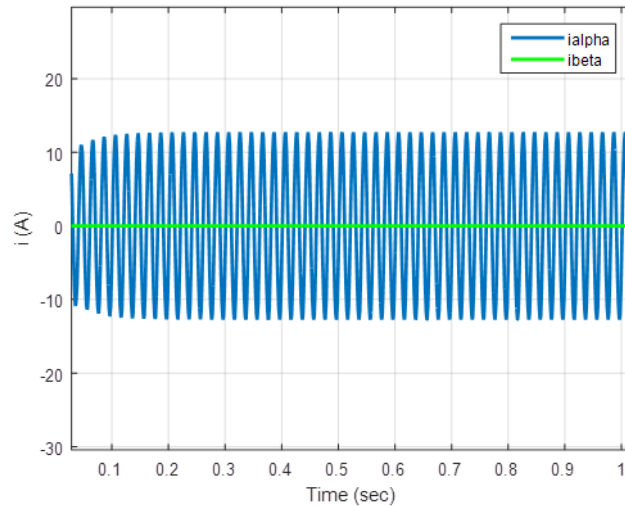r coil of a seven-phase motor, as it is clear that the current in all phases is equal, which compensates for the nonlinearity caused by connecting the seven phases of the motor to a three-phase power supply. Figure 4.60 displays the THD percentage of the three-phase grid current from the source side, which remains below 0.26%. The reason for this good current quality is the SM controller's ability to regulate the system suffering from disturbance caused by unbalanced loads and uneven current flow across motor phases in this case. It is important to mention that the THD in the i_{ag} is greater than in the other two phases. This is because the equivalent inductance related to the first phase grid current is less than the equivalent inductance related to

102

the other phases. Figure 4.61 depicts the currents passing through the motor coils in a stationary reference frame. Essentially, the α component is only created on the torque-producing (α-β) plane. Consequently, the field is pulsating, which disables the generation of initial torque. Figure 4.62 shows that for the values of the components of the grid current (i_d,i_q), the q-component remains constant at zero, whereas the d-component adheres to its reference without any leftover mistakes. Figure 4.63 shows the active power and reactive power of the charger, as the value of the power gained from the system is 7750 W.

4.2.2.3 PI Controller with separation method

The PI controller was used to overcome the unbalanced state by separating the components of the network current into positive and negative sequences, then eliminating the negative series that is generated due to connecting a three-phase source to a seven-phase motor and inverter within integrated charging.

Table 4.10 The PI parameters for charging mode with 3-phase source

|		k_p	k_i
inner loop	i_d+	6777	861
	i_q+	8000	2700
	i_d-	8000	2700
	i_q-	8000	2700
outer loop		0.1	3
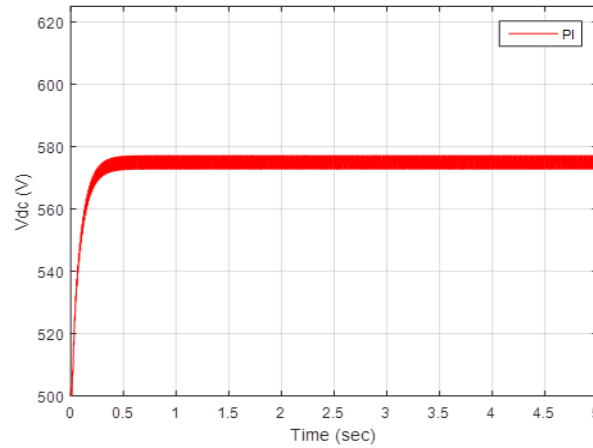
Figure 4.64 The DC output voltage with the PI controller

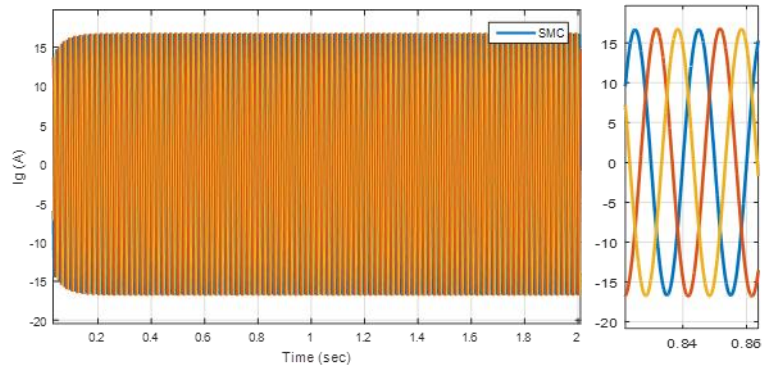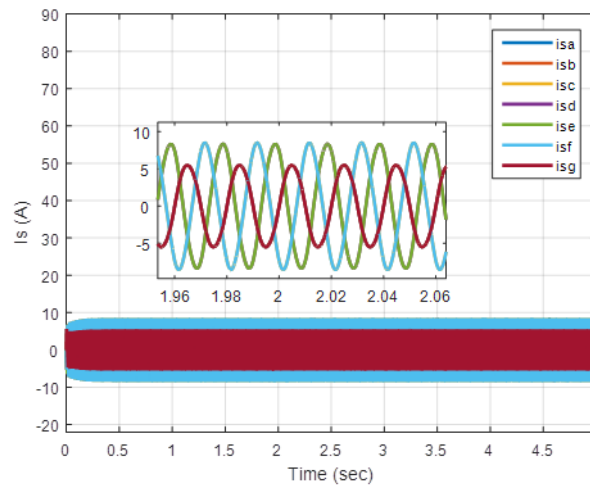Figure 4.65 The stator current supplied from the three-phase source in the PI controller

Figure 4.64 illustrates the control of the DC bus voltage V_{dc} and the reference voltage (575 V). It showcases the system's responsiveness with a settling time less than 0.32 seconds and confirms that the system does not have any static error with a percentage of V_{dc} ripple equal to 1.3%. Figure 4.65 shows the current passing through the seven phases of the motor coils, noting that the current passing through coils A, B, and G is equal to each other but contain a lower amplitude compared to the current passing through the other coils.
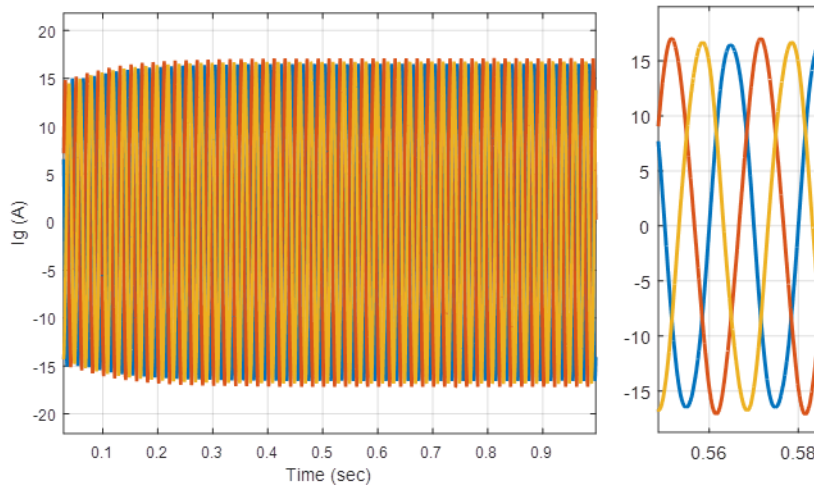
Figure 4.66 The grid current supplied from the three-phase source in the PI controller
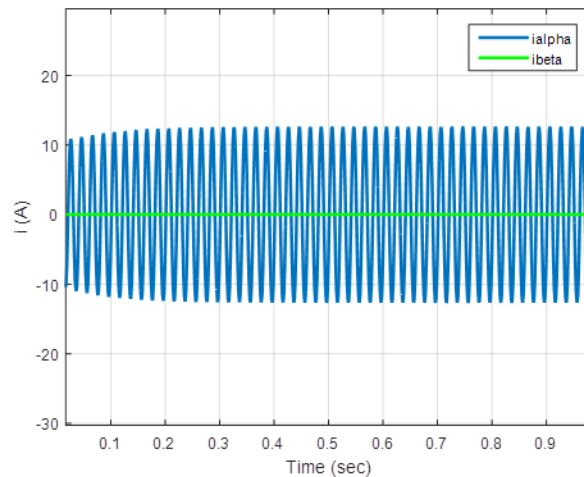
Figure 4.67 The source currents in a stationary reference frame for the first plane with the PI controller

Figure 4.66 shows the grid current supplied to the stator coil of a seven-phase motor, as it is clear that the current in all phases is equal, which compensates for the nonlinearity caused by connecting the seven phases of the motor to a three-phase power supply. Figure 4.67 depicts the currents passing through the motor coils in a stationary reference frame. Essentially, the α component is created on the torque-producing (α-β) plane. Consequently, the field is pulsating, which disables the generation of initial torque.
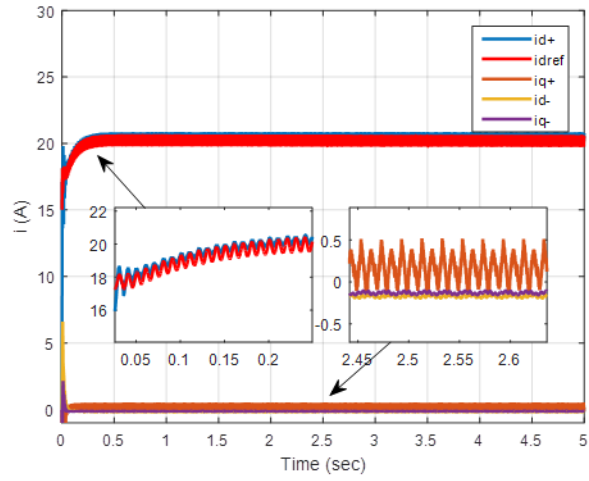
Figure 4.68 The idg and i$_{qg}$ response with the PI controller
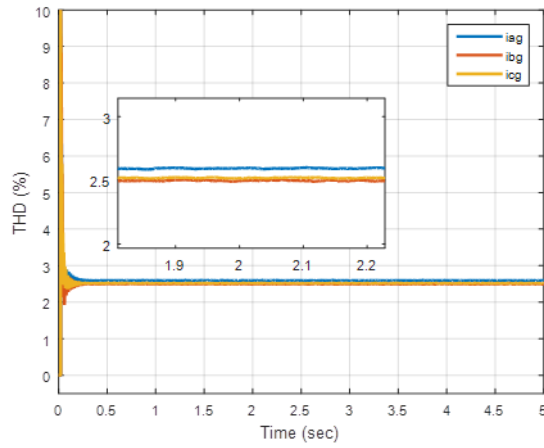
Figure 4.69 The harmonic description of the grid current with the PI controller
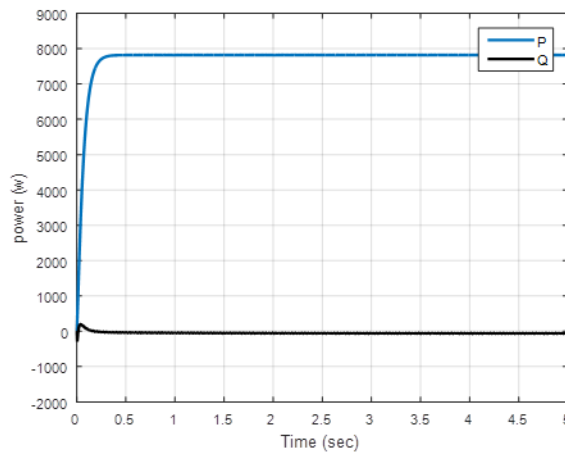
Figure 4.70 The active and reactive power gained with the three-phase supply in the PI controller

Figure 4.68 shows that the values of the components of the grid current (i_d^+, i_q^+, i_d^-, i_q^-), the i_q^+, i_d^-, i_q^- component remains constant at zero to eliminate the negative component aligned with achieving unity power factor, whereas the d-component adheres to its reference without any leftover mistakes. The absence of excessive ripple in these currents is evident, thanks to the isolation process applied to the network current components. This isolation process enables the PI controller to effectively regulate these currents. Figure 4.69 displays the THD percentage of the three-phase grid current from the source side, which remains below 2.5%. The reason for this good current quality is the isolation block through which the current components were isolated into positive and negative components, where the negative components were eliminated. It is important to mention that the THD in the i_{ag} is greater than in the other two phases. This is because the equivalent inductance related to the first phase grid current is less than the equivalent inductance related to the other phases. Figure 4.70 shows the active power and reactive power of the charger, as the value of the power gained from the system is 7750 W.

The SM controller demonstrates greater effectiveness when dealing with disturbances compared to other controllers, specifically selective harmonic elimination SHE approaches. This occurs because selective controllers only address a certain harmonic and do not provide any therapy for additional harmonics if they are present.

Table 4.11 Comparison of controlling methods for three-phase source

	Ripple of V_{dc} (%)	Settling time of V_{dc} (sec)	THD of i_{ag}	N. of controllers
Virtual proportional integral	1	0.25	2.5	5
Proportional integral	1.3	0.37	3.2	5
Sliding mode control	0.3	0.19	0.25	3

When comparing the results of charging from a seven-phase source with a three-phase source, we observe that, under identical circumstances, the overall power output of the system using a three-phase source is equivalent to that of the system using a seven-phase source. However, the three-phase system requires twice as much current from the grid.

CHAPTER 5 : Conclusion

5.1 Introduction

In the last few years, with the increase in population, means of transportation consume energy sources, especially fossil fuels, which are the main source of greenhouse gas emissions. Transportation   contributes to 15% of global heat emissions, and it is anticipated to maintain its position while progressing in the direction of the future. In addition to the limited availability of fossil fuels and the escalating difficulties associated with climate change, it is suggested that the utilization of internal combustion engine vehicles will reduce substantially in the upcoming years as they are progressively substituted by electric-powered vehicles. To achieve this objective, the primary factors for successive shifting are to design and create suitable battery chargers in addition to a reliable driving system. These chargers should be integrated into the vehicle to charge the battery quickly. The biggest challenge facing this type of charger is rotating the motor during the charging period. Multi-phase motors can give greater freedom in solving the problem of engine rotation during charging, in addition to being more reliable during driving.

5.2 Conclusions

1. In the propulsion mode, sliding mode controllers (SMC, ISMC) regulate motor speed better than the PI controller when system components change.
2. However, adjusting rotor flux to maintain a consistent flux value despite motor parameter changes for avoiding magnetic saturation.

3. The sliding mode controllers (SMC, ISMC) enhances reference signal tracking, proving that the motor speed retains its reference value even with external torque.

4. The sliding mode controllers (SMC, ISMC) maintain the motor's current and voltage values within their rated values without an unacceptable increase in these values, unlike the PI controller.

The second part of the thesis dealt with the driving elements, which represent the inverter and the motor coils, which represent a filter for passing AC currents from the grid and obtaining a DC voltage by applying VOC technique. The process of passing current through open motor windings must ensure that no torque is generated. It was analyzed mathematically and proven in the simulation part, adhering to the published literature in this field.

1. Employing a seven-phase network ensures that no electric field is excited in the motor coils.

2. The system charging from a three-phase source has pulsing torque in the stator coils but cannot generate torque.

3. Special controllers were used to control the components of the current in the inner loop, such as the VPI, SMC, and PI with separation part to overcome the unbalance current from three-phase source.

4. The efficiency of the sliding-mode controller in eliminating harmonics is greater than the ability of selective controllers, in addition to achieving a higher response speed and a lower fluctuation in the output voltage than other controllers.

5.3 Future Works

1. Investigation of the effects of the charging procedure on the driving equipment during integration charging.
2. Studying the impact of this type of engine on users when charging the vehicle.
3. Studying the behavior of MP motors in driving and charging operations during the presence of a defect in one of the stator coils.
4. Investigation of the behavior of this type of charger in the case of a disturbance in the network voltage while selecting a suitable PLL to deal with this disturbance.
5. Using multi-level inverters with multi-phase motors to obtain the fastest integrated charging, overcoming off-board charging.
6. Providing a study on connecting the active filter with the integrated charging circuit to avoid using the motor windings as a filter and to ensure the elimination of the motor rotation problem.

References

[1] D. L. Bleviss, "Transportation is critical to reducing greenhouse gas emissions in the United States," *WIREs Ener. Env.*, no. pp. 1–16, 2020, doi: 10.1002/wene.390.

[2] D. Purushothaman, R. Narayanamoorthi, A. Elrashidi, and H. Kotb, "A Comprehensive Review on Single-Stage WPT Converter Topologies and Power Factor Correction Methodologies in EV Charging," *IEEE Access*, vol. PP. 135529 - 135555, 2023, doi: 10.1109/ACCESS.2023.3338164.

[3] J. De Santiago *et al.*, "Electrical Motor Drivelines in Commercial All-Electric Vehicles : A Review," *IEEE Trans. Transp.,* vol. 61, no. 2, pp. 475–484, 2012.

[4] M. M. Alwan, Yasir M.Y. Ameen "Analysis and Simulation of Integrated onboard chargers of EV with multi-phase propulsion system," M.Sc. Thesis in Electrical Engineering / Electrical Engineering, College of Engineering, University of Mosul, 2024.

[5] S. Sharma, M. V. Aware, and A. Bhowate, "Integrated Battery Charger for EV by Using Three-Phase Induction Motor Stator Windings as Filter," *IEEE Trans. Transp. Electrif.*, vol. 6, no. 1, pp. 83–94, 2020, doi: 10.1109/TTE.2020.2972765.

[6] M. Y. Metwly, M. S. Abdel-Majeed, A. S. Abdel-Khalik, R. A. Hamdy, M. S. Hamad, and S. Ahmed, "A Review of Integrated On-Board EV Battery Chargers: Advanced Topologies, Recent Developments and Optimal Selection of FSCW Slot/Pole Combination," *IEEE Access*, vol. 8, pp. 85216–85242, 2020, doi: 10.1109/ACCESS.2020.2992741.

[7]   E. Levi and S. Member, "Multiphase Electric Machines for Variable-Speed Applications," *IEEE Trans. Transp.,* vol. 55, no. 5, pp. 1893–1909, 2008.doi: 10.1109/TIE.2008.918488.

[8]   M. Jones, S. N. Vukosavic, D. Dujic, and E. Levi, "A synchronous current control scheme for multiphase induction motor drives," *IEEE Trans. Energy Convers.*, vol. 24, no. 4, pp. 860–868, 2009, doi: 10.1109/TEC.2009.2025419.

[9]   E. Machines and M. W. Wyspianskiego, "Field-oriented control of five-phase induction motor with open-end stator winding," *Arch. Elect. Eng.*,vol. 65, no. 3, pp. 395–410, 2016, doi: 10.1515/aee-2016-0029.

[10] O. Paper, "High-performance discrete-time chattering-free sliding mode-based speed control of induction motor ˇ," *Electrical Engineering*, 2016, doi: 10.1007/s00202-016-0386-1.

[11] R. Roumaine, K. Iffouzar, M. F. Benkhoris, P. Nantes, H. Aouzellag, and K. Ghedamsi, "DIRECT ROTOR FIELD ORIENTED CONTROL OF POLYPHASE INDUCTION MACHINE BASED ON FUZZY LOGIC CONTROLLER," *Rev. Roum. Sci. Techn.– Électrotechn. et Énerg.* Vol. 62, 1, pp. 42–47, Bucarest, 2017.

[12] S. Khadar, H. A. Abu-rub, and K. Abdellah, "Sensorless Field-Oriented Control for Open-End Winding Five-Phase Induction Motor with Parameters Estimation," *IEEE Op. Jour. of the Indus.Elect. Soc.* Vol. 2, PP. 266 - 279, , 2021, doi: 10.1109/OJIES.2021.3072232..

[13] M. A. Mossa, H. Echeikh, N. El Ouanjli, and H. H. Alhelou,

"Enhanced Second-Order Sliding Mode Control Technique for a Five-Phase Induction Motor," *Int. Trans. Electron. Ene. Syst.,* , vol. 2022, 2022.

[14] K. Rahman *et al.*, "Field-Oriented Control of Five-Phase Induction Motor Fed from Space Vector Modulated Matrix Converter," *IEEE Access*, vol. 10, pp. 17996–18007, 2022, doi: 10.1109/ACCESS.2022.3142014.

[15] A. Iqbal, B. P. Reddy, S. Rahman, and M. Meraj, "Modelling and indirect field-oriented control for pole phase modulation induction motor drives," *IET Power Electron.*, vol. 16, no. 2, pp. 268–280, 2023, doi: 10.1049/pel2.12381.

[16] R. Surada, S. Member, A. Khaligh, and S. Member, "A Novel Approach towards Integration of Propulsion Machine Inverter with Energy Storage Charger in Plug-In Hybrid Electric Vehicles," *IEEE Indus. Electron. Annual Conf. IECON*, pp. 2493–2498, 2010.

[17] I. Subotic, N. Bodo, and E. Levi, "An EV Drive-Train with Integrated Fast Charging Capability," *IEEE Trans. Power Electron.*, vol. 31, no. 2, pp. 1461–1471, 2016, doi: 10.1109/TPEL.2015.2424592.

[18] B. Kollar and Z. Varga, "Features of Segment Winded PMSM for a Low Voltage Supply System," *2016 Internatio. Conference on Electri. Syst. for Aircr., Rail., Ship Pro. and Road Vehic. & Inte. Transp. Electrificat. Confere. (ESARS-ITEC)*, pp. 0–5, 2016.

[19] K. A. Chinmaya and G. K. Singh, "Integrated onboard single-stage battery charger for PEVs incorporating asymmetrical six-phase induction machine," *IET Electr. Syst. Transp.*, vol. 9, no. 1, pp. 8–

15, 2019, doi: 10.1049/iet-est.2018.5015.

[20] D. Herrera, J. Villegas, E. Galván, and J. M. Carrasco, "Synchronous reluctance six-phase motor proved based EV powertrain as charger/discharger with redundant topology and ORS control," *IET Electr. Power Appl.*, vol. 13, no. 11, pp. 1857–1870, 2019, doi: 10.1049/iet-epa.2018.5338.

[21] S. Foti *et al.*, "An Integrated Battery Charger for EV applications based on an Open End Winding Multilevel Converter configuration . Keywords 2 . AHMC OW - motoring mode," *2019 21st Eur. Conf. Power Electron. Appl. (EPE '19 ECCE Eur.*,P. P.1- 8.

[22] U. Singh, "Three-phase On-board Integrated Bidirectional EV Battery Charger With Power Factor Correction," *2019 6th Int. Conf. Signal Process. Integr. Networks*, pp. 335–340, 2019.

[23] U. Singh, "Single-Phase On-board Integrated Bi-directional Charger with Power Factor Correction for an EV," *2019 6th Int. Conf. Signal Process. Integr. Networks*, pp. 716–721, 2019.

[24] M. Tong, M. Cheng, S. Wang, and W. Hua, "An On-Board Two-Stage Integrated Fast Battery Charger for EVs Based on a Five-Phase Hybrid-Excitation Flux-Switching Machine," *IEEE Trans. Ind. Electron.*, vol. 68, no. 2, pp. 1780–1790, 2021, doi: 10.1109/TIE.2020.2988242.

[25] H. J. Raherimihaja, Q. Zhang, T. Na, M. Shao, and J. Wang, "Transactions on Power Electronics A Three-Phase Integrated Battery Charger for EVs based on Six-phase Open-end Winding Machine," *IEEE Trans. on Power Electron.* vol. 35, P.P 12122 - 12132 , no. c, 2020, doi: 10.1109/TPEL.2020.2986798.

[26] P. Pescetto, "Integrated Isolated OBC for EVs with 6-phase Traction Motor Drives," *IEEE Ene. Conve. Congr.and Exp. (ECCE)* , pp. 4112–4117, 2020.

[27] M. S. Abdel-majeed, A. Shawier, A. S. Abdel-khalik, M. S. Hamad, M. M. Sedky, and N. A. Elmalhy, "General Current Control of Six-Phase-Based Non-Isolated Integrated On-Board Charger with Low Order Harmonic Compensation," *Sustainability*, PP.1-20, 2022.

[28] A. T. Abdel-wahed, Z. Ullah, A. S. Abdel-khalik, M. S. Hamad, S. Ahmed, and N. A. Elmalhy, "Design and Finite-Element-Based Optimization for a 12-Slot / 10-Pole IPM Motor with Integrated Onboard Battery Charger for Electric Vehicle Applications," *Machines*, vol. 11, no. 5, p. 534, 2023.

[29] D. Jiang, Y. Shuai, Z. Liu, B. Li, and M. Zhou, "Control Strategy of Series-End Winding Single-Phase Integrated On-Board Charger System," *IEEE Trans. Transp. Electrif.*, vol. PP, p. 1, 2023, doi: 10.1109/TTE.2023.3323525.

[30] Z. Liang *et al.*, "Full Integration of On-Board Charger, Auxiliary Power Module, and Wireless Charger for Electric Vehicles Using Multipurpose Magnetic Couplers," *IEEE Trans. Ind. Electron.*, vol. PP, pp. 1–6, 2023, doi: 10.1109/TIE.2023.3331082.

[31] E. E. Ward and H. Härer, "Preliminary investigation of an invertor-fed 5-phase induction motor," *Proc. Inst. Electr. Eng.*, vol. 116, no. 6, p. 980, 1969, doi: 10.1049/piee.1969.0182.

[32] A. Salem and M. Narimani, "A Review on Multiphase Drives for Automotive Traction Applications," *IEEE Trans. Transp. Electrif.*, vol. 5, no. 4, pp. 1329–1348, 2019, doi:

10.1109/TTE.2019.2956355.

[33] T. M. Jahns, "Improved Reliability in Solid-State AC Drives by Means of Multiple Independent Phase-Drive -Uiits," *IEEE Trans. Transp. Indust. Appl,* vol. I, no. 3, 1980.

[34] S. He, X. Sui, D. Zhou, and F. Blaabjerg, "Torque ripple minimization of seven-phase induction motor under more-than-two-phase fault," *Proc. - 2020 Int. Conf. Electr. Mach. ICEM 2020*, pp. 2222–2228, 2020, doi: 10.1109/ICEM49940.2020.9270772.

[35] E. Levi, R. Bojoi, F. Profumo, H. A. Toliyat, and S. Williamson, "Multiphase induction motor drives – a technology status review", *IET Electr. Power Appl.*, 2007, 1, (4), pp. 489–516 , doi: 10.1049/iet-epa.

[36] E. Semail, M. Ieee, X. Kestelyn, A. Bouscayrol, and M. Ieee, "Right Harmonic Spectrum for the Back-Electromotive Force of a n -phase Synchronous Motor," *IEEE Indus. Appl. Conference* , no. 1, pp. 71–78, 2004.

[37] F. Mekri, S. Ben Elghali, M. El, H. Benbouzid, and S. Member, "Fault-Tolerant Control Performance Comparison of Three- and Five-Phase PMSG for Marine Current Turbine Applications *IEEE Trans. on Sust.Ene.* , vol. 4, no. 2, pp. 425–433, 2013.

[38] T. M. Jahns and W. L. Soong, "Pulsating Torque Minimization Techniques for Permanent Magnet AC Motor Drives-A Review," *IEEE Trans. Indus. Electron.*, vol. 43, no. 2, 1996.

[39] W. L. Soong, "Field-weakening performance of brushless synchronous AC motor drives," *IEEE Proc-Electr. Power Appl.*,vol. 141, no. 6, 1994.

[40] J. Wai and T. M. Jahns, "A New Control Technique for Achieving Wide Constant Power Speed Operation with an Interior PM Alternator Machine," *IEEE Indus. Appl. Conference* , vol. 00, no. C, pp. 807–814, 2001.

[41] R. Schiferl and T. A. Lip, "POWER CAPABILITY OF SALIENT POLE PERMANENT MAGNET," *IEEE Indus. Appl. Conference* , 1988.

[42] R.krishnan "Electric Motor Drives Modeling, Analysis, And Control," Upper Saddle River, New Jersey 2001.

[43] H. A. Toliyat and T. A. Lip, "Transient analysis of cage induction machines under stator, rotor bar and end ring faults," *IEEE Trans. Energy Convers.*,vol. 10, no. 2, pp. 241–247, 1995. doi: 10.1109/60.391888.

[44] A. Iqbal, "MODELLING AND CONTROL OF SERIES-CONNECTED FIVE-PHASE AND SIX- PHASE TWO-MOTOR DRIVES Atif Iqbal," PhD. Thesis of Liverpool John Moores University August, 2005.

[45] A. Iqbal, S. Moinuddin, and M. R. Khan, "A Novel Three-Phase to Five-Phase Transformation Using a Special Transformer Connection," *IEEE Trans. on Power Deliv.*, vol. 25, no. 3, pp. 1637–1644, 2010. doi: 10.1109/TPWRD.2010.2042307.

[46] S. Moinoddin, A. Iqbal, H. Abu-Rub, M. Rizwan Khan, and S. Moin Ahmed, "Three-phase to seven-phase power converting transformer," *IEEE Trans. Energy Convers.*, vol. 27, no. 3, pp. 757–766, 2012, doi: 10.1109/TEC.2012.2201483.

[47] A. Iqbal, S. Moinuddin, and M. R. Khan, "Space Vector Model of

A Five-Phase Voltage Source Inverter," *IEEE Inte. Conference on Indus. Tech.* , pp. 488–493, 2006.

[48] C. Cfrj, "Comparing the indirect fieldoriented control with a scalar method," *IEEE Trans. On IE*， pp. 475–480, 1991.

[49] K. Ohishi and E. Hayasaka, "High Performance Speed Servo System Considering Voltage Saturation," *IEEE Trans. On IE*, 53(3), 795-802., pp. 804–809,2002. doi: 10.1109/TIE.2006.874274.

[50] H. Echeikh, R. Trabelsi, A. Iqbal, N. Bianchi, and M. F. Mimouni, "Comparative study between the rotor flux oriented control and non-linear backstepping control of a five-phase induction motor drive - an experimental validation," *IET Power Electron.*, vol. 9, no. 13, pp. 2510–2521, 2016, doi: 10.1049/iet-pel.2015.0726.

[51] D. G. Holmes, B. P. McGrath, and S. G. Parker, "Current regulation strategies for vector-controlled induction motor drives," *IEEE Trans. Ind. Electron.*, vol. 59, no. 10, pp. 3680–3689, 2012, doi: 10.1109/TIE.2011.2165455.

[52] P. Anantachaisilp and Z. Lin, "Fractional order PID control of rotor suspension by active magnetic bearings," *Actuators*, vol. 6, no. 1, pp. 1–31, 2017, doi: 10.3390/act6010004.

[53] T. Sreekumar and K. S. Jiji, "Comparison of Proportional-Integral (P-I) and Integral-Proportional (I-P) controllers for speed control in vector controlled induction Motor drive," *ICPCES 2012 - 2012 2nd Int. Conf. Power, Control Embed. Syst.*, 2012, doi: 10.1109/ICPCES.2012.6508089.

[54] J. K. Jain, S. Ghosh, and S. Maity, "Concurrent PI Controller Design for Indirect Vector Controlled Induction Motor," *Asian J.*

Control, vol. 22, no. 1, pp. 130–142, 2020, doi: 10.1002/asjc.1911.

[55] J. Y. Hung, W. Gao, and J. C. Hung, "Variable Structure Control : A Survey," *IEEE Trans. Ind. Electron.*, vol. 40, no. 1, pp. 23–36, 1993.

[56] V. I. Utkin, "Sliding Mode Control Design Principles and Applications to Electric Drives," *IEEE Trans. Ind. Electron.*, vol. 40, no. 1, pp. 23–36, 1993.

[57] X. Zhang, L. Sun, K. Zhao, and L. Sun, "Nonlinear Speed Control for PMSM System Using Sliding-Mode Control and Disturbance," *IEEE Trans. Ind. Electron.*, vol. 28, no. 3, pp. 1358–1365, 2013.

[58] O. Barambones, A. J. Garrido, and F. J. Maseda, "Integral sliding-mode controller for induction motor based on field-oriented control theory," *IET Control Theory Appl.*, no. 3, pp. 786–794, 2007, doi: 10.1049/iet-cta.

[59] M. Jouini, S. Dhahri, and A. Sellami, "Combination of integral sliding mode control design with optimal feedback control for nonlinear uncertain systems," *Trans. Inst. Meas. Control.*, 2018, doi: 10.1177/0142331218777562.

[60] S. K. Sahoo and T. Bhattacharya, "A synchronized sinusoidal PWM based Rotor Flux Oriented Controlled Induction Motor Drive for Traction Application," *IEEE Applied Power Electronics Conference*, pp. 797–804, 2013.

[61] V. Deshpande, J. G. Chaudhari, and P. P. Jagtap, "Development and simulation of SPWM and SVPWM control induction motor drive," *2009 2nd Int. Conf. Emerg. Trends Eng. Technol. ICETET 2009*, vol. 2, pp. 748–752, 2009, doi: 10.1109/ICETET.2009.78.

[62] M. Valente, T. Wijekoon, F. Freijedo, P. Pescetto, G. Pellegrino, and R. Bojoi, "Integrated on-board EV battery chargers: New perspectives and challenges for safety improvement," *Proc. - 2021 IEEE Work. Electr. Mach. Des. Control Diagnosis, WEMDCD 2021*, pp. 349–356, 2021, doi: 10.1109/WEMDCD51469.2021.9425666.

[63] J. Gao, B. Li, D. Jiang, and M. Zhou, "Review of Torque Cancellation Methods for Integrated Motor Drive and Charger System," *2021 IEEE Int. Electr. Mach. Drives Conf. IEMDC 2021*, pp. 0–8, 2021, doi: 10.1109/IEMDC47953.2021.9449500.

[64] E. Levi, M. Jones, S. Vukosavic, and H. A. Toliyat, "A novel concept of a multiphase, multimotor vector controlled drive system supplied from a single voltage source inverter," *IEEE Trans. Power Electron.*, vol. 19, no. 2, pp. 320–335, 2004, doi: 10.1109/TPEL.2003.823241.

[65] I. Subotic, E. Levi, M. Jones, and D. Graovac, "Multiphase integrated on-board battery chargers for electrical vehicles," *2013 15th Eur. Conf. Power Electron. Appl. EPE 2013*, pp. 3–5, 2013, doi: 10.1109/EPE.2013.6631935.

[66] I. Subotic, N. Bodo, and E. Levi, "Integration of Six-Phase EV Drivetrains into Battery Charging Process with Direct Grid Connection," *IEEE Trans. Energy Convers.*, vol. 32, no. 3, pp. 1012–1022, 2017, doi: 10.1109/TEC.2017.2679280.

[67] M. A. Frikha, J. Croonen, K. Deepak, Y. Benômar, M. El Baghdadi, and O. Hegazy, "Multiphase Motors and Drive Systems for Electric Vehicle Powertrains: State of the Art Analysis and Future Trends," *Energies*, vol. 16, no. 2, 2023, doi: 10.3390/en16020768.

[68] T. J. C. Sousa, D. Pedrosa, V. Monteiro, and J. L. Afonso, "A Review on Integrated Battery Chargers for Electric Vehicles," *Energies*, vol. 15, no. 8, 2022, doi: 10.3390/en15082756.

[69] J. Hu, J. Zhu, and D. G. Dorrell, "In-depth study of direct power control strategies for power converters," *IET Power Electron.*, vol. 7, no. 7, pp. 1810–1820, 2014, doi: 10.1049/iet-pel.2013.0632.

[70] S. L. Sanjuan, "Voltage Oriented Control of Three - Phase Boost PWM Converters" *Master Thesis in Electric Power Engineering, Dep.of Energy and Env ironm. Div. of Electric Power Engineering*, Chalmers University Of Technology Göteborg, Sweden, 2010 ..

[71] F. SEVİLMİŞ and H. KARACA, "Performance analysis of SRF-PLL and DDSRF-PLL algorithms for grid interactive inverters," *Int. Adv. Res. Eng. J.*, vol. 3, no. 2, pp. 116–122, 2019, doi: 10.35860/iarej.412250.

[72] S. Golestan, J. M. Guerrero, and J. C. Vasquez, "Three-Phase PLLs: A Review of Recent Advances," *IEEE Trans. Power Electron.*, vol. 32, no. 3, pp. 1894–1907, 2017, doi: 10.1109/TPEL.2016.2565642.

[73] F. Sebaaly, H. Vahedi, H. Y. Kanaan, N. Moubayed, and K. Al-Haddad, "Design and Implementation of Space Vector Modulation-Based Sliding Mode Control for Grid-Connected 3L-NPC Inverter," *IEEE Trans. Ind. Electron.*, vol. 63, no. 12, pp. 7854–7863, 2016, doi: 10.1109/TIE.2016.2563381.

[74] J. Listwan and K. Pieńkowski, "Comparative analysis of control methods with model reference adaptive system estimators of a seven-phase induction motor with encoder failure," *Energies*, vol. 14, no. 4, 2021, doi: 10.3390/en14041147.

الخلاصة

إن الانتشار الكبير للسيارات الكهربائية (EVs) في الآونة الأخيرة جعل المستخدمين يتجهون نحو اختيار طريقة شحن مناسبة تغني عن محطات الشحن. قدمت هذه الدراسة تحليل ومحاكاة للشاحن المتكامل على متن السيارات الكهربائية، اذ تتم عملية الشحن عبر العناصر المخصصة للقيادة بحيث يتم الاستفادة من العاكس الكهربائي سباعي الطور مجتمعا مع المحرك الحثي سباعي الطور أثناء فترة الشحن. إن استخدام ملفات الجزء الثابت الخاص بالمحرك اثناء عملية الشحن كمرشح لتيار الشبكة يواجه عديد من المعوقات، منها تعرضه للدوران بسبب مرور تيار متناوب من خلال الملفات آنفة الذكر، لذلك يميل مستخدمو الشحن المتكامل للسيارات الكهربائية الى استخدام المحركات متعددة الاطوار لما لها من مزايا تمكنها من التخلص من عزم الدوران أثناء الشحن، ولضمان بقاء المحرك ساكناً أثناء الشحن، تم تنفيذ نقلة إضافية لأطوار المحرك بهدف فصل وظائف الشحن عن الدفع.

قدمت هذه الدراسة تحليل و محاكاة للمحرك الحثي سباعي الطور مع تقنية التحكم الموجهة للفيض (FOC) من اجل التحكم في السرعة في ما يخص طور القيادة. استخدامت في هذه الدراسة انواع مختلفة من المتحكمات بما في ذلك المتحكم التكاملي-التناسبي (PI)، والمتحكم ذو النمط المنزلق (SM)، اضافة الى المتحكم ذو النمط المنزلق التكاملي (ISM) بهدف تحقيق نظام أكثر كفاءة للتحكم بالسرعة ضد الاضطرابات الخارجية. عندما تم دمج المتحكم ذو النمط المنزلق SM والمتحكم ذو النمط المنزلق التكاملي ISMمع خوارزمية FOC؛ أظهرت المحاكاة أداءً أفضل وأكثر دقة من المتحكم PI في تحقيق السرعة والفيض بدقة بالرغم من وجود اضطرابات في معلمات المحرك. حيث اضهرت نتائج المحاكاة ان سرعة النظام مع المتحكم PI يحتوي على نسبة تجاوز ٠٫٠٥% و زمن استقرار يقدر ب ١٫٢ ثانية ، بينما بالنسبة للمتحكم SMC فان نسبة التجاوز تكون معدومة اما زمن الاستقرار يكون ٠٫٢٥ ثانية ، و المتحكم ISMC يكون نسبة التجاوز لمنحني السرعة معدومة اما زمن الاستقرار يكون ٠٫٥ ثانية.

إضافة إلى كل ما سبق، تعمل هذه الدراسة على تقديم شواحن متكاملة للسيارات الكهربائية بالاعتماد على مصادر الشبكة ذات الأطوار السبعة والثلاثة. في ما يخص الشحن من مصدر الشبكة سباعي الاطوار ، تكون كمية التيار المسحوبة من الشبكة متوازنة خلال جميع ملفات الجزء الثابت مانعةً بذلك من تولد عزم الدوران للمحرك. اما الشاحن ذو مصدر الشبكة ثلاثية

الأطوار فقد أظهرت توزيعا غير متساوٍ للتيار بين أطوار الشبكة، ونتيجة لذلك كانت جميع اطوار الشبكة في حالة من عدم المساواة. استخدمت هذه الدراسة تقنية VOC مع أنواع مختلفة من تقنيات التحكم بالتيار لتنظيم عملية الشحن، بحيث يحتوي على نظام التحكم ذو النمط المنزلق، والمتحكم التناسبي التكاملي الموجه (VPI) ، والمتحكم PI بالإضافة إلى كتلة فصل مركبات تيار الشبكة. تم تنفيذ هذه المتحكمات بشكل خاص للتعامل مع عدم التوازن وإنهاء التوافقية الثانية الناتجة عن عدم توازن تيار الشبكة وضمان تحقيق مستويات متطابقة من التيار. إن استخدام المتحكم ذو النمط المنزلق بدلاً من المتحكمات الأخرى أضاف درجة قليلة نسبيا من التوافقيات في تيار الشبكة إلى أدنى مستوى له. اظهرتنتائج المحاكاة ان المتحكم VPI يملك ١,٠% نسبة تجاوز و ٢,٥% من THD ، بينما ا لمتحكم SMC يحتوي على نسبة تجاوز ٣,٠% و ٢٥,٠ من THD ، و المتحكم PI يكزن ٣,١% من نسبة التجاوز و ٢,٣% من THD لموجة الفولتية الناتجة . وأخيرا، إنشاء طرق إدارة الشحن والقيادة تم محاكاة النظام مع المتحكمات المقترحة من خلال MATLAB/Simulink .

جامعة نينوى

كلية هندسة الالكترونيات

قسم الالكترونيك

الشحن المتكامل عالي القدرة للسيارة الكهربائية

علي حسين سلطان

رسالة في هندسة الالكترونيك

بإشراف

الاستاذ المساعد الدكتور

حارث احمد محمد البدراني

١٤٤٥ه ٢٠٢٤م

الشحن المتكامل عالي القدرة للسيارة الكهربائية

رسالة تقدم بها

علي حسين سلطان

إلى

مجلس كلية هندسة الالكترونيات- جامعة نينوى
وهي جزء من متطلبات نيل شهادة الماجستير
علوم في هندسة الالكترونيك

بإشراف

الأستاذ المساعد الدكتور

حارث احمد محمد البدراني